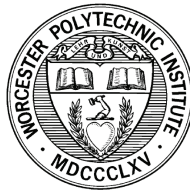


Wireless Communications and Spectrum Characterization in Impaired Channel Environments

Srikanth Pagadarai



Department of Electrical & Computer Engineering
Worcester Polytechnic Institute
Worcester, Massachusetts, USA

January 2012

APPROVED:

Professor Alexander M. Wyglinski, Primary Advisor

Professor Andrew G. Klein

Professor William R. Michalson

Professor Christopher R. Anderson

A dissertation submitted to Worcester Polytechnic Institute in partial fulfillment of the requirements for the degree of Doctor of Philosophy.

Abstract

The demand for sophisticated wireless applications capable of conveying information content represented in various forms such as voice, data, audio and video is ever increasing. In order to support such applications, either additional wireless spectrum is needed or advanced signal processing techniques must be employed by the next-generation wireless communication systems. An immediate observation that can be made regarding the first option is that radio frequency spectrum is a limited natural resource. Moreover, since existing spectrum allocation policies of several national regulatory agencies such as the Federal Communications Commission (FCC) restrict spectrum access to licensed entities only, it has been identified that most of the licensed spectrum across time and frequency is inefficiently utilized. To facilitate greater spectral efficiency, many national regulatory agencies are considering a paradigm shift towards spectrum allocation by allowing unlicensed users to temporarily borrow unused spectral resources. This concept is referred to a *dynamic spectrum access* (DSA). Although, several spectrum measurement campaigns have been reported in the published literature for quantitatively assessing the available vacant spectrum, there are certain aspects of spectrum utilization that need a deeper understanding.

First, we examine two complementary approaches to the problem of characterizing the usage of licensed bands. In the first approach, a linear mixed-effects based regression model is proposed, where the variations in percentage spectrum occupancy and activity period of the licensed user are described as a function of certain independent regressor variables. The second approach is based on the creation of a geo-location database consisting of the licensed transmitters in a specific geographical region and identifying the coverage areas that affect the available secondary channels. Both of these approaches are based on the energy spectral density data-samples collected across numerous frequency bands in several locations in the United States. We then study the mutual interference effects in a coexistence scenario consisting of licensed and unlicensed users. We numerically evaluate the impact of interference as a function of certain receiver characteristics. Specifically, we consider the unlicensed user to utilize OFDM or NOFDM symbols since the appropriate subcarriers can be turned off to facilitate non-contiguous spectrum utilization. Finally, it has been demonstrated that multiple-input and multiple-output (MIMO) antennas yield significant throughput while requiring no increase in transmit power or required bandwidth. However, the separation of spectrally overlapping signals is a challenging task that involves

the estimation of the channel. We provide results concerning channel and symbol estimation in the scenario described above. In particular, we focus on the MIMO-OFDM transmission scheme and derive capacity lower bounds due to imperfect channel estimation.

Acknowledgments

I have been extremely fortunate for having been associated with Professor Alex Wyglinski's research groups at the University of Kansas and at Worcester Polytechnic Institute for more than six years during my graduate studies. I can confidently claim that I have benefitted immensely under his guidance. His patience and nurturing management style have played a major role in my development as an engineer. I am grateful to him for his continual support, encouragement and the opportunities that he has given me to mature as a researcher. It would be an understatement to say that I would miss working with him.

I am deeply thankful to Professor William Michalson, Professor Andrew Klein and Professor Christopher Anderson for their feedback and suggestions at every stage of my research. Their insight and comments have helped me in improving both my ideas and this dissertation document. In particular, the knowledge that I gained by taking a class on information theory with Professor Klein has helped me in developing the ideas presented in Chapter 6. Over the course of the ONR-funded project, I had the pleasure of working with Professor Anderson. The regular discussions that I had with him have been of great help in my work on this project.

During my graduate studies, I have been financially supported by National Science Foundation (NSF) via grant CNS-0754315, Toyota InfoTechnology Center and the Office of Naval Research (ONR) via grant N00014-10-1-0065. I have also been supported by the Department of Electrical and Computer Engineering through a teaching assistantship from August 2008 through December 2009. I would like to acknowledge these funding agencies as well as Dr. Fred Loofth for their support.

My association with the Wireless Innovation Laboratory has given an opportunity to work with numerous graduate and undergraduate students who have enriched my Ph.D. experience. I thank them for being wonderful colleagues and friends. In particular, I would like to thank Si Chen, Di Pu, Jingkai Su, Sean Rocke and Zhu Fu for their friendship and support.

As always, my parents and my brother have supported me during the course of this degree and throughout my life. I am deeply indebted to them for their unconditional love and encouragement.

Contents

1	Introduction	1
1.1	Context	1
1.2	Background	3
1.3	Problem Statement	4
1.4	Dissertation Organization	5
2	The Wireless Spectrum	7
2.1	Introduction	7
2.2	The Complex Baseband Wireless Channel	8
2.3	Channel Estimation for Cyclic-Prefixed Block Transmissions	16
2.4	Orthogonal Frequency Division Multiplexing	17
2.5	Opportunistic Spectrum Access	19
2.6	Chapter Summary	24
3	Characterization of Wireless Spectrum in Urban Environments	25
3.1	Introduction	25
3.2	Time, Frequency and Spatial Characterization of Urban Environments	26
3.3	Spectrum Measurement Model Employing Linear Mixed Effects	31
3.4	Chapter Summary	36
4	Characterization of Wireless Spectrum in Vehicular Environments	38
4.1	Introduction	38
4.2	Measurement Campaign	40
4.3	Geo-Location Database Approach for Determining Vacant Channels	43
4.4	Implications for Transceiver Design	50

4.5	Chapter Summary	51
5	Non-contiguous Multicarrier Communications in DSA Systems	53
5.1	Introduction	53
5.2	Multicarrier Transmission Techniques for Opportunistic Communications .	55
5.3	Non-contiguous Data Transmission	59
5.4	Spectral Agility in Real-world Transmission Scenarios	62
5.5	Chapter Summary	69
6	Time-Selective MIMO-OFDM Channel Tracking in Low-Mobility Scenarios	71
6.1	Introduction	71
6.2	System Model	74
6.3	Decoupled Channel and Symbol Estimation	78
6.4	Blockwise Kalman Tracking	84
6.5	Capacity Bounds with Sequential MMSE Channel Estimation	88
6.6	Simulation Results	92
6.7	Chapter Summary	94
7	Conclusions and Future Work	97
7.1	Future Work	100
A	Linear Mixed Effects Model	102
B	An Overview of Complex-Valued Matrix Differentiation	105
C	Proof of Theorem 6.1	107
D	Proof of Theorem 6.2	111
E	Proof of Lemma 6.1	113
F	Proof of Theorem 6.4	117
G	Proof of Theorem 6.5	119
	References	121

List of Figures

1.1	Marconi in Newfoundland: The 1901 Transatlantic Radio Experiment. [1] .	2
2.1	Block diagram of a digital communications system. In this chapter, we will not review Source Encoding/ Decoding and Channel Encoding/ Decoding.	8
2.2	An energy spectral density plot of TV Channels from 470–806 MHz observed on 06/12/2009 in West Stockbridge, MA (top) and in Newton, MA (bottom)	20
2.3	A schematic example of OFDM-based dynamic spectrum access (DSA) . . .	21
2.4	An illustration of VDSA on a major inter-state highway.	23
3.1	A photograph of the mobile wireless spectrum measurement testbed employed in this research. Components of the testbed include a mini-discone/ridged-horn antenna, a spectrum analyzer and a laptop with SQUIRREL installed.	28
3.2	Cumulative distribution functions showing spectrum occupancy for the four cities surveyed.	29
3.3	An example showing the spatial variation of spectrum usage.	31
3.4	Quantile-quantile plots for the proposed linear mixed-effects models [2]. . .	37
4.1	A map of the forty eight locations close to I-90 between Boston, MA and West Stockbridge, MA over which spectrum measurements were collected on 06/07/2009, 06/11/2009 and 06/12/2009.	40
4.2	A photograph of the mobile wireless spectrum measurement testbed employed in this research. Components of the testbed include a mini-discone/ridged-horn antenna, a spectrum analyzer and a laptop with SQUIRREL installed.	41

4.3	Spectrogram plot for the TV frequencies in the frequency range, 600 - 750 MHz over 550 time sweeps on I-90 between Boston, MA and West Stockbridge, MA. The measurement setup was located in a vehicle moving at an average velocity of 60 miles/hr.	42
4.4	A map of the forty eight locations close to I-90 between Boston, MA and West Stockbridge, MA over which spectrum measurements were collected on 06/07/2009, 06/11/2009 and 06/12/2009.	43
4.5	TV Channel availability at different locations along I-90 in the state of Massachusetts, USA [3].	48
4.6	WSD power constraints on the available TV channels at different locations along I-90 in the state of Massachusetts, USA [3].	49
4.7	The total available bandwidth for secondary usage at different locations along I-90 in the state of Massachusetts, USA [3].	50
4.8	Maximum contiguous bandwidth and the number of non-contiguous channel blocks at different locations along I-90 in the state of Massachusetts, USA [3].	51
5.1	Signal processing and representation in GMC transmission link (a) and the time-frequency (T-F) representation of the transmit signal $s(t)$ (b); Δf - subcarriers distance, Δt - sampling period. L, N, M, N_t denote: the duration of the pulse-shaping filter impulse response $\gamma[k]$ in samples (equal to the duration of the dual-filter impulse response $g[k]$ at the receiver), the oversampling rate, the number of subcarriers, and the number of pulses in time, respectively [4]	55
5.2	An illustration of the non-contiguous OFDM (shown in green) and non-contiguous NOFDM (shown in red) transmissions in the paging band (928 MHz - 948 MHz). Paging transmission is shown in blue [4].	60
5.3	Normalized interference as a function of the filter order [5].	65
5.4	Normalized interference as a function of the threshold difference [5].	66
5.5	Normalized interference as a function of the filter order in the event of false detection of PU [5].	68
5.6	Complexity of NOFDM and NC-OFDM transmissions as a function of the number of subcarriers. L, N, M denote: length of the pulse $\gamma[k]$ or $g[k]$ in samples, oversampling rate and the number of subcarriers, respectively [5].	70

6.1	Block diagram of a digital MIMO communications system	74
6.2	MMSE of channel coefficients	93
6.3	MMSE of information symbols	94
6.4	Capacity bounds for optimal Power allocation versus equi-powered allocation.	95
6.5	MMSE of information symbols for optimal Power allocation versus equi-powered allocation.	96

List of Tables

3.1	List of locations where the measurements were taken.	27
3.2	Fixed Effects for eq. (3.2) [2].	34
3.3	Fixed Effects for eq. (3.4) [2].	35
4.1	Protected Service Contour Levels for TV Channels	44
4.2	Required Interference Protection Ratios for TV Channels	45

Chapter 1

Introduction

1.1 Context

Historically speaking, Guglielmo Marconi's series of demonstrations on wireless telegraphy towards the end of the Twentieth century in Europe and in the United States had marked a turning point for the field of wireless communications. The subsequent decades were marked with episodes of enthusiasm towards wireless systems such as the adoption of wireless telegraphy by the shipping industry [6], the installation of wireless radios for law-enforcement vehicles in the United States [7], followed by commercial audio [8] and television broadcasting [9] using wireless radio transmitters. However, due to the technological constraints involved, the application of wireless systems had not gained widespread utilization until the 1970s except for the specialized examples listed above and mainstream communications' operations such as telephony relied on classic wireline implementations. Nevertheless, researchers as early as 1947¹ had envisioned dividing large geographical areas into *cells* in order to provide affordable mobile-radio service to the general public. Throughout the 1950s and the 1960s, several researchers [11–17] have advanced the theory of cellular communications, culminating in Bell Telephone Laboratories Inc. submitting a proposal to the Federal Communications Commission (FCC) in December 1971 for offering cellular mobile communications. Following extensive FCC-authorized field trials, a Bell Telephone Laboratories Inc. subsidiary, Advanced Mobile Phone Service Inc. (AMPS) was granted commercial licenses. The complete series of papers that describe the original

¹D. H. Ring at the Bell Telephone Laboratories Inc. in an internal memo [10, Section 2.4]



Fig. 1.1 Marconi in Newfoundland: The 1901 Transatlantic Radio Experiment. [1]

AMPS architecture can be found at [18].

During the past four decades, the field of wireless communications has experienced a sustained period of advancement both in terms of the research and development of innovative techniques as well as the market penetration in the consumer sector. Beginning with the introduction of the first generation wireless telephone system, Advanced Mobile Phone Service (AMPS) [10] in 1983, there has been a tremendous improvement in the data-rates offered by the wireless communications' service providers to meet the unceasing demands of the subscribers. During the subsequent decades, wireless communications' technology progressed from the analog 1G to the digital 2G and continued its expansion by incorporating many other advanced signal processing principles. More importantly, this evolution was driven by the increasingly diverse nature of the information content that needed to be transported between several users. As a result, a clear challenge emerged in the regulation and the standardization of the "prime" wireless spectrum *i.e.*, from DC to 3 GHz towards different types of wireless services [19–22].

The Federal Communications Commission (FCC) was established by the Seventy-third Congress of the United States in an act entitled, "Public, No. 416" and approved on June 19, 1934 [23] for the purpose of regulating communication by wire and radio with public

interest as its primary focus. Thus, although the FCC has been in charge of developing and enforcing the regulations that are necessary for the support of various laws enacted by the U.S. Congress to govern the commercial use of the spectrum for several decades, it was during the mid-1980s that an era of a rethinking of spectrum regulation had begun. In contrast to the public interest focused approach that had existed until then, the FCC and several other regulatory authorities around the world started spectrum assignment based on a new market focused approach particularly for frequency bands such as those corresponding to cellular communications via various forms of auction.

With increased licensing of prime radio frequency (RF) spectrum, the expansion of the existing services or the allocation of spectrum for additional services was an important technical challenge identified by the FCC. The traditional spectrum allocation techniques relying on segmenting the available spectrum and assigning the fixed blocks to the licensed users do not permit unlicensed users to access the already licensed bands. As a result of this prohibition on the unlicensed access to licensed spectrum, heavily populated and highly interference-prone frequency bands have to be accessed. Clearly, this results in reduced system performance.

1.2 Background

Spectrum measurement studies have been carried out in the United States for the past several years for the purpose of gaining insights into wireless spectrum occupancy characteristics, and there by implement appropriate technical and legislative actions in order to support continued growth in the wireless sector, see for example [24–26]. However, spectrum measurement studies conducted in the recent times [27, 28] have focused primarily on characterizing the under-utilization with the purpose of their utility for the design of *dynamic spectrum access networks* (DSA) which enable highly spectrally agile wireless platforms called *cognitive radios* [29] to temporarily borrow licensed spectrum while ensuring that the interference caused to primary license holders is almost negligible. Owing to the increasing evidence of the under-utilization of wireless spectrum as demonstrated by [27, 28] and several others, an important policy step taken by the FCC is the enabling of cognitive access by secondary devices in TV broadcast spectrum [30]. Although the paradigm shift in wireless spectrum regulatory approaches is based on the assumption that the majority of wireless spectrum is extensively underutilized by the incumbent license holders, which re-

lies on several independently conducted measurement campaigns, there still exists a definite need to obtain a deeper understanding of this natural resource.

A diametrical approach to improving spectral efficiency was put forward around the end of the last decade by Foschini *et al* in the seminal paper [31]. They showed that several independent data streams transmitted over co-channels across multiple antennas can be successfully recovered. This argument is based on the assumptions that each data stream experiences a distinct spatial signature and there are sufficient receiving antennas for the demodulation of the data streams. This revolutionary approach to data transmission has been shown to yield high data-rates while conserving the spectral resources at the same time, thus offering an impressive solution to providing high-speed wireless services. As part of an ongoing research project, We are working on an approach for the estimation of the wireless channels that impair the information data streams in the interference-corrupted, multiple-input multiple-output (MIMO) setting described above.

The important idea that bridges these two seemingly diverse topics is orthogonal frequency division multiplexing (OFDM). When OFDM signal is transmitted with a cyclic-prefix, the Toeplitz channel matrix in time-domain is converted into a diagonal matrix in the frequency domain. As a result, frequency-domain equalization is rendered simple. OFDM is also attractive for DSA based systems since subcarriers can be turned off in the frequency range that carries primary user's information and a non-contiguous frequency range can be utilized to provide fast data-rates to unlicensed users. On the other hand, OFDM combined with multiple-input/multiple-output antennas has become the de facto approach towards leveraging spatial and frequency diversity such that fast data-rates are provided.

1.3 Problem Statement

Based on the brief discussion on the background provided in the previous section, our aim in this dissertation is to answer the following questions:

- What is the wireless spectrum occupancy in average case urban environments as opposed to the worst case scenarios that are considered in the published literature? Can we demonstrate spatial, temporal and frequency-wise variations in spectrum occupancy? Since these variations are expected, how can we model these variations

parsimoniously such that meaningful conclusions regarding the influence of various parameters on wireless spectrum occupancy?

- Can we also extend this wireless spectrum occupancy analysis to vehicular settings which are increasingly reaching a point of “spectrum scarcity” due to the desire for faster data-rates? How feasible is the freed-up UHF DTV band for vehicular DSA? Given that the FCC has formulated certain restrictions on the use of UHF TV band, how do we incorporate them and quantify the available channels as a function of distance from TV transmitters?
- What are the co-existence issues that arise when licensed and unlicensed users transmit in neighboring frequency bands? What characteristics of the transmitter and the receiver influence these co-existence issues? How do orthogonal and non-orthogonal FDM schemes compare in a non-contiguous opportunistic spectrum access scenario?
- Focusing on OFDM alone, how do multiple-input/multiple-output antennas result in faster data-rates? How is channel acquisition optimal in such a scenario and what is the optimal training design? Specifically, in the presence of imperfect channel estimates, how much does the channel capacity reduce compared to the upper bound?

Each chapter whose description is given briefly in the next section addresses the questions indicated above by providing a theoretical framework followed by supporting simulation examples.

1.4 Dissertation Organization

Following Chapter 2 which provides the background material on several topics relevant to this dissertation, we present a statistical analysis in Chapter 3 for the wireless spectrum occupancy across the spatial, temporal, and frequency dimensions using measurements collected in four mid-size US cities, namely: Rochester, NY; Buffalo, NY; Pittsburgh, PA; Worcester, MA. Although we have collected these measurements across several bands within the 88 MHz-3 GHz frequency range, results pertaining to only certain bands are presented for the purpose of brevity.

We then present quantitative and qualitative results obtained as a result of a TV spectrum measurement campaign in Chapter 4. We used these measurements to characterize

vacant TV channels along a major interstate highway (I-90) in the state of Massachusetts, USA. By characterizing the availability of vacant TV channels in the 470-806 MHz frequency range, we show the trends in the availability of vacant channels from a vehicular dynamic spectrum access perspective. We also describe the design constraints imposed on a point-to-multipoint communications based architecture in such a setting. Specifically, we described a general geo-location database approach to create a spectral map of available channels in a given geographical area and presented the results obtained by applying such a technique in the state of MA over several locations on I-90.

In Chapter 5, we investigated two approaches for enabling non-contiguous multicarrier modulation that can be used to facilitate spectrally opportunistic cognitive radio systems. One of the approaches is a variant of orthogonal frequency division multiplexing (OFDM), called non-contiguous OFDM (NC-OFDM), while the other approach is based on the non-contiguous version of the filter bank approach, non-orthogonal frequency division multiplexing (NOFDM), referred to as noncontiguous NOFDM (NC-NOFDM). The performance of these two approaches is assessed in terms of interference mitigation, which involves the use of actual spectrum measurement data, as well as computational complexity.

Finally, in Chapter 6, we analyze the channel tracking characteristics of a MIMO-OFDM setup. We derive this setup as a solution that meets an orthogonality criterion that is required in order to decouple channel estimation from data detection. We then derive a training design that is optimal in MMSE sense. By utilizing certain diagonality properties, we simplify the structure of the sequential channel estimator. We analyze upper and lower bounds on the channel capacity for this setup and understand the impact of channel state predictions on the data-rate.

The dissertation is wrapped up in Chapter 7 by drawing several conclusions and providing directions for future research.

Chapter 2

The Wireless Spectrum

2.1 Introduction

In contrast to analog communications where a continuum of values are employed to transfer information over space or time, digital communications which is ubiquitous in today's world uses binary digits, or *bits*. At the transmitter end, these information bits are represented as a discrete sequence of voltage levels. However, the physical medium over which the information is transmitted is analog in nature. As a result, the discrete voltage levels are mapped to voltage waveforms such that analog electromagnetic waves containing the original information bits are transmitted over the physical channel. The physical channel distorts the transmitted waveform depending on the particular context under consideration. For the case of a wireline channel, the system impairments can be modeled as linear and time-invariant whereas for the case of a wireless mobile channel, the system may be linear but possibly time-varying. At the receiver end, the channel-impaired analog waveform is sampled to produce a discrete sequence of voltage levels followed by a mapping operation to produce the original information bits. A block representation of the above order of operations is provided in Fig. 2.1. Although, the concise description provided above clearly skips several points pertaining to a digital communication link operating over a wireless fading channel, in this chapter, we provide a general overview regarding some of the details relevant to this dissertation. We then discuss a special property concerning OFDM symbols that is of interest in the final chapter. Additionally, the use of a wireless channel is regulated by national regulatory authorities such as the Federal Communications Commission (FCC) in the United States or the Office of Communications (Ofcom) in the

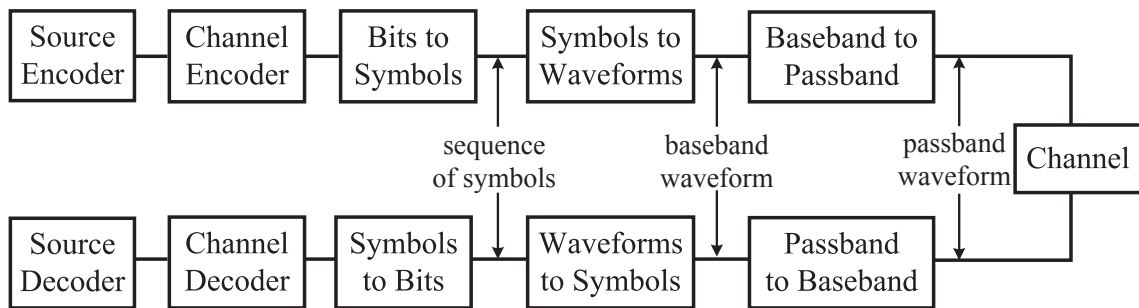


Fig. 2.1 Block diagram of a digital communications system. In this chapter, we will not review Source Encoding/ Decoding and Channel Encoding/ Decoding.

United Kingdom. The traditional approach is to auction portions of wireless spectrum to licensed entities and guarantee assured access to spectrum. We provide some details on these general spectrum regulatory policies adopted so far and the need for the regulatory bodies to let unlicensed users access spectrum dynamically when certain conditions are met.

2.2 The Complex Baseband Wireless Channel

As mentioned previously, we employ real-valued passband signals from transmission and reception in the physical world. However, a complex baseband representation of a digital communications system which contains all of the relevant information without resorting to using a large sampling rate for the corresponding passband signal is preferred for the sake of ease of analysis. This representation also helps in moving all of the analog processing closer to the antennas such that modern digital signal processors (DSPs) can digitally perform the necessary analysis independent of the actual passband channel employed. We first obtain a continuous-time complex baseband model followed by a discrete-time complex baseband model. Along the way, as the necessity arises, we also discuss certain parameters which characterize the frequency and time coherence of a wireless channel.

2.2.1 Continuous-time Model

The electromagnetic field impinging on a receive antenna due to the presence of a far field transmitting antenna radiating into free space can be determined by applying Maxwell's

partial differential equations []. In practical settings, the presence of arbitrarily moving reflectors and absorbers, the impact of mobility and other imperfections can also be taken into account and solved by Maxwell's equations. However, a simpler method which is often applied is a procedure termed *ray tracing*. In applying this procedure, we assume that the received electromagnetic waveform, $y_p(t)$ is a superposition of multiple copies of the transmitted passband waveform, $x_p(t)$ with each copy attenuated by a factor, $\gamma_i^p(t)$ and delayed by $\tau_i(t)$. In other words,

$$y_p(t) = \sum_i \gamma_i^p(t) x_p(t - \tau_i(t)) + z_p(t) \quad (2.1)$$

where $z_p(t)$ is zero-mean additive white Gaussian noise (AWGN) with power spectral density $N_0/2$. By writing (2.1) using a continuous-time convolution operation as, $y_p(t) = h_p(\tau, t) \star x_p(t) + z(t)$, it can be observed that the response of the channel at time t to an impulse transmitted at time $t - \tau$ is given by the expression,

$$h_p(\tau, t) = \sum_i \gamma_i^p(t) \delta(t - \tau_i(t)) \quad (2.2)$$

The propagation delay associated with each path, $\tau_i(t)$ is directly related to the distance travelled by the path, d_i as shown below:

$$\tau_i(t) = \frac{d_i}{c} \pm \frac{v_i t}{c} - \frac{\angle \phi_i}{2\pi f} \quad (2.3)$$

where v_i is the velocity with which the i th path length is changing and $\angle \phi_i$ indicates that the phase changes at the transmitter, receiver or due to the reflectors.

We now recognize that a passband signal is represented as a function of the continuous-time complex baseband signal as shown below:

$$x_p(t) = \sqrt{2}x^{(c)}(t) \cos(2\pi f_c t) - \sqrt{2}x^{(s)}(t) \sin(2\pi f_c t) = \sqrt{2}\Re(x(t)e^{j2\pi f_c t}) \quad (2.4)$$

where $x(t) = x^{(c)}(t) + jx^{(s)}(t)$ is the continuous-time complex-baseband signal with $x^{(c)}(t) = \Re(x(t))$ and $x^{(s)}(t) = \Im(x(t))$ being the in-phase component and the quadrature-phase components of $x(t)$ respectively. By writing $y_p(t)$ and $x_p(t)$ in (2.1) as a function of the

corresponding complex baseband signals, we now have

$$\begin{aligned}\sqrt{2}\Re(y(t)e^{j2\pi f_c t}) &= \sum_i \sqrt{2}\Re(x(t - \tau_i(t))e^{j2\pi f_c(t - \tau_i(t))}) + z_p(t) \\ &= \sqrt{2}\Re\left(\left\{\sum_i \gamma_i^p(t)x(t - \tau_i(t))e^{-j2\pi f_c \tau_i(t)}\right\}e^{j2\pi f_c t}\right) + z_p(t)\end{aligned}\quad (2.5)$$

Hence, the equivalent continuous-time complex baseband received signal is,

$$\text{Time-Varying case: } y(t) = \sum_i \gamma_i(t)x(t - \tau_i(t)) + z(t)\quad (2.6a)$$

$$\text{Time-Invariant case: } y(t) = \sum_i \gamma_i x(t - \tau_i) + z(t)\quad (2.6b)$$

where the complex baseband channel impulse response is,

$$\begin{aligned}h(\tau, t) &= \sum_i \gamma_i^p(t)e^{-j2\pi f_c \tau_i(t)}\delta(t - \tau_i(t)) \\ &= \sum_i \gamma_i(t)\delta(t - \tau_i(t))\end{aligned}\quad (2.7)$$

From (2.6a) and (2.6b), we can see that the passband physical channel with real-valued attenuation factors has been transformed into an equivalent baseband channel with complex-valued attenuations which depend on the carrier frequency used for transmission. The discussion in the next subsection involves obtaining the discrete-time complex baseband channel impulse response based on (2.7). Before moving on, we now briefly discuss two relevant parameters that will be needed for this purpose.

Delay Spread and Coherence Bandwidth An important parameter that determines the finite support over which the total energy of the impulse response, $h(\tau, t)$ is contained is the *delay spread*. It is defined based on the criterion, $\int_0^\infty |h(\tau, t)|^2 d\tau \approx \int_0^{T_d} |h(\tau, t)|^2 d\tau$ as follows:

$$T_d = \max_{i,j} |\tau_j(t) - \tau_i(t)|\quad (2.8)$$

In other words, taking into account all the paths that contribute significantly to the total energy of the channel impulse response, T_d is the maximum difference between the longest

and the shortest paths. Furthermore, it is clear that delay spread is defined in an order of magnitude sense since the approximation can be made arbitrarily accurate by taking more paths into account. We now look at the frequency response of (2.7),

$$H(f, t) = \sum_i \gamma_i(t) e^{-j2\pi f \tau_i(t)} \quad (2.9)$$

and notice that the differential phase caused by multiple paths undergoes changes when f changes by an order of magnitude comparable to the inverse of T_d . This quantity termed the *coherence bandwidth* is defined as shown below:

$$W_c = \frac{1}{2T_d} \quad (2.10)$$

When the coherence bandwidth of a channel is much greater than the bandwidth of a signal being transmitted, appreciable variations in frequency response as a function of frequency are not noticed. In this case, the fading wireless channel is considered *flat* or *frequency non-selective* and a single filter-tap (cf., Subsection 2.2.2) is sufficient to describe the channel. Conversely, when the coherence bandwidth of a channel is lesser than the bandwidth of a signal being transmitted, it is considered *frequency selective* and multiple filter-taps are necessary to describe the channel. Thus, the coherence bandwidth or the delay spread characterizes the frequency-selectivity of a wireless channel.

2.2.2 Discrete-time Model

From the previous subsection, we see that the information to be transmitted over a real passband waveform can be encoded onto a continuous-time complex baseband waveform. From Nyquist's sampling theorem [32] we see that if this complex baseband waveform is bandlimited to $[-\frac{1}{2T}, \frac{1}{2T}]$, then it can be completely described by its samples $\{x[nT]\}$ at rate $1/T$. Moreover, $x(t)$ can be recovered from its samples using the interpolation formula:

$$x(t) = \sum_n x[n] g(t - nT) \quad (2.11)$$

where $g(t) = \text{sinc}(t/T)$. Based on (2.11), we can construct the complex baseband waveform from a sequence of symbols, $\{x[n]\}$ which are drawn from a general complex-valued constellation with $1/T$ termed as *symbol rate*. In the absence of noise, the received waveform

is given as,

$$\bar{y}(t) = \sum_n x[n] h(t - nT) \quad (2.12)$$

where the time-invariant channel impulse response is $h(t) = g(t) \star g_c(t) = g_{\text{Tx}}(t) \star g_c(t) \star g_{\text{Rx}}(t)$. The filter, $h(t)$ is required to meet Nyquist's criterion for inter-symbol interference (ISI) avoidance so that $\bar{y}(nT) = x[n]$. Since the channel filter, $g_c(t)$ is not within the control of the designer, the usual practice is to design $g(t)$ to be Nyquist and handle the ISI introduced by $g_c(t)$ by a different mechanism. Although the sinc pulse is the minimum bandwidth Nyquist pulse, other pulses which have a faster time-decay than the sinc pulse and more robust against timing errors are used in practice at the expense of fractional excess bandwidth than what is dictated by the Nyquist criterion. One example of a pulse that is widely used is the raised cosine:

$$g_{RC}(t) = \text{sinc} \left[\frac{t}{T} \right] \cos \left[\frac{\pi \beta \frac{t}{T}}{1 - 4\beta^2 \frac{t^2}{T^2}} \right] \quad (2.13)$$

where the roll-off factor, β with $0 \leq \beta < 1$ indicates the use of a fractional excess bandwidth of $\frac{\beta}{2T}$. Moreover, $g_{RC}(t)$ has a finite *spread*, T_p i.e., $g_{RC}(t) \approx 0 \quad \forall t \notin (-t_0, T_p - t_0)$. We now substitute (2.11) in (2.6a) for the case of a raised-cosine pulse,

$$y(t) = \sum_i \sum_n \gamma_i(t) x[n] g_{RC}(t - nT - \tau_i(t)) + z(t) \quad (2.14)$$

Sampling the received waveform at multiples of T , we have

$$\begin{aligned} y(\bar{m}T) &= \sum_i \sum_n \gamma_i(\bar{m}T) x[n] g_{RC}(\bar{m}T - nT - \tau_i(\bar{m}T)) + z(\bar{m}T) \\ &= \sum_n x[n] \left(\sum_i \gamma_i(\bar{m}T) g_{RC}(\bar{m}T - nT - \tau_i(\bar{m}T)) \right) + z(\bar{m}T) \end{aligned} \quad (2.15)$$

By defining,

$$h[\bar{m} - n; \bar{m}] = \sum_i \gamma_i(\bar{m}T) g_{RC}(\bar{m}T - nT - \tau_i(\bar{m}T)) \quad (2.16)$$

and taking the channel delay spread as well as the pulse spread into account, we observe that

$$h[\bar{m} - n; \bar{m}] \approx 0 \quad \forall (\bar{m} - n) \notin \left\{ -\left\lceil \frac{t_0}{T} \right\rceil, \dots, \left\lceil \frac{T_p + T_d - t_0}{T} \right\rceil \right\} \quad (2.17)$$

By letting $l = \bar{m} - n$ in (2.15), we can write the discrete convolution operation of the transmitted symbol sequence with a *non-causal* FIR channel filter as follows:

$$y[\bar{m}] = \sum_{l=-\lceil \frac{t_0}{T} \rceil}^{\lceil \frac{T_p + T_d - t_0}{T} \rceil} h[l; \bar{m}]x[\bar{m} - l] + z[\bar{m}] \quad (2.18)$$

By replacing, \bar{m} with $m - \lceil \frac{t_0}{T} \rceil$ and defining $L = \lceil \frac{T_p + T_d}{T} \rceil$, the received sequence is left-shifted so that we can write the discrete convolution operation of the transmitted symbol sequence with respect to a *causal* FIR channel filter as follows:

$$\text{Time-Varying case:} \quad y[m] = \sum_{l=0}^L h[l; m]x[m - l] + z[m] \quad (2.19a)$$

$$\text{Time-Invariant case:} \quad y[m] = \sum_{l=0}^L h[l]x[m - l] + z[m] \quad (2.19b)$$

where the FIR channel filter taps are as shown below:

$$\begin{aligned} h[l; m] &= \sum_i \gamma_i(mT) g_{RC}(lT - \tau_i(mT)) \\ &= \sum_i \gamma_i(mT) \text{sinc} \left[l - \frac{\tau_i(mT)}{T} \right] \cos \left[\frac{\pi\beta \left(l - \frac{\tau_i(mT)}{T} \right)}{1 - 4\beta^2 \left(l - \frac{\tau_i(mT)}{T} \right)^2} \right] \\ &= \sum_i \gamma_i^p(mT) e^{-j2\pi f_c \tau_i(mT)} \text{sinc} \left[l - \frac{\tau_i(mT)}{T} \right] \cos \left[\frac{\pi\beta \left(l - \frac{\tau_i(mT)}{T} \right)}{1 - 4\beta^2 \left(l - \frac{\tau_i(mT)}{T} \right)^2} \right] \end{aligned} \quad (2.20)$$

Finally, the discrete-time complex Gaussian noise process, $\{z[m]\}$ in (2.19a) and (2.19b) is obtained by down-converting, low-pass filtering and sampling the continuous-time real-valued Gaussian noise process, $z_p(t)$ at multiples of T . It can be shown that $\{z[m]\}$ is a white

noise process, *i.e.*, independent over time. Moreover, the real and imaginary components of $\{z[m]\}$ are independent with equal variances, $N_0/2$. Due to the independence of the real and imaginary components of $\{z[m]\}$, it is also circularly-symmetric.

At the end of the previous subsection, we discussed two parameters which characterize the frequency-selectivity of the channel. We now provide a brief overview about two complementary parameters by observing the expression for the discrete-time complex baseband channel filter taps obtained in (2.20). These parameters explain the time-selectivity of the channel. In the next section, we will utilize the review of these quantities in summarizing the parsimonious models that are extensively used in the published literature for modeling time-selective wireless fading channels.

Doppler Spread and Coherence Time From (2.20), we notice that the phase term corresponding to the i th multipath that contributes to the l th channel filter tap undergoes a change of $\pi/2$ when the delay on the path changes by $\frac{1}{4f_c}$ or when the path length changes by a quarter wavelength, *i.e.*, by $\frac{c}{4f_c}$. Since the i th path length is changing with a velocity v_i , the time required for this phase change is $\frac{c}{4f_c v_i}$. By defining the Doppler shift of the i th path as $\eta_i = \frac{f_c v_i}{c}$, we now recognize that the phase change of the channel filter tap which depends on the phase changes occurring on several physical multipaths are determined by the inverse of the largest difference between the Doppler shifts, termed the *Doppler spread* as defined below:

$$D_s = \max_{i,j} |\eta_j - \eta_i| \quad (2.21)$$

Consequently, $h[l; m]$ experiences significant variations as a function of *coherence time* defined as:

$$T_c = \frac{1}{4D_s} \quad (2.22)$$

We observe from the above definitions that the time-selectivity is primarily dictated by the phase variations. That is, in (2.20), the time-variations caused on each path due to its corresponding attenuation factor and the raised cosine pulse are negligible compared to those that occur due to the phase term since it is dependant on the carrier frequency.

2.2.3 Statistical Characterization of Wireless Channels

An observation of (2.20) reveals that each FIR channel filter tap is obtained as a superposition of several attenuated and delayed samples taken over the Nyquist pulse employed for pulse-shaping. Clearly, while it is inconceivable to model the unpredictable nature of the physical mechanisms that give rise to the attenuation factors and propagation delays, statistical models which provide an insight into the aggregate properties of the channel filter taps are necessary in order to test the functioning of different wireless systems. Moreover, the possible limited range of operating conditions under which such models are valid provides further knowledge on the specific limitations of the wireless systems tested.

A simple probabilistic model that is based on the application of the Central Limit Theorem is based on the assumption that the real and imaginary parts of the channel filter taps are a sum of numerous independent random variables. Further, the phase of each tap is assumed to be uniformly distributed. Such assumptions can be claimed to be reasonable in the presence of several reflectors. As a result of the above assumptions, each channel filter tap is a complex Gaussian random variable. Hence, its magnitude is drawn from Rayleigh distribution and exhibits large variations due to the constructive and destructive superposition of the underlying independent random variables. This model is addressed in the literature as corresponding to a *Rayleigh fading channel*. A variation on the above model involves taking a large line-of-sight path into account. In this case, the magnitude of at least one path can be shown to be Rician distributed and is therefore, addressed as a *Rician fading channel*.

Modeling Time-Variations Another aspect of the characterization of the channel filter taps in addition to the complex random variable description provided above lies in taking their time-variations into consideration. A common assumption on the random process that drive the time-variations of the channel filter taps is its wide sense stationarity. In other words, the mean and the auto-correlation functions of each filter tap are assumed to be independent of time with latter being a function of the time-difference alone. Further, each tap at a given time instant is assumed to be independent of every other tap at any time instant. Together these two assumptions give rise the wide-sense stationary, uncorrelated scattering (WSSUS) model.

Autoregressive Model: A widely applied approach to model time variations of a WSSUS

channel is by a general P th order autoregressive (AR) random process. If we form a vector, \mathbf{h}_m by the following stacking operation,

$$\mathbf{h}_m = [h[0; m] \ h[0; 1] \ \dots \ h[L; m]]^\top \quad (2.23)$$

where L is the order of the discrete-time complex baseband wireless channel, the AR model that helps us to specify the correlation between the current state of the system and the past states of the system is as shown below:

$$\mathbf{h}_m = \sum_{p=1}^P \mathbf{A}_p \mathbf{h}_{m-p} + \mathbf{B} \mathbf{u}_m \quad (2.24)$$

In (2.24), each element in $\{\mathbf{A}_p\}$ is termed as an AR coefficient matrix or a state-transition matrix and \mathbf{u}_m as the excitation or driving noise vector. The eigen values of each element in $\{\mathbf{A}_p\}$ are assumed to be less than 1 in magnitude and the driving noise are assumed to be i.i.d and complex Gaussian distributed with zero mean. The AR model admits the following Yule-Walker equations to describe the covariance function of the process [33].

$$\mathbf{R}_h[m] = \sum_{p=1}^P \mathbf{A}_p \mathbf{R}_h[m-p] + \sigma_u^2 \mathbf{B} \mathbf{B}^H \quad (2.25)$$

Assuming that $\mathbf{R}_h[0]$ and $\{\mathbf{A}_p\}$ are known, we can apply the fact that $\mathbf{R}_h[m] = \mathbf{R}_h[-m]$, and recursively find $\{\mathbf{R}_h[m]\}$ for $m = 1, 2, \dots, P$. We can also find a non-unique \mathbf{B} by computing the square-root of (2.25) for $m = 0$ [34, p. 358].

2.3 Channel Estimation for Cyclic-Prefixed Block Transmissions

The problem of channel estimation is one of fundamental importance for wireless communication systems. Channel state information (CSI) at the receiver is critical for channel equalization and coherent data detection. On the other hand, the availability of CSI at the transmitter through a feedback channel helps in designing precoders and decoders that meet various criteria [35]. Although, CSI at the transmitter can be leveraged to provide fast data-rates, rapid variations in the wireless channel render the CSI that is feedback to the transmitter outdated. As a result, a practical approach is to gather CSI at the receiver

alone while the transmitter is designed to be independent of the channel characteristics. In this section, we examine some of relevant work in the published literature for the latter approach *i.e.*, those dealing with channel independent transmitters and coherent receivers that extract CSI using the transmitted signals.

One way of acquiring CSI is by employing *blind* techniques that are based solely on the symbol properties of the original data such as finite alphabet, constant modulus etc. or on the statistics of the received symbols [36]. These blind channel estimation techniques which can be broadly categorized as statistical or deterministic methods depending on whether the statistical knowledge about the source is exploited or not suffer from certain inadequacies. While deterministic methods allow closed-form solutions, avoid local minima and offer high speed of convergence, they also suffer from channel length indeterminacies and require that the corresponding channel transfer function be irreducible [37, 38]. On the other hand, statistical methods are robust to channel length overdeterminacies and in the case of statistical maximum likelihood (ML)- based approaches, no assumption is required on the knowledge of channel length. However, these techniques are optimal only for large data sets and require proper initialization to avoid the possibility of attaining local minima [36, 39].

Another approach for acquiring CSI which is more popular and adopted in all the prevailing wireless communications standards is by transmitting pilot symbols that are known *a priori* to the receiver. Although valuable system resources are sacrificed for transmitting pilot symbols, investing a fraction of the total power and data-rate budget for pilot symbols optimally makes the CSI acquisition problem solvable by well-known estimation theoretic techniques [40].

2.4 Orthogonal Frequency Division Multiplexing

From (2.19a) and (2.19b), it is clear that due to the multipath fading channel acting as an FIR filter, the transmitted symbol at a given time instant is corrupted by symbols that were transmitted in the past. An optimal way of managing this ISI in sequential communications is to employ a minimum mean square error (MMSE) equalizer, together with the successive interference cancelation (SIC) technique. This MMSE equalizer designed such that the SINR of the transmit symbol at the output of the filter is maximized is a standard way of ameliorating the effects of ISI for time-invariant channels. On the

other hand, Orthogonal Frequency Division Multiplexing (OFDM) has found widespread usage for block communications due to an attractive feature that simplifies equalization. In order to explore this idea further, we first write the IDFT-modulated information symbol sequence followed by a matrix formulation of the convolution operation shown in (2.19b).

Assuming that each OFDM symbol block spans over P subcarriers, the complex-baseband OFDM signal can be expressed as,

$$x[n] = \frac{1}{\sqrt{P}} \sum_{p=0}^{P-1} \tilde{x}[p] \exp \left\{ \frac{j2\pi np}{P} \right\} \quad 0 \leq n \leq P-1 \quad (2.26)$$

In the above equation, the information symbols, $\tilde{x}[p]$ are drawn from a general M-PSK or M-QAM constellation. Moreover, in order to facilitate block-wise processing of received symbols a guard-interval is inserted by copying the last L inverse discrete Fourier transform (IDFT) samples to the beginning of the OFDM block. That is, in order to generate one OFDM transmit symbol vector, we form an information symbol vector consisting of P symbols, $\tilde{\mathbf{x}} \triangleq [\tilde{x}(0) \dots \tilde{x}(P-1)]^T$ and pre-multiply it with the IDFT matrix, \mathbf{W}^H , where $[\mathbf{W}]_{n,p} = \frac{1}{\sqrt{P}} \exp\{-j2\pi np/P\}$ for $0 \leq n \leq P-1$ and $0 \leq p \leq P-1$. After adding cyclic-prefix, the transmitted OFDM symbol block is given by the matrix product,

$$\mathbf{x} = \mathbf{C}_T \mathbf{W}^H \tilde{\mathbf{x}} \quad (2.27)$$

where $\mathbf{C}_T = [[\mathbf{0}_{L \times (P-L)} \quad \mathbf{I}_L]^T \quad \mathbf{I}_P]^T$ with $\bar{P} = P + L$. The received symbol vector is now,

$$\mathbf{y} = \mathbf{H}_T \mathbf{x} + \mathbf{H}_{\text{ISI}} \mathbf{x}_{(-1)} + \mathbf{z} \quad (2.28)$$

where, \mathbf{H}_T is a column-wise Toeplitz matrix of dimensions, $\bar{P} \times \bar{P}$ whose first column is $[h[0] \dots h[L] \quad \mathbf{0}]^T$. Moreover, in (2.28), the effect of the ISI from the previous symbol is included by defining the row-wise Toeplitz matrix, \mathbf{H}_{ISI} whose first row is $[\mathbf{0} \quad h[L] \dots h[0]]$. After removing the cyclic prefix and performing the DFT operation, the received signal that is unaffected by the ISI from the previous symbol is expressed by the matrix product,

$$\begin{aligned} \tilde{\mathbf{y}} &= \mathbf{W} \mathbf{C}_R \mathbf{H}_T \mathbf{C}_T \mathbf{W}^H \tilde{\mathbf{x}} + \mathbf{v} \\ &= \tilde{\mathbf{H}} \tilde{\mathbf{x}} + \mathbf{v} \end{aligned} \quad (2.29)$$

where, $\mathbf{C}_R = [\mathbf{0}_{P \times L} \ \mathbf{I}_P]^\top$, $\tilde{\mathbf{H}} \triangleq \mathbf{W} \mathbf{H} \mathbf{W}^H$ and $\tilde{\mathbf{z}} \triangleq \mathbf{W} \mathbf{C}_R \mathbf{z}$. Furthermore, it is straightforward that $\mathbf{H} \triangleq \mathbf{C}_R \mathbf{H}_T \mathbf{C}_T$ is a circulant matrix whose first column is, $[h[0] \ \dots \ h[L] \ \mathbf{0}]^\top$ and first row is, $[h[0] \ \mathbf{0} \ h[L] \ \dots \ h[1]]$.

We first denote the q th column of \mathbf{H} as $\mathbf{H}_{(:,q)}$ and q th row of \mathbf{W} as $\mathbf{W}_{(q,:)}$ to understand the structure of $\tilde{\mathbf{H}}$ as follows:

$$\begin{aligned}
\tilde{\mathbf{H}}[n, p] &= \sum_{q=0}^{P-1} [\mathbf{W} \mathbf{H}_{(:,q)} \mathbf{W}_{(q,:)}^*]_{n,p} \\
&= \sum_{q=0}^{P-1} \left[[\mathbf{W} \mathbf{H}_{(:,q)}]_{(n,1)} \mathbf{W}_{(q,p)}^* \right]_{n,p} \\
&= \frac{1}{P} \sum_{q=0}^{P-1} \sum_{l=0}^L h[l] \exp \left\{ \frac{-j2\pi n(q+l)}{P} \right\} \exp \left\{ \frac{j2\pi qp}{P} \right\} \\
&= \frac{1}{P} \sum_{l=0}^L h[l] \exp \left\{ \frac{-j2\pi n l}{P} \right\} \sum_{q=0}^{P-1} \exp \left\{ \frac{-j2\pi q(n-p)}{P} \right\} \\
&= \sum_{l=0}^L h[l] \exp \left\{ \frac{-j2\pi n l}{P} \right\} \delta[n-p] \tag{2.30}
\end{aligned}$$

where the final equality stems from the fact that the summation of r th roots of unity is zero for $r > 1$. Due to (2.30), $\tilde{\mathbf{H}} = \text{diag} [\tilde{\mathbf{H}}[0,0], \dots, \tilde{\mathbf{H}}[P-1, P-1]]$. That is, irrespective of the channel filter coefficients, the IDFT and DFT operations at the transmitter and the receiver respectively have transformed an ISI constrained channel (cf., (2.19b)) into a collection of parallel flat-fading channels

$$\tilde{\mathbf{y}}[p] = \tilde{\mathbf{H}}[p,p] \tilde{\mathbf{x}}[p] + \mathbf{v}[p] \tag{2.31}$$

and a one-tap frequency-domain per-tone equalizer is sufficient to undo their effect resulting in a collection of parallel AWGN channels.

2.5 Opportunistic Spectrum Access

Due to impact on commerce, and various organizations, governmental or private, spectrum regulation has historically been regarded as an area of policy that is more about economics, politics, lobbying efforts and current perceived public opinion than it is about

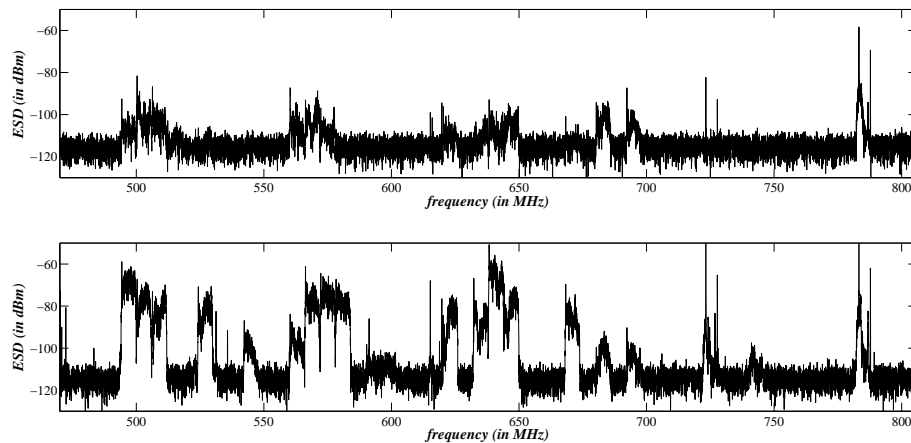


Fig. 2.2 An energy spectral density plot of TV Channels from 470 – 806 MHz observed on 06/12/2009 in West Stockbridge, MA (top) and in Newton, MA (bottom)

the details of a specific promising new technology. As mentioned in the previous chapter, due to the rapid pace of the development of the technologies involved in wireless communications, a market-based approach was adopted by the FCC in the mid-1980s. The four primary demands that dictate the regulation policies by the FCC are as follows [41]: applications, coverage, duty cycle and performance.

Traditionally, regulatory authorities have followed a command-and-control policy for spectrum allocation. However, several spectrum occupancy measurement studies show that wireless spectrum is generally under-utilized in both the frequency and temporal domains. Spectrum measurement campaigns have shown that such an allocation causes a waste of the spectrum both in frequency and time. A brief survey of other related works in the published literature is as follows. A comprehensive summary of spectrum occupancy for New York City and several locations in the state of Virginia were reported in [27]. Reference [42] presents similar results for locations in the state of Georgia. Spectrum occupancy variations as a function of varying thresholds and across the different angles of arrival at the receiver were presented. In [28], analytical and simulation based results are provided to support the use of spectral signatures that help a cognitive radio in identifying the active transmitters in a band of interest. More recently, closed-form probability distributions are presented for several fixed bandwidth signalling channels, and for proportional bandwidths, such as pre-selectors and low noise amplifiers [43] using the datasets presented in [44]. Spectrum

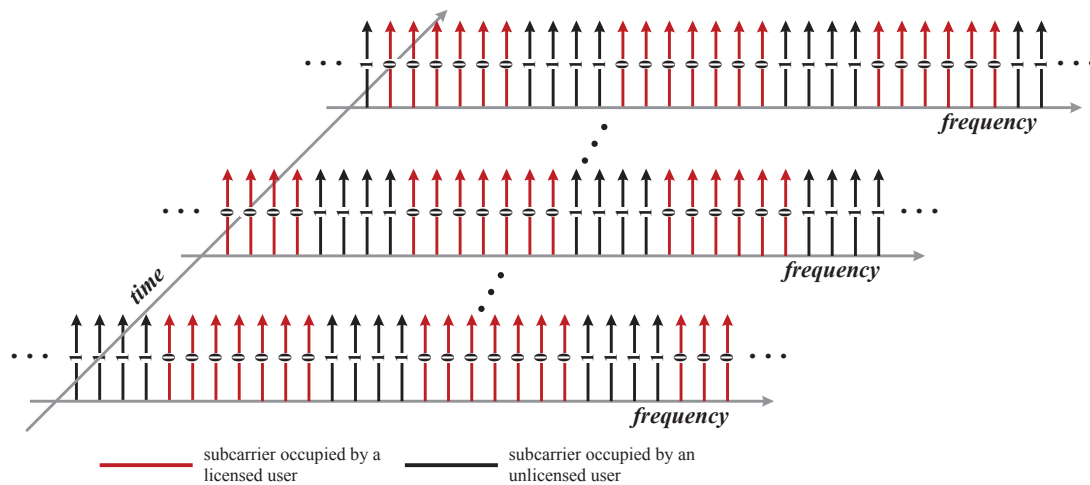


Fig. 2.3 A schematic example of OFDM-based dynamic spectrum access (DSA)

measurement-based studies similar to those described above have also been conducted outside of the United States. In [45], spectrum occupancy for several bands in the frequency range of 806 MHz to 2750 MHz in urban Auckland, New Zealand are provided. In [46], four spectrum sensing methods have been proposed and their performance is compared for UMTS uplink and GSM 1800 uplink bands. In [47], a methodology has been developed to identify TVWS frequencies, using digital TV coverage maps in conjunction with a database containing their locations.

As an example, Fig. 2.2 shows a measurement campaign conducted in Western MA between West Becket and Lee on 06/27/2009. The spectral occupancy from 470 – 806 MHz is shown. From this figure, it is observed that there are several spectral white spaces in the licensed portions of the spectrum demonstrating that the allocated spectrum is under-utilized. Thus, the result of this under-utilization caused by existing spectrum allocation policies causes an apparent scarcity of spectrum [48]. Hence, there is a need for a novel spectrum allocation policy.

2.5.1 The DSA Paradigm

The basic objective of the new spectrum allocation policy is the promotion of secondary utilization of unused portions of the spectrum in the form of *spectrum pooling*, wherein, unlicensed users rent licensed portions of the spectrum from a common pool of spectral

resources from different owners [49]. An illustration of secondary utilization of wireless spectrum in a spectrum pooling system is shown in Fig. 2.3. It should be remembered that although, the utilization of the spectral resources potentially generates additional revenue to the licensed users, the implementation of a spectrum pooling system raises many technological, economic and political questions, that need to be answered for the successful coexistence of the legacy¹ and rental systems. Efficient pooling of the radio spectrum is achieved by using a *cognitive radio* [50], which is a multi-band, spectrally agile radio that employs flexible communication techniques and detects the presence of primary user transmissions over different spectral ranges to avoid interference to the licensed users.

The concepts of spectrum pooling and cognitive radio were first introduced in [50]. This paper outlines the basic factors that need to be considered in determining the pooling strategy and in designing the radio etiquette. Reference [51] provides an understanding and mathematical analysis of the design principles behind the architecture of a software defined radio. Other physical design issues such as the adaptive nature of the transmitter both in selecting the frequency range over wideband frequencies, the different power levels, and the signal processing involved at the receiver, which are important aspects in the design of a cognitive radio, have been discussed at length in [52]. Further insight into the notion of spectrum pooling is provided by [49]. Some of the issues pertaining to spectrum pooling that are detailed in this paper include: detecting a spectrum, collecting and broadcasting the spectrum access measurements, and mutual interference caused by a rental system to a legacy system and vice-versa. Mutual interference in OFDM-based spectrum pooling systems is discussed in greater detail in [53]. This paper also discusses simple techniques to counter the effects of mutual interference caused by the sidelobes of an OFDM symbol in a spectrum pooling scenario. Similar research efforts involving the many related areas of cognitive radio such as efficient spectrum usage, supporting reliable communication and standardization efforts to promote fair use of spectrum resources among cognitive radio devices have been reported in [54] and [55] also.

¹In this dissertation, the terms *legacy systems* and *primary systems* are used to refer to the licensed owners of the RF spectrum whereas the terms *rental systems* and *secondary systems* are used to refer to the users that utilize the idle licensed portions of the spectrum.

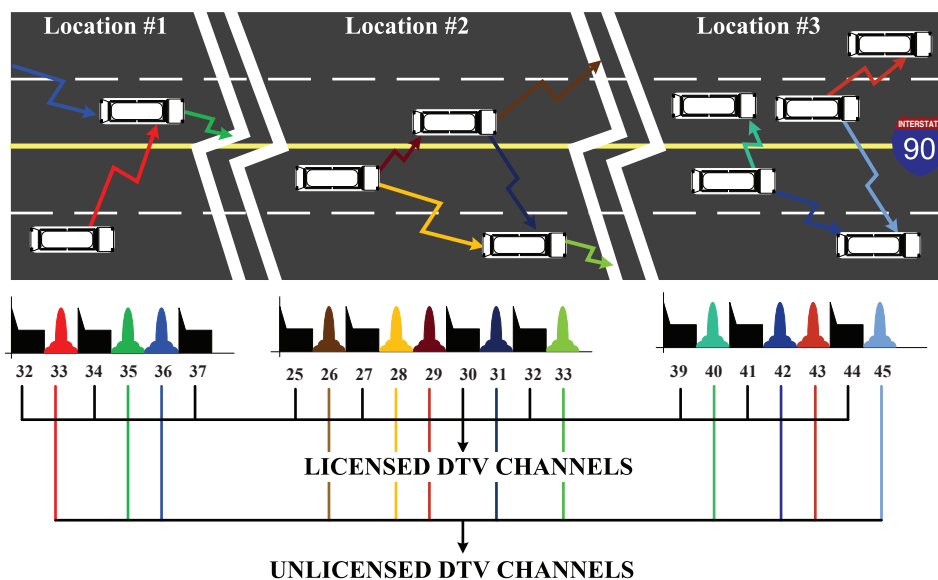


Fig. 2.4 An illustration of VDSA on a major inter-state highway.

2.5.2 A Practical Application: Vehicular Dynamic Spectrum Access

Vehicular communication research is becoming a major research focus in wireless communications research community to provide safety, comfort and information to the driver. Significant activities like the United States Department of Transportation (DOT) IntelliDrive [56] program are underway to develop vehicular communication technologies. The applications proposed by IntelliDrive aim to provide connectivity between vehicles, between vehicles and roadway infrastructure and infrastructure/consumer devices inside vehicles. Similarly, researchers have proposed methods like local peer group (LPG) [57] to organize vehicles into manageable groups to efficiently share safety messages. Proliferation of vehicular communication applications beyond safety in dense vehicular traffic environment necessitates efficient usage of wireless channel and spectrum resources. Therefore, future vehicular applications require dynamic spectrum access (DSA) methods to efficiently utilize available spectrum while providing stringent QoS required by vehicular applications. We envision that communication nodes enabled by cognitive radio capabilities like DSA will support future vehicular communication needs in challenging environments.

Although the many related areas of cognitive radio have been studied for the past few years, vehicular cognitive radio is a fairly recent research topic [58, 59] primarily focused on

offering reliable communications for vehicles in challenging spectrum environments through spectrum sensing, spectrum coordination and dynamic spectrum access. The application of dynamic spectrum access (DSA) to vehicular communication networks enables secondary utilization of licensed wireless channels for both vehicle-to-vehicle (V2V) and vehicle-to-infrastructure (V2I) communications [60], which results in an increase of transmission capacity and efficient spectral utilization, while simultaneously guaranteeing the rights of incumbent wireless transmissions. When applying the DSA concept to vehicular networks in order to create a vehicular dynamic spectrum access (VDSA) framework, the slowly time-varying spectral occupancy characteristics of TV spectrum is essential for realizing unlicensed vehicular wireless communications within licensed frequency bands. This is due to the high level of mobility of the wireless devices within a VDSA network, where the TV spectral occupancy characteristics that once appeared to be static at a fixed geographical location now appears to be changing based on the direction and speed of mobile wireless device. As opposed to other frequency bands, where spectral occupancy changes may occur relatively quickly over time and geography, TV spectrum possesses the advantage of having relatively slow spectral occupancy variations over large distances and periods of time. An illustration diagram depicting a vehicular DSA scenario is shown in Fig. 2.4.

2.6 Chapter Summary

This chapter has provided a brief overview of the discrete-time channel model followed by a review of miscellaneous topics related to OFDM signal transmission. Moreover, the existing literature on spectrum measurement campaigns conducted in the U.S. and elsewhere has been surveyed. While highlighting the contributions made by these studies in showing that the spectrum utilization is low, we indicated the possible areas in which further research can be conducted to better understand the characteristics in spectrum occupancy. We then provided a description of the dynamic spectrum access and its emerging application in vehicular environments. In the following chapters, this background material is referenced without loss of continuity.

Chapter 3

Characterization of Wireless Spectrum in Urban Environments

3.1 Introduction

Although the modification of wireless spectrum regulations are based on the assumption that the majority of wireless spectrum is extensively underutilized, which is based on several independently conducted measurement campaigns, there still exists a need to obtain a deeper understanding of this natural resource. By gaining this insight into wireless spectrum, appropriate technical and legislative actions can be taken in order to support continued growth in the wireless sector. In this chapter, we present statistical results for wireless spectrum occupancy across the space, time and frequency dimensions using measurements collected in four mid-size US cities, namely, Rochester (NY), Buffalo (NY), Pittsburgh (PA) and Worcester (MA). Even though we have collected these measurements across several bands, results pertaining to only a few bands are presented for the purpose of brevity.

3.2 Time, Frequency and Spatial Characterization of Urban Environments¹

The allocation of spectrum for a specific wireless application is uniform across the nation. However, its usage varies from region to region causing the location and the size of spectrum holes to vary randomly with respect to time and geography. The measurement campaigns conducted so far have focused mostly on the worst cases in terms of spectrum occupancy, such as very large cities and/or special events that result in increased communication traffic. Moreover, these measurement studies have mostly assessed the spectrum occupancy across a small geographical region. As a result, we do not fully understand the broader spectrum usage picture with respect to the temporal, spatial and band-wise variations of a large geographical area. Therefore, we characterize the availability of prime spectrum in mid-size American cities, i.e. the average case that most commonly occurs, for secondary access via theoretical and experimental techniques. Using these measurements, we will determine the long-term behavior and trends of spectrum occupancy and quantitatively compute the rate at which spectrum scarcity is occurring. Finally, we assess the temporal, spatial and band-wise characteristics over a large metropolitan area using the spectrum measurements and develop a linear mixed-effects model, which will be validated using these data points.

3.2.1 Measurement Campaign

In our measurement campaign, we used two antennas for scanning different frequency ranges broadly classified to two groups, namely, low frequency and high frequency. For the low frequency range *i.e.*, from 88 MHz to 1240 MHz, we used a Diamond D-220 mini-discone antenna with an operating frequency range of 100 – 1600 MHz. For the high frequency range *i.e.*, from 1850 MHz to 2686 MHz, we used an Advanced Technical Materials (ATM) 07-18-440-*NF* horn antenna with an operating frequency range of 0.7 – 18 GHz and an aperture of 60°. This helped us in observing the variation in spectrum usage across different angles of arrival. During our operation, one of these antennas is wired to an Agilent CSA series *N1996A* spectrum analyzer with frequency range ranging from 100 kHz - 3

¹The work included in this section has been funded by the National Science Foundation via grant CNS-0754315 and published at the *4th International Conference on Cognitive Radio Oriented Wireless Networks and Communications* (CROWNCOM) 2009 [61]

Table 3.1 List of locations where the measurements were taken.

Location	City			
	ROCHESTER, NY 19 th & 20 th June 2008	BUFFALO, NY 21 st & 22 nd June 2008	PITTSBURGH, PA 23 rd & 24 th June 2008	WORCESTER, MA 17 th , 26 th , & 27 th July 2008
SITE 1	S. Plymouth & Exchange Blvd	E. Huron St. & Washington St.	16th St Bridge & N of 1711 Penn. Av.	SE of Boynton Hall WPI
SITE 2	Jay St. & Verona St.	Swan St. & E. Michigan Av.	Sheraton St. & Fort Pitt Bridge	Vernon St. & Dorchester St.
SITE 3	Prince St. & Univ. Av.	Pearl St. & Church St.	Riverfront Park next to Birmingham bridge	Bell Hill Park (off Belmont St.)
SITE 4	Mortimer St. & N. Clinton St.	W. Genesee St. & Seventh St.	Craig St. & N. 5th Av.	Major Taylor Blvd. & Thomas St.
SITE 5	Pearl St. & Averill Av.	Oak St. & Clinton St.	Grandview St. & Ulysses St.	Gateway Park (Parking lot) WPI

GHz and consisting of a low noise amplifier (LNA). We use an in-house software tool called SQUIRREL (Spectrum Query Utility Interface for Real-time Radio Electromagnetics) to communicate remotely with the spectrum analyzer via commands issued through a simple graphical user interface on a laptop. The GUI accepts details, such as the center frequency, the span around the center frequency, and the resolution bandwidth. SQUIRREL communicates with the spectrum analyzer using TCL (Tool Command Language) over TCP/IP. After the sweep action is performed by the spectrum analyzer, the data points are returned to the GUI in a comma spaced value format. In its current format, the GUI and the server are written in JAVA and can be deployed on a variety of operating systems and computers. A photograph of the mobile wireless spectrum measurement testbed is shown in Fig. 3.1. The details about the locations and the dates of our spectrum measurement campaign is given in Table I.

Fig. 3.2 shows the trend in the occupancy irrespective of the cities, sites, time and frequency. In the following subsections, we provide finer details of occupancy values by grouping the collected data points appropriately. Moreover, in order to show a comparison of spectrum usage as a function of the variables mentioned above, an optimum threshold is computed using Otsu's gray-level thresholding algorithm [62] for each of the datasets.

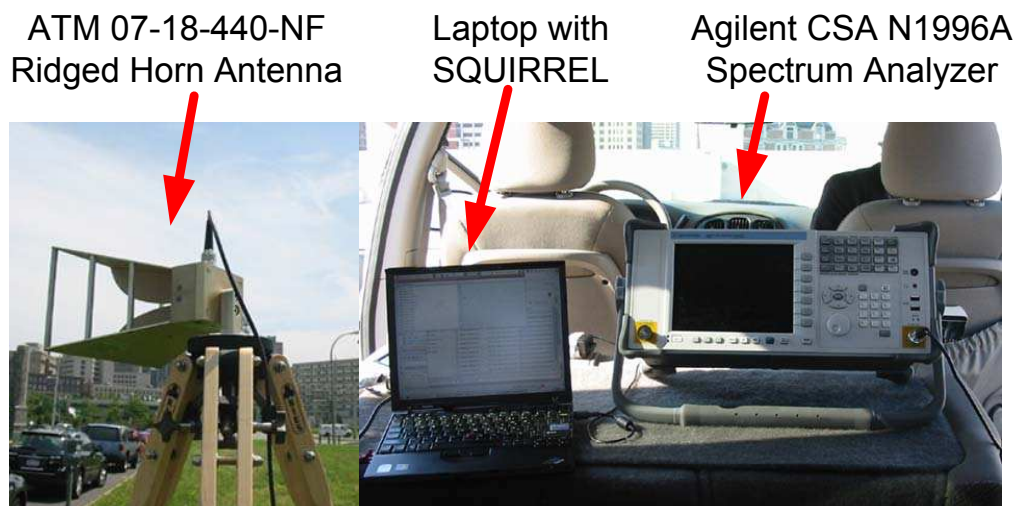


Fig. 3.1 A photograph of the mobile wireless spectrum measurement testbed employed in this research. Components of the testbed include a mini-discone/ridged-horn antenna, a spectrum analyzer and a laptop with SQUIRREL installed.

Otsu's optimum threshold² provides a maximum separation between the two classes of data, namely the signal and the noise.

3.2.2 Spatial, Temporal and Band-wise Variations of Spectrum Usage

As mentioned earlier, we chose five locations which were at least a mile apart from each other, so that we would be able to capture the spatial variation as we go higher in the radio frequency (RF) spectrum. We measured usage activity across approximately 70% of the wireless spectrum from 88 MHz to 2686 MHz. We omitted those bands in which the average usage has been previously reported to be extremely low. Thus, we focused on the remaining bands of interest. Also, in our measurement procedure, we sweep a particular frequency band, for example, Personal Communications Service (PCS) from 1850 MHz to 1990 MHz, completely for a specific number of times and then proceed to the next band instead of scanning a wide frequency range. By performing the sweeps in this manner, our goal was to capture temporal variations over small periods of time. We chose a constant resolution bandwidth of 20 kHz and the number of sweeps recorded per band per site is

²There are alternative approaches for computing the threshold, some of which are explained in [63, 64].

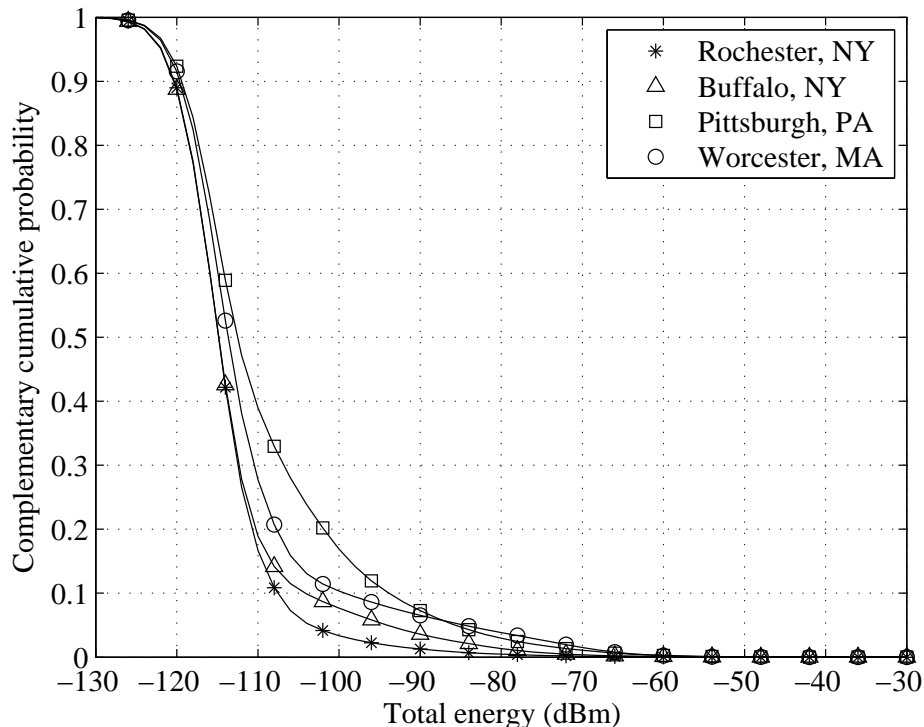


Fig. 3.2 Cumulative distribution functions showing spectrum occupancy for the four cities surveyed.

25. Fig. 3.2 provides a first step summary of all the data points collected across all the frequencies in bins of 20 kHz. This plot which is a complementary cumulative distribution function shows the spectrum occupancy in each of the four cities as a function of energy.

Our measured data is in fact samples of energy spectral density (ESD) across a band of concentration and not time-samples. We cannot apply traditional signal-detection based techniques due to total absence of phase information. Therefore, we detect the presence of the signal in the data purely from the point of view of separating data into two distinct distributions. The optimal threshold calculated using Otsu's algorithm is known to maximize the variance between the two classes of data, namely the signal and the noise classes. Therefore, we employ this algorithm in our analysis.

To apply Otsu's algorithm, a matrix, $\mathbf{M}(t_j, f_i)$ is formed from the collected data points where the row, t_j contains data points over all the frequency locations in the band of interest during one particular time instant and the column, f_i represents the data points

observed in that frequency bin over all time sweeps during the measurement process. The next step is to transform the contents of this matrix into gray scale values by applying the procedure given by:

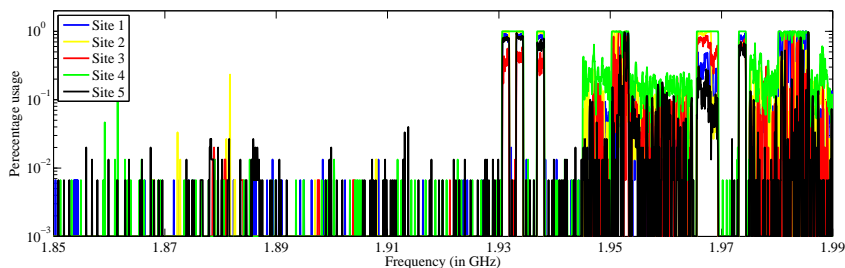
$$\mathbf{I}(t_j, f_i) = \frac{1.0 - 0.0}{\max\{M\} - \min\{M\}} \times (\mathbf{M}(t_j, f_i) - \min\{M\}) \quad (3.1)$$

Applying Otsu's algorithm to the matrix, $\mathbf{I}(t_j, f_i)$ gives the required optimum threshold using which, all the values that are below are classified as noise and the rest as signal.

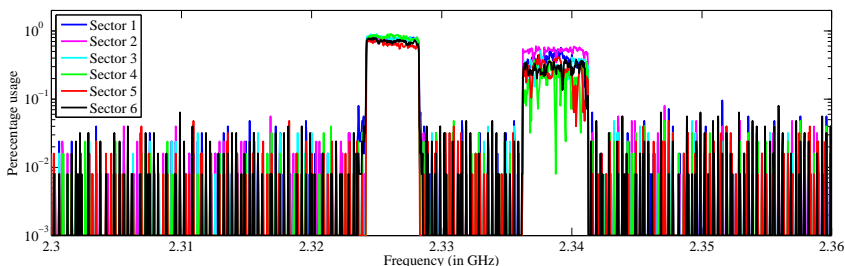
Since the number spectrum licenses issued in a geographical area, say a city, are dependent on several factors like the population density, it is obvious that, the usage varies significantly among different cities. Moreover, the channels that are allocated to a particular wireless service differ greatly between cities and therefore the usage pattern over any specific frequency is not expected to be similar. In contrast, in a mid-size city, the wireless channels that are allocated are more-or-less similar within a certain area and hence the same specific channels are expected to be used across different sites.

However, due to the random nature of the wireless channel, as well as the reduced received power due to the distance from the transmitter, the actual usage would differ widely across different locations within the same city. Furthermore, in the case of a band where the licensed user signals appear on a bursty basis, several allocated bands would only be used intermittently. This is illustrated in Fig. 3.3(a) which shows the percentage occupancy for the city of Rochester in the PCS band. From the figure, it is clear that at Site 4, the occupancy is considerably higher compared to the other sites in the frequency ranging from approximately 1940 MHz to 1990 MHz. Other sites also show a variation in the percentage occupancy.

Another form of spatial variation that depends on the direction in which the receiver antenna is "listening" is shown in Fig. 3.3(b) across the Wireless Communications Service/Digital Audio Radio Satellite Service (WCS/DARS) ranging from 2300 MHz to 2360 MHz. As shown in this figure, there is a considerable amount of variation in the percentage usage across different sectors of our horn antenna. The difference in the usage is as high as 40% between Sector 2 and Sector 4 in a frequency bin near 2340 MHz. Fig. 3.3 has been generated using frequency bins of 40 kHz. Note that in generating this plot, we simply count the number of time sweeps when the signal is observed at a particular channel and divide it with the total number of time sweeps.



(a) Percentage usage of 40 kHz channels across five different locations in the PCS band (1850 MHz to 1990 MHz) in Rochester, NY on 06/19/2008 [61].



(b) Percentage usage of 40 kHz channels across six different sectors in the WCS band (2300 MHz to 2360 MHz) in Rochester, NY on 06/19/2008 [61].

Fig. 3.3 An example showing the spatial variation of spectrum usage.

3.3 Spectrum Measurement Model Employing Linear Mixed Effects³

Although Figs. 3.2, 3.3(a) and 3.3(b) serve the purpose of summarizing the measured results, a great deal of detail remains hidden in the data both with respect to the occupancy characteristics over time, frequency and space as well as their dependence on other influencing factors. One way of analyzing the occupancy results is presented in [61] where, we have provided occupancy values in percentages across different channels, along different angles of arrival and over several time sweeps as observed during the measurement duration. Another way of performing the analysis is from the point of associating the measured data with certain *predictor variables* in a *linear mixed effects* model as we explain below.

³The work included in this section has been funded by the National Science Foundation via grant CNS-0754315 and published in the *EURASIP Journal on Wireless Communications and Networking* [2]

3.3.1 Mathematical Formulation

Due to the differences in the signal modulation involved as well as the differences in the bandwidths utilized by each channel, energy spectral densities corresponding to signals transmitted for different wireless services can be expected to be different. Thus, the four different wireless services analyzed namely paging, TV, WCS and PCS correspond to four different predictor variables. Similarly, the four US cities are also predictor variables. Assuming that the spectrum usage is dependant on two other factors namely, the time of the day and day of the week, those are incorporated as well. Due to the fact that our data corresponds to only four mid-size US cities, we do not claim that our model is a representative of all the mid-size US cities. This is the reason why although our model is not as general as we would like it to be, due to practical constraints involved, we nevertheless believe that it is indicative of the general trends in spectrum occupancy characteristics that can be expected in any typical US city. Moreover, we considered the population densities associated with the measurement sites as our random effects term to reflect this fact. In the following sections, we provide more details regarding the occupancy values by grouping the appropriate collected data points as functions of several predictor variables.

3.3.2 Regression Fit for Percentage Spectrum Occupancy

The model for the performed analysis on the spectrum occupancy percentage using a linear mixed model is as follows:

$$\begin{aligned} \text{Occ.Perc}_{ij} = & \beta_0 + \beta_1 \text{TV}_{ij} + \beta_2 \text{PCS}_{ij} + \beta_3 \text{WCS}_{ij} \\ & + \beta_4 \text{roch}_{ij} + \beta_5 \text{buff}_{ij} + \beta_6 \text{pitt}_{ij} + \beta_7 \text{AN}_{ij} \\ & + \beta_8 \text{weekend}_{ij} + b_{i0} + b_{i1} \text{PD}_{ij} + \varepsilon_{ij}. \end{aligned} \quad (3.2)$$

As seen from the above model, we have selected three indicator variables (*i.e.*, either 1 or 0) for the types of the wireless service (TV, PCS, WCS), three indicator variables for the cities (Rochester, Buffalo, Pittsburgh), one indicator variable for afternoon/before noon, and one indicator variable for weekend/weekday. The intercept represents the spectrum occupancy in the paging band for Worcester, Massachusetts. As mentioned previously, the response variable in the regression analysis that we considered is the percentage spectrum occupancy which is calculated after applying Otsu's thresholding algorithm. Also, notice

that the population density of the sites is chosen as the random effects term which is specific to each one out of 20 groups (4 cities \times 5 sites). Since, we collected 25 wireless spectrum sweeps in each of the 5 sites from each city, the population density is chosen as the random effect that is different among the sites. Moreover, the population density is rounded off to the next highest multiple of 100. Thus, discrete values are considered which helps in the interpretation of the obtained results. Fitting the linear mixed model gives the following results in Table 3.2. The parameters associated with the random effects are as follows: standard deviation of the intercept = 2.14, standard deviation of the population density = 0.12 and the correlation coefficient of the population density = 0.007.

From the above random effects, the covariance matrix of the random effects [65] can be calculated as follows:

$$\begin{aligned}\sigma^2\mathbf{D} &= \begin{bmatrix} 2.14^2 & 2.14 \times 0.12 \times 0.007 \\ 2.14 \times 0.12 \times 0.007 & 0.12^2 \end{bmatrix} \\ &= \begin{bmatrix} 4.58 & 1.8e-3 \\ 1.8e-3 & 0.0144 \end{bmatrix}.\end{aligned}\tag{3.3}$$

Interpretation of the Obtained Regression Fit From Table 3.2 ⁴, we see that the percentage spectrum occupancy for Worcester in the paging band is 13.28% with a p-value of < 0.0001 . With all other regressors remaining constant, the percentage spectrum occupancy for the city of Rochester in the paging band increases to 14.65% *i.e.*, it is 1.37% higher than that of the city of Worcester with the associated p-value being 7×10^{-4} . Similarly, with the city under consideration, the type of the wireless service and the time of the day remaining constant, the spectrum occupancy decreases by 1.12% on the weekends for a p-value of < 0.0001 . Notice that, we have obtained all of the above coefficients at very low p-values indicating the statistical significance of each of the regressors. Also, the structure of the \mathbf{D} matrix which is almost diagonal suggests that the assumed normality assumption on the random-effects is valid. The plot of the standardized residuals shown in Fig. 3.4(a) also supports this assumption on the residuals since approximately 95% of the residuals lie in the range $[-1.96, 1.96]$, *i.e.*, they follow a standard normal distribution very closely.

⁴In Tables 3.2 and 3.3, DF is short for degrees of freedom

Table 3.2 Fixed Effects for eq. (3.2) [2].

	Coefficient	Std. Error	DF	t-value	p-value
(Intercept)	13.28	0.244	473	54.354	< 0.0001
TV	5.82	0.317	473	18.36	< 0.0001
PCS	4.33	0.225	473	19.23	< 0.0001
WCS	4.08	0.202	473	20.11	< 0.0001
Roch	1.37	0.423	473	3.23	7e-4
Buff	4.98	0.273	473	18.21	< 0.0001
Pitt	3.67	0.356	473	10.29	< 0.0001
AN	0.5	0.159	473	3.15	9e-4
weekend	-1.12	0.116	473	-9.68	< 0.0001

3.3.3 Regression Fit for Activity Period

The model for the performed analysis on the ON time duration of the licensed signal transmissions in the four bands considered is similar to that of the spectrum occupancy percentage. Thus, it follows that:

$$\begin{aligned}
 \text{ON.time}_{ij} = & \beta_0 + \beta_1 \text{TV}_{ij} + \beta_2 \text{PCS}_{ij} + \beta_3 \text{WCS}_{ij} \\
 & + \beta_4 \text{roch}_{ij} + \beta_5 \text{buff}_{ij} + \beta_6 \text{pitt}_{ij} + \beta_7 \text{AN}_{ij} \\
 & + \beta_8 \text{weekend}_{ij} + b_{i0} + b_{i1} \text{PD}_{ij} + \varepsilon_{ij}.
 \end{aligned} \tag{3.4}$$

In this case, the response variable in the regression analysis performed is the ON time duration which is calculated after applying Otsu's thresholding algorithm. We calculated the amount of time during which the licensed signal transmission was consistently above the calculated threshold. The regressor variables are the same. Fitting the linear mixed model gives the following results presented in Table 3.3. The parameters associated with the random effects are as follows: standard deviation of the intercept = 1.58, standard deviation of the population density = 0.34 and the correlation coefficient of the population density = 0.005.

From the above random effects, the covariance matrix of the random effects can be

Table 3.3 Fixed Effects for eq. (3.4) [2].

	Coefficient	Std. Error	DF	t-value	p-value
(Intercept)	2.33	0.12	473	19.44	< 0.0001
TV	2.21	0.132	473	16.73	< 0.0001
PCS	1.02	0.056	473	18.23	< 0.0001
WCS	1.24	0.24	473	5.16	< 0.0001
Roch	2.12	0.474	473	4.47	< 0.0001
Buff	3.26	0.778	473	4.19	< 0.0001
Pitt	2.74	0.769	473	3.56	2e-4
AN	2.03	0.76	473	2.67	< 0.0001
weekend	-1.87	0.227	473	-8.23	< 0.0001

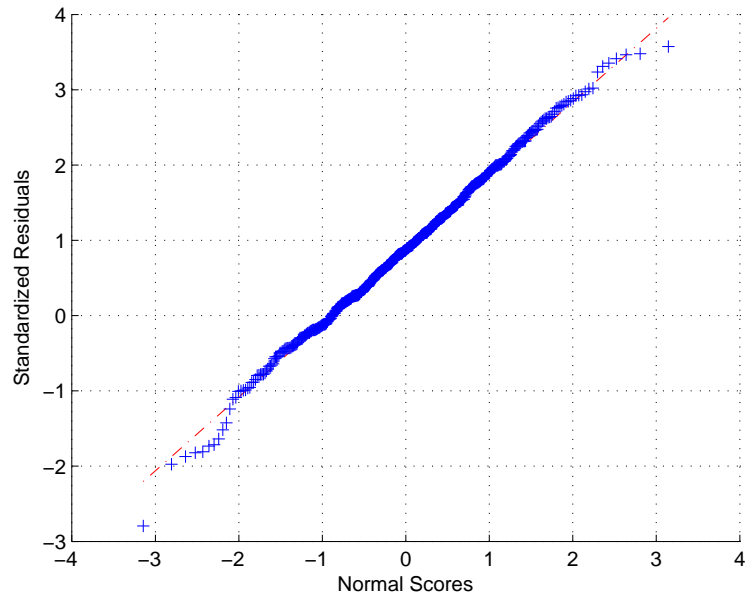
calculated as follows:

$$\begin{aligned} \sigma^2 \mathbf{D} &= \begin{bmatrix} 1.58^2 & 1.58 \times 0.34 \times 0.005 \\ 1.58 \times 0.34 \times 0.005 & 0.34^2 \end{bmatrix} \\ &= \begin{bmatrix} 2.49 & 2.7e-3 \\ 2.7e-3 & 0.1156 \end{bmatrix}. \end{aligned} \quad (3.5)$$

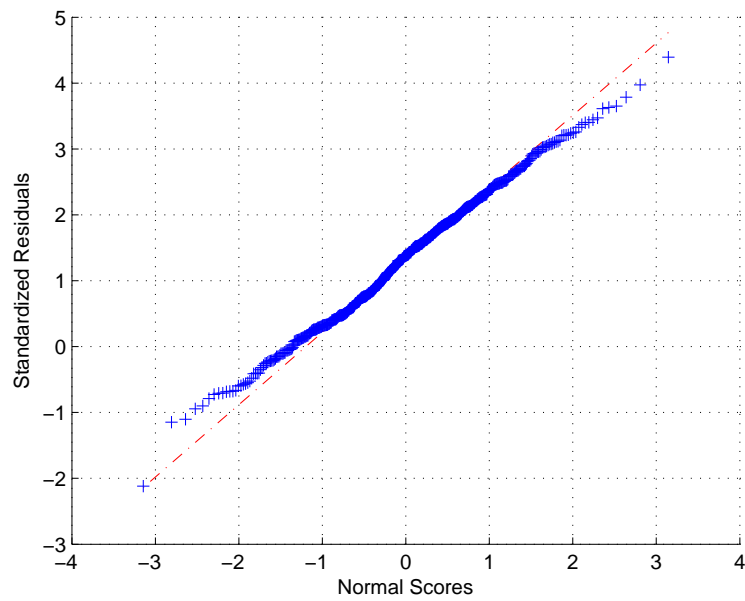
Interpretation of the Obtained Regression Fit From Table 3.3, we see that the ON time duration for the city of Worcester in the PCS band is 3.35s with a p-value of < 0.0001. It is 1.02 higher than that of the paging band. With all other regressors remaining constant, the ON time duration of the licensed signal transmissions for the city of Pittsburgh in the PCS band increases to 6.09s *i.e.*, it is 3.76s higher than that of the city of Worcester with the associated p-value being 2×10^{-4} . Similarly, with the city under consideration, the type of the wireless service and the time of the day remaining constant, the ON time duration decreases by 1.87s on the weekends for a p-value of < 0.0001. Again, we have obtained all of the above coefficients at very low p-values indicating the statistical significance of each of the regressors. Again, the normality assumption on the random-effects is validated by the structure of the \mathbf{D} matrix which is almost diagonal. We also show the quantile-quantile plot of the standardized residuals in Fig. 3.4(b). Even though, towards the lower tail of the distribution, there is a slight deviation from the normal scores, we believe that it is not significant enough to seriously violate the normal distribution assumption.

3.4 Chapter Summary

In this chapter, we utilized the spectrum measurement samples collected in several mid-size U.S. cities and obtained a regression fit for the percentage occupancy and the activity period response variables. Even though practical constraints forced us to describe the collected data samples in a model that is only indicative of the cities that we studied, general observations can be made regarding the spectrum occupancy trends in cities with similar characteristics. The results that we obtained indeed confirm our original hypothesis that considerable spatial, temporal and frequency-wide variations exist in the occupancy characteristics.



(a) Quantile-quantile plot for the fit shown in Eq. (3.2)



(b) Quantile-quantile plot for the fit shown in Eq. (3.4)

Fig. 3.4 Quantile-quantile plots for the proposed linear mixed-effects models [2].

Chapter 4

Characterization of Wireless Spectrum in Vehicular Environments

4.1 Introduction¹

Although opening up of the TV spectrum for secondary access presents an exciting opportunity for efficiently utilizing a valuable national resource, several key technological and legislative considerations need to be addressed to make DSA a success. The most critical of these is the potential interference analysis as experienced by the primary license holders i.e., broadcast television viewers from unlicensed users. A straight-forward strategy for the white space devices (WSDs) is to employ a “listen before talk” approach wherein each secondary device would utilize spectrum sensing techniques [60, 66] for detection of signals from the nearby TV stations, or auxiliary broadcasting services such as wireless microphones and other authorized transmitters followed by a detection methodology to determine which TV channels are occupied and which are vacant. Then, via a combination of distributed coordination [58], and transmission channel selection [59], certain channels are deemed to be vacant and are utilized by the WSD in compliance with the regulatory requirements on transmissions in those channels.

The sensing-only techniques available in the existing literature can be classified into four categories namely, energy detection, matched filtering, cyclostationary detection and wavelet detection [67]. By applying these techniques, the WSDs must determine if a licensed

¹The work included in this chapter has been funded by the Toyota InfoTechnology Center, USA and published at the *IEEE Vehicular Networking Conference* [3]

user's signal is over a certain threshold, for example, -116 dBm for DTV signal detection as proposed by IEEE 802.22 [68]. However, there are certain advantages of using geo-location based techniques over sensing-only approaches which are listed in the following paragraphs. Reference [69] provides additional details on the implementation of spectrum-sensing techniques based on utilizing the geo-location databases. Specifically, considerations about geo-location database resolution, implementation costs involved in building geo-location databases, location uncertainty issues for highly mobile WSDs (which is critical for vehicular DSA), periodical updates of the database after the secondary device is deployed etc. Reference [70] provides an overview of the spectrum sensing techniques at MAC and PHY layers that are part of the IEEE 802.22 draft standard as of Aug. 2007. Of particular relevance to our study are the standard PHY layer sensing techniques such as the comparison of the measured squared FFT values with a threshold for pilot-energy sensing and the comparison of the number of times a particular location is chosen as the maximum against a threshold for the pilot-location sensing. For instance, in order to determine the presence of the licensed user, either the number of times during which the squared FFT value goes above threshold is counted and compared with a certain number or the average of all the sensing windows is compared against a threshold. Reference [71] provides information on the deployment of fixed solutions for rural broadband connectivity in the United States. The approach proposed is the now standard combination of geo-location information pertaining to the location of TV stations and spectrum sensing of the environment to identify white spaces combined with Motorola's Adaptive Radio Technology.

In this chapter, we apply the constraints imposed by the FCC on the protection of TV broadcast services from secondary transmissions and present the obtained allowed transmit power values on the secondary devices operating along several locations on I-90 in the state of Massachusetts. Specifically, we apply a geo-location database approach to show the variations as a vehicle moves along I-90 and provide a discussion from the point of view of the total number of channels available, the number of non-contiguous blocks and the implications on the design of the transceiver that utilizes channels in such a non-contiguous scenario.

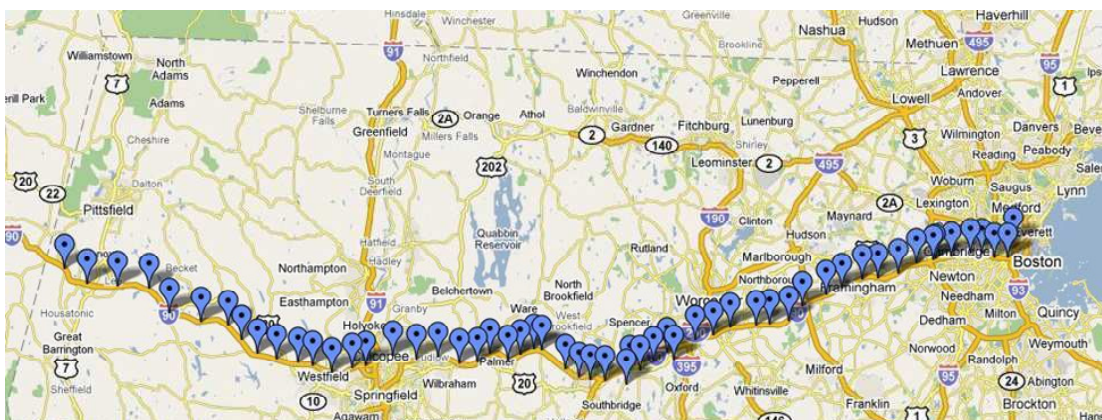


Fig. 4.1 A map of the forty eight locations close to I-90 between Boston, MA and West Stockbridge, MA over which spectrum measurements were collected on 06/07/2009, 06/11/2009 and 06/12/2009.

4.2 Measurement Campaign

We conducted the first phase of the spectrum measurement campaign on 06/07/2009 and 06/11/2009 across 48 locations between Boston, MA and West Stockbridge, MA. The second phase which consisted of collecting spectrum measurements in a vehicle traveling at approximately 60 miles/hr. between the same locations was done on 06/30/2009. We selected a frequency resolution of 20 kHz and collected 10 sweeps per site. Since the goal of the project is to characterize DTV spectrum over several locations on I-90 in the state of Massachusetts, most sites were chosen to be within half mile from I-90 for the purpose of avoiding interference to the ongoing traffic. The locations were also selected such that they were spaced approximately 2 miles apart. The map of the measurement sites is shown in Fig. 4.1. The measurement setup used to collect spectrum measurements in the TV band is shown in Fig. 4.2. The mini-disccone antenna is fixed to a bike-rack mounted on the trunk of a car in order to make the entire setup portable.

In Fig. 4.3, we show the data points collected on 07/30/2009 where the measurement setup was mounted on a moving vehicle travelling on I-90 at an average velocity of 60 miles/hr. Essentially, Fig. 4.3 shows the energy spectral density plot for the TV bands in the higher frequency range which is the region primarily identified as the suitable for dynamic spectrum access. In this figure the x-axis represents the frequencies swept during our study and the y-axis represents the sweep index. We reduced the frequency range swept in order to obtain finer time resolution. That is instead of the entire UHF TV range, we

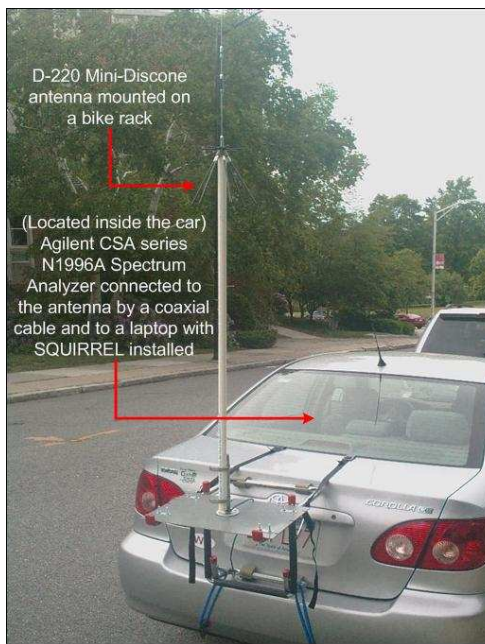


Fig. 4.2 A photograph of the mobile wireless spectrum measurement testbed employed in this research. Components of the testbed include a mini-discone/ridged-horn antenna, a spectrum analyzer and a laptop with SQUIRREL installed.

selected 600 - 750 MHz and captured 4 sweeps per minute on average along the length of I-90. The sweep index increases from 1 on the top left corner of each figure and indicates our drive as we travel along I-90 in the state of MA from west to east. The western most point in our study was West Stockbridge, MA and the eastern most point was Boston, MA. The intensity of each pixel indicates the energy level observed during the study. From this figure, a clear indication of the variation in the energy levels across any particular channel is evident. The total absence of any signal towards the end of our drive (around sweep index 520-530) was during the time when moving vehicle was in the Big Dig of Boston metropolitan area. An interesting thing to note is that, as we go farther away from Boston towards Palmer (which corresponds to a sweep index of around 220), the energy values decrease in general. However, going from Palmer towards West Stockbridge (which corresponds to a sweep index of around 120), the energy values show an increasing trend indicating that we were approaching a nearby TV transmitter. Another observation from this figure is that there are several locations close to Boston, MA where we observed strong signals of the order of -60 dBm indicating that our measurement sites were close to TV

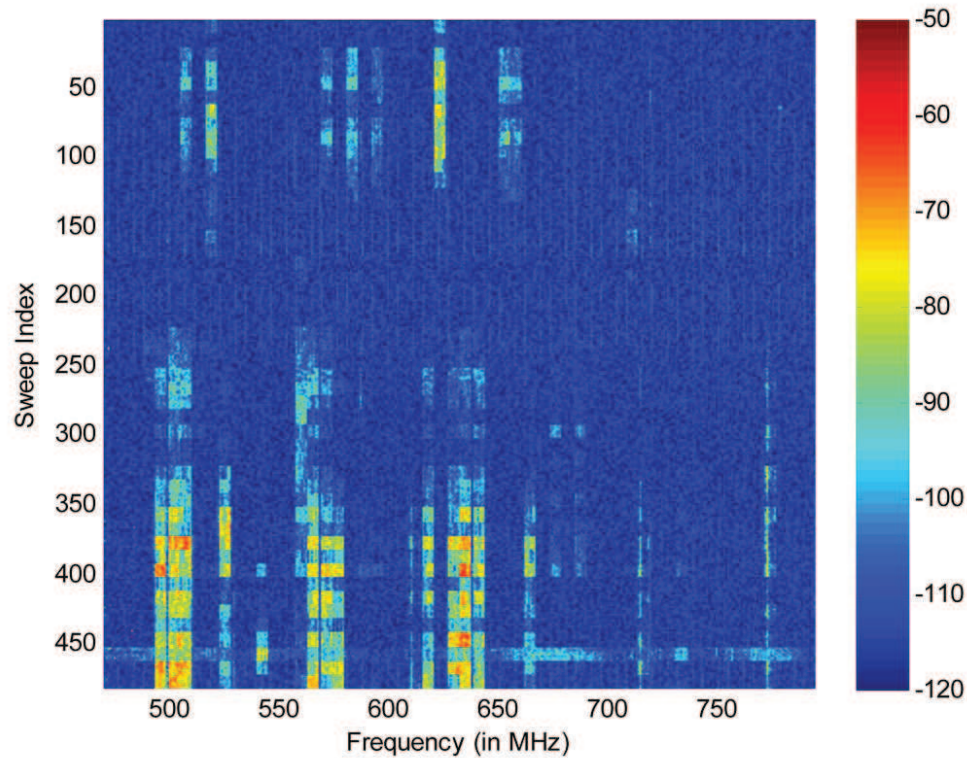


Fig. 4.3 Spectrogram plot for the TV frequencies in the frequency range, 600 - 750 MHz over 550 time sweeps on I-90 between Boston, MA and West Stockbridge, MA. The measurement setup was located in a vehicle moving at an average velocity of 60 miles/hr.

transmitters.

As an illustration of the wireless spectrum environment encountered by a WSD in motion, consider Fig. 4.4. Referring to this figure, we observe that at various locations along a highway the spectral occupancy behavior changes. Nevertheless, this change in spectral occupancy is gradual enough to allow for the vehicular wireless devices to spectrally sense the frequency locations of the TV broadcasts and take the appropriate actions, such as dynamically change the transmission band in order to avoid interference with the TV signals. Furthermore, given the predictable, well-defined transmission characteristics of TV broadcasts, by studying TV spectral occupancy measurements across several locations along a transportation route, it is possible characterize the behavior of this frequency band,

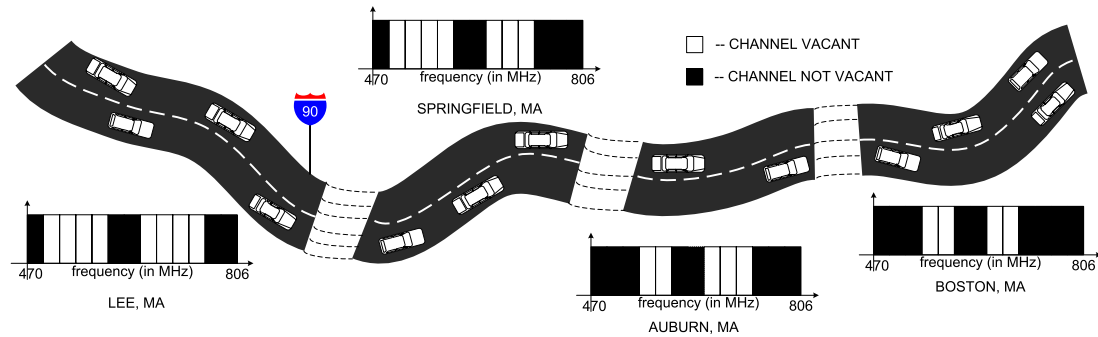


Fig. 4.4 A map of the forty eight locations close to I-90 between Boston, MA and West Stockbridge, MA over which spectrum measurements were collected on 06/07/2009, 06/11/2009 and 06/12/2009.

thus allowing for VDSA communications that do not interfere with the incumbent TV broadcasts. An important point to note here is that the availability of vacant channels will most likely be non-contiguous with widely differing allowed transmit power constraints on the WSD across different channels. The implications of this observation will be highlighted in the following section.

4.3 Geo-Location Database Approach for Determining Vacant Channels

In a “Notice of Proposed Rule Making” [72], the FCC has also suggested that the WSD’s sensing approach could potentially be improved with geo-location information of the incumbents in addition to their own, which is determined by a variety of means such as GPS, distributed sensing and/or beacon identification techniques. Several factors have been identified in [72] that must be taken into consideration in establishing an optimum detection threshold. The considerations are as follows:

1. protecting the rights of the TV receiver which is attempting to receive a weak signal in the presence of a strong signal from a WSD, both of which are geographically close but relatively far from the TV transmitter is addressed through the first consideration.
2. the appropriate spectrum utilization in the spatial dimension, in the presence of false-positives and false-negatives.

Table 4.1 Protected Service Contour Levels for TV Channels

Type of Station	Protected Contour		
	Channel	Contour (dBu)	Propagation Curve
Analog TV	Low VHF (2-6)	47	F(50,50)
	High VHF (7-13)	56	F(50,50)
	UHF (14-69)	64	F(50,50)
Analog Class A, LPTV, translator and booster	Low VHF (2-6)	62	F(50,50)
	High VHF (7-13)	68	F(50,50)
	UHF (14-69)	74	F(50,50)
Digital TV	Low VHF (2-6)	28	F(50,90)
	High VHF (7-13)	36	F(50,90)
	UHF (14-51)	41	F(50,90)
Digital Class A	Low VHF (2-6)	43	F(50,90)
	High VHF (7-13)	48	F(50,90)
	UHF (14-51)	51	F(50,90)

- the question of failure to detect an occupied channel due to the presence of an obstruction between the WSD and the incumbent receiver. Most importantly, the impact of collaborative spectrum sensing in preventing false-negatives, thereby protecting the rights of the incumbent user.

There are primarily, four types of licensed incumbents present in the TV bands in the U.S. today. Currently, both full power analog and digital stations, as well as low power analog and digital stations operate in the TV bands. The full power analog broadcast stations are off the air since the total digital switchover that was performed on June 12, 2009 by FCC order, though numerous low power analog TV (LPTV) stations are expected to remain in service after that date, and will be entitled to protection. Detailed information about U.S. TV band allocations can be found in the FCC's Consolidated DataBase System (CDBS), which can be accessed via the FCC TV Query website [73]. Each type of licensed incumbent system listed above has a service contour determined by the electric-field levels summarized in Table I. Reference [72] also describes common interference protection ratios that are typically specified in terms of desired-to-undesired (D/U) signal levels. These

Table 4.2 Required Interference Protection Ratios for TV Channels

Type of Station	Protected Contour		
	Channel Separation	D/U ratio (dB)	Propagation Curve
Analog TV, Class A, LPTV, translator and booster	Co-channel	34	F(50,10)
	Upper adjacent	-17	F(50,50)
	Lower adjacent	-14	F(50,50)
Digital TV and class A	Co-channel	23	F(50,10)
	Upper adjacent	-26	F(50,50)
	Lower adjacent	-28	F(50,50)

ratios take into account the effects of full power TV transmitter splatter (or Out of Band Emissions, OOBE). Table II summarizes these specifications.

Utilizing geo-location based information i.e., the directives issued by the FCC as summarized above and combining it with spectrum measurement data in order to sense the presence of incumbents has several advantages over a sensing-only approach. Some of them are as follows:

- In a sensing-only approach, since no information is made available about the protected service contours of the nearby TV transmitters, WSDs must sense incumbent signals down to very low levels (e.g., -116 dBm for DTV signal detection as proposed by IEEE 802.22 [68]) in order to combat hidden-node effects and other localized sensing phenomena. Due to such a low threshold which is uniformly applied across all geographic locations irrespective of the protected service contour considerations, large areas are potentially unused leading to inefficient spectrum utilization.
- Moreover, even though certain types of TV transmissions employ the same modulation, the constraints based on which the protected contours are determined differ greatly. In such a scenario, sensing-only WSDs cannot differentiate between low-power DTV signals and full-power DTV signals, as they both employ ATSC modulation. Therefore, a WSD will be forced to protect low-power DTV stations assuming the same constraints as that of its full-power variant.

In the following paragraphs, the algorithm for calculating the transmit power constraints on a WSD based on the keep-out region around a DTV transmitter for a given effective radiated power (ERP) and a fixed height above average terrain (HAAT) is explained. Each TV transmitter has a protected contour region around it over which the FCC stipulates that the required performance criteria on the signal strength are met. For instance, the FCC specifies the use of F(50,90) curves in order to identify the protected contour region where F(50,90) indicates that the field strength will exceed the value specified by the curves at 50% of the locations for 90% of the time. The desired field strength on the edge of the protected contour for different transmitter types is given in Table I. Similarly, the keep-out region is the area around the protected contour wherein the presence of a secondary transmitter with a given ERP would interfere with the DTV receivers on the edge of the protected contour. That is, a secondary transmitter with a given ERP has to be located outside of the keep-out region. With this knowledge combined with the desired-to-undesired signal levels given in Table II, the steps involved in calculating the transmit power constraints on a WSD based on the keep-out region around a TV transmitter are as follows:

Step 1 Create a look-up table of the TV transmitters in the area of interest and identify the protected contours based on [74]. Notice that the the minimum required parameters are the ERP of the TV transmitter, its HAAT, its location in GPS coordinates and the type of transmission *i.e.*, analog/digital and full-power/low-power. In our analysis, we created a look-up table consisting of 47 TV transmitters in the state of Massachusetts (MA) plus 5 from the state of Connecticut (CT), 2 from the state of New York (NY), and 1 from the state of Rhode Island (RI) which were considered to have a significant impact on the coverage of I-90 in the state of MA².

Step 2 For $i = 1$ through *Number of Transmitters*, repeat steps 3 to 6.

Step 3 For $j = 1$ through *Number of Measurement Sites*, repeat steps 4 and 6.

Step 4 Geo-locate the desired point of interest and calculate its distance from the TV transmitter under study. This can be done by using the polar-coordinate flat-earth formula

$$D(i, j) = R\sqrt{\theta_i^2 + \theta_j^2 - 2\theta_1\theta_2 \cos(\Delta\lambda)} \quad (4.1)$$

²Due to space constraints, the list consisting of these 55 TV transmitters has not been included in this dissertation.

where, $D(i, j)$ is the distance between i^{th} TV transmitter and j^{th} measurement site, R , Radius of the earth = 6371 km, $\theta_i = \frac{\pi}{180}(90 - latitude_i)$, $\theta_j = \frac{\pi}{180}(90 - latitude_j)$ and $\Delta\lambda = \frac{\pi}{180}(longitude_i - longitude_j)$.

Step 5 If $D(i, j)$ is less than *Protected Contour* of *Transmitter, i*, then the channel number corresponding to *Transmitter, i* is unavailable at *Measurement Site, j* and the allowed WSD transmit power corresponding to *Measurement Site, j* and *Transmitter, i* is zero.

Step 6 Else, the channel number corresponding to *Transmitter, i* is available at *Measurement Site, j*. That is, if the distance is lesser than the protected contour radius, the channel is unavailable at this geographical location, so, continue to the next transmitter geo-location. If the above check succeeds, the channel over which the TV transmitter under study operates is available in that particular location and proceed further. Fig. 4.5 shows the results at the end of this step for all of our measurement sites. However, this result does not yet provide any information on the power constraints imposed on a WSD when using a particular channel

Step 7 For $j = 1$ through *Number of Measurement Sites*, repeat steps 8 and 11.

Step 8 Delete duplicate entries of available channel information for each of the TV transmitters which use the same channel (but, are geographically separated by sufficient distance). Make sure that the transmitter which is closest (and hence requires smaller ERP values in order to conform to the FCC guidelines) is noted and create a reduced set of available channels.

Step 9 For $k = 1$ through the *Number of Available Channels from the reduced set at Measurement Site, j*, repeat steps 10 and 11.

Step 10 If the current channel is a co-channel to the nearest incumbent transmitter, calculate the allowed WSD transmit power corresponding to *Measurement Site, j* and *Transmitter, k* from [74]. That is, for a fixed value of HAAT, use F(50,10) curves [74] to identify the ERP on the secondary transmitter that interferes with the incumbent receivers on the edge of the protected contour at 50% of the locations for 10% of the time. This value is the allowed ERP on a secondary transmitter without violating the FCC's directives on using DTV spectrum on a secondary basis. Notice that,

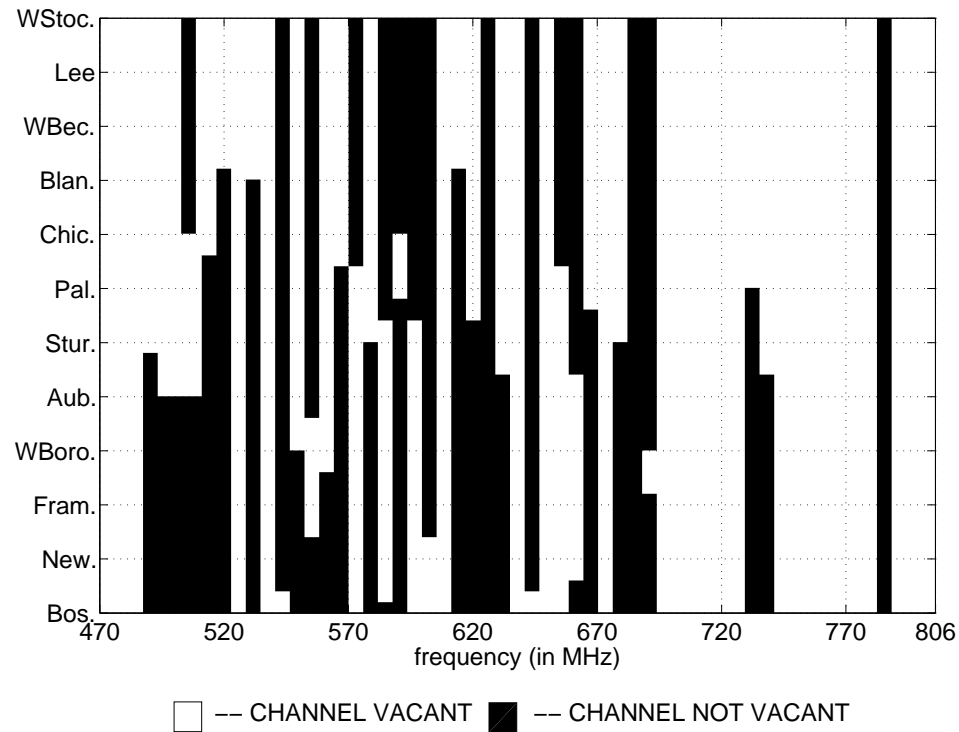


Fig. 4.5 TV Channel availability at different locations along I-90 in the state of Massachusetts, USA [3].

the $D(k, j)$, *i.e.*, the distance between k^{th} TV transmitter and j^{th} measurement site is used in doing this calculation.

Step 11 If the current channel is an adjacent channel to the nearest incumbent transmitter, calculate the allowed WSD transmit power corresponding to *Measurement Site, j* and *Transmitter, k* from [74] using the above procedure but use the *DU* ratios from Table II.

The above algorithm has been implemented for all the locations at which we visited near I-90 in the state of MA. A snapshot of the available channels across all the measurement locations is shown in Fig. 4.5³ as previously mentioned. The white spaces in this figure indicates the vacant portions of the TV spectrum. As evident from this figure and as

³In fig.s 4.5 and 4.6, the abbreviations on the y-axis are as follows: WStoc. - West Stockbridge, Lee - Lee, WBec. - West Becket, Blan. - Blandford, Chic. - Chicopee, Pal. - Palmer, Stur. - Sturbridge, Aub. - Auburn, WBoro. - Westborough, Fram. - Framingham, New. - Newton, Bos. - Boston.

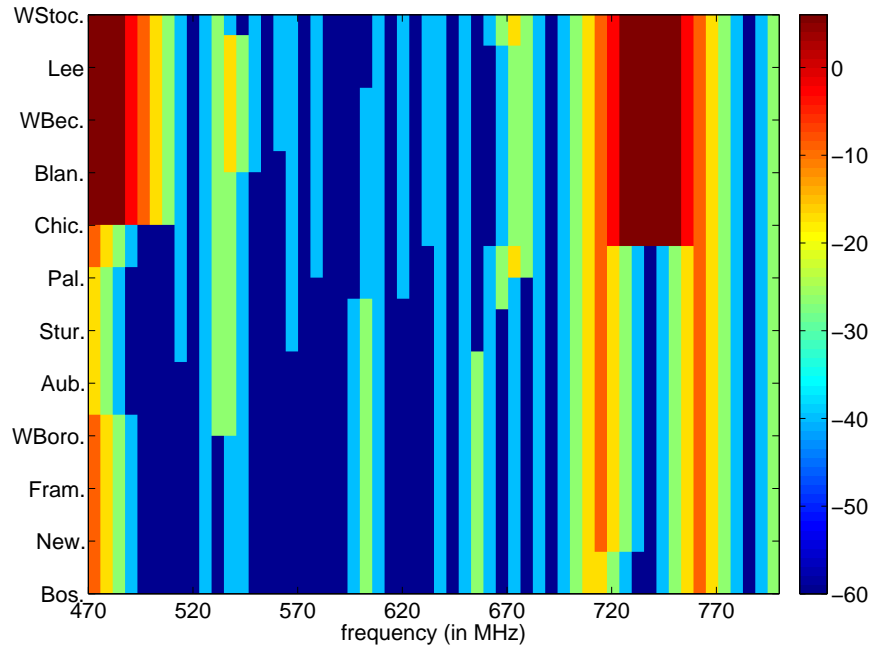


Fig. 4.6 WSD power constraints on the available TV channels at different locations along I-90 in the state of Massachusetts, USA [3].

previously noted from Fig. 4.3, the number of vacant channels in the western part of MA are more in number compared to the eastern part. Fig. 4.6 shows a map of the allowed power levels on the WSD transmitter for the state of MA. As seen from this figure, the channels that are vacant as shown in Fig. 4.5 are assigned power values based on the proximity to the neighboring licensed TV channels. The maximum allowed power of 4 W [68] is assigned only when there are a sufficiently wide range of vacant channels. For example, around the cities of West Stockbridge, MA to Chicopee, MA, the frequency range of (720-770) MHz is completely free of licensed user transmissions and hence the WSDs are allowed to use the maximum allowed transmit power. Figs 4.7 and 4.8 which are derived from Fig. 4.5 further highlight the non-contiguous nature of the channel availability in the UHF TV band. For example, in Framingham, MA, even though the total bandwidth available for secondary usage is around 100 MHz, there are 11 non-contiguous blocks of vacant spectrum of which a maximum of 24 MHz is available as one contiguous block.

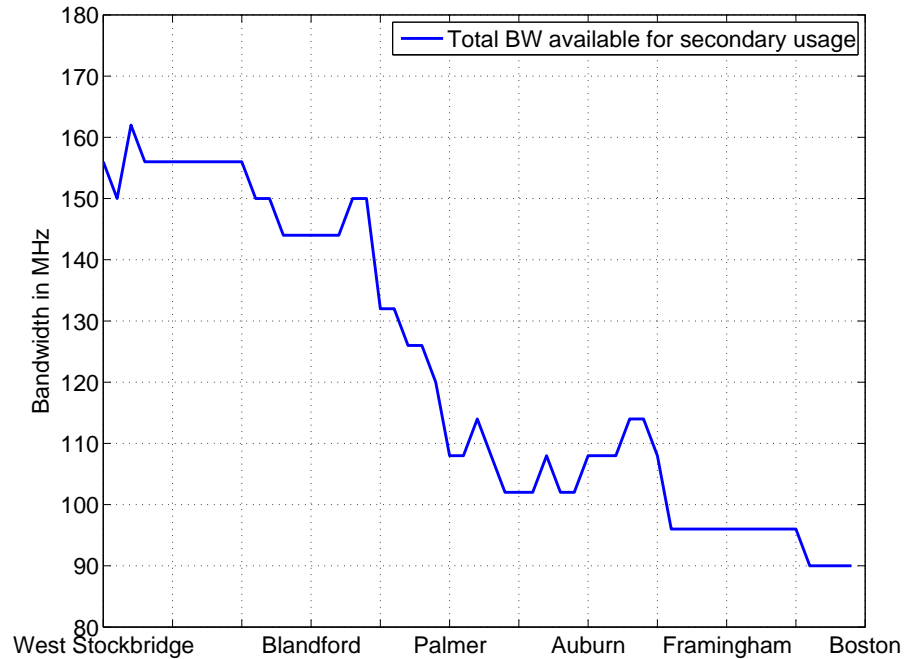


Fig. 4.7 The total available bandwidth for secondary usage at different locations along I-90 in the state of Massachusetts, USA [3].

4.4 Implications for Transceiver Design

Based on the results obtained from Figs 4.5, 4.6 4.7 and 4.8, we see that, as a WSD moves along I-90 in MA, non-contiguous channel bonding needs to be performed by the cognitive transceivers. This necessitates several important design requirements on the WSD to efficiently utilize the available vacant wireless spectrum. Some of them are as follows.

- An important requirement on the WSD transmitter, particularly for the non-contiguous case, is the means of communicating the channels used for data transmission. Since, potentially several non-contiguous channels could be used, the WSD-based MAC has to be tailored to accommodate the varying number and location of available TV channels.
- With this knowledge assumed to be available, the next challenge is for the WSD receiver to tune into these channels and perform frequency/timing synchronization. Hardware reconfigurability is crucial to enable this feature.

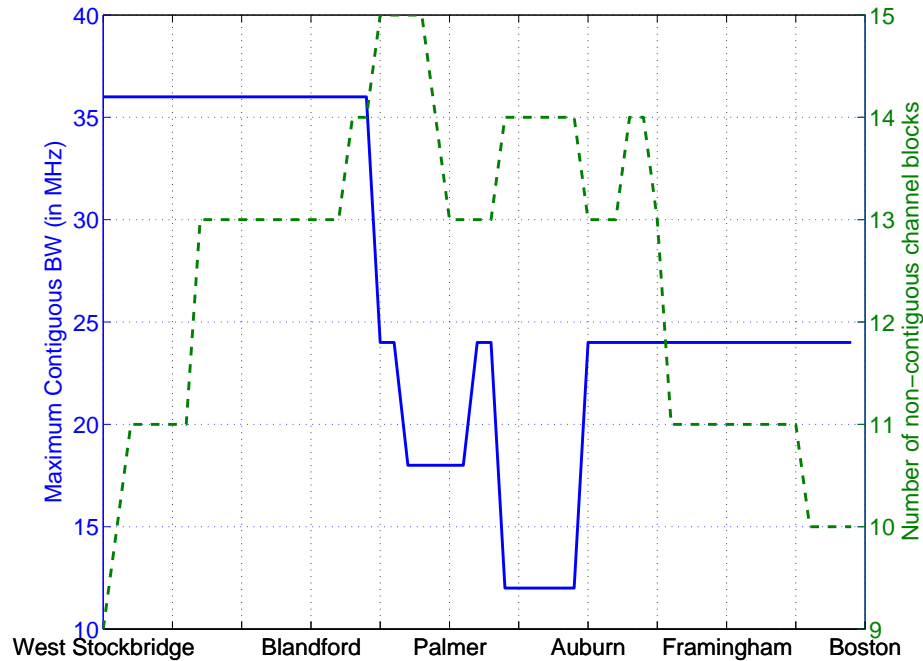


Fig. 4.8 Maximum contiguous bandwidth and the number of non-contiguous channel blocks at different locations along I-90 in the state of Massachusetts, USA [3].

- Also note that the number of FFT operations in case of an OFDM-based transceiver is a varying quantity with several frequencies pruned in order to meet the interference-avoidance criteria set to protect the incumbent transmissions.
- Another important constraint imposed due to the varying nature of allowed power levels in different bands is the need to identify which channels meet the QoS requirements. This requires elaborate channel sensing across several non-contiguous channels.

4.5 Chapter Summary

In this chapter, we studied an alternative approach to spectrum characterization which is based on the examination of the coverage areas around a DTV transmitter that affect a particular geographic region. This approach directly follows the directives of the FCC

that a sensing-only approach may not benefit from known information on the presence of licensed transmitters. As a result of the geo-location database approach, we have seen that as a function of distance on I-90, the available bandwidth for secondary usage increases as a mobile unit travels from Eastern MA to Western MA.

Chapter 5

Non-contiguous Multicarrier Communications in DSA Systems

5.1 Introduction¹

Dynamic spectrum access (DSA) is a wireless access approach designed to enhance spectrum utilization efficiency, where unlicensed (i.e., *secondary*) wireless users are permitted to temporarily “borrow” unoccupied spectral bandwidth from licensed (i.e., *primary*) frequency bands [72]. At the same time, the secondary wireless users must ensure that the rights of the incumbent primary wireless transmissions are respected, especially with respect to mitigating any potential interference effects towards the primary users [75]. As a result, there has been extensive research into devising communication systems and networks that can facilitate this form of wireless access, especially with respect to the concept of *cognitive radio* [76].

Although the process of accessing unoccupied frequency spectrum by secondary wireless devices is a viable concept, one of the primary challenges with this wireless access approach is finding a contiguous unoccupied frequency band that is capable of accommodating a secondary wireless transmission. Despite the fact that the aggregate bandwidth of the unoccupied spectrum might be sufficient for accommodating many of the secondary wireless transmissions, it is possible that this unoccupied spectrum can be fragmented, with

¹The work included in this chapter has been funded by the National Science Foundation via grant CNS-0754315 and published in the IET Radar, Sonar and Navigation Journal [5] and the IEEE Communications Magazine [4]

the individual frequency bands not being large enough to support most of the secondary users. Consequently, it is necessary for secondary wireless transceivers to require a degree of *spectral agility* in order to operate in the presence of primary signals, especially across several unoccupied but fragmented frequency bands whose aggregate bandwidth satisfies the secondary transmission requirements. Moreover, the characteristics of the energy spectral densities (ESD) corresponding to signals transmitted over different licensed frequency bands are different, which in turn are dependent on the particular signal processing operations performed before transmitting the signal. As a result, different licensed frequency bands have different requirements related to secondary signal transmissions such as the allowed spectral masks, the stipulated receiver operating characteristics (ROC) of the secondary user, the required time duration (and hence the number of samples that need to be processed) before making a decision on the availability of a specific channel etc. In this paper, we focus only on a subset of channels that correspond to the paging band in the United States.

Several researchers have proposed a spectrally agile data transmission technique based on *multicarrier modulation* capable of deactivating subcarriers located within the frequency vicinity of primary wireless transmissions [66, 77]. This technique, referred to as *non-contiguous multicarrier modulation*, possesses the ability to efficiently use fragmented spectrum opportunities in conjunction with spectrum shaping in order to suppress interference that may affect nearby primary wireless transmissions. In this paper, we present a performance analysis of two approaches for enabling non-contiguous multicarrier modulation with respect to interference mitigation and computational complexity. One of the approaches is a variant of *orthogonal frequency division multiplexing* (OFDM), called *non-contiguous OFDM* (NC-OFDM), while the other approach is based the non-contiguous version of the filter bank approach *non-orthogonal frequency division multiplexing* (NOFDM), referred to as *non-contiguous NOFDM* (NC-NOFDM).

The rest of this paper is organized as follows: An overview of spectrally opportunistic transmission employing multicarrier modulation is presented in Section 5.2. In Section 5.3, details on how non-contiguous data transmission is performance are provided. A performance evaluation of spectrally agile wireless data transmission under real-world conditions is then provided in Section 5.4, including a comparison of the two approaches in terms of interference and computational complexity. Finally, several concluding remarks are made in Section 5.5.

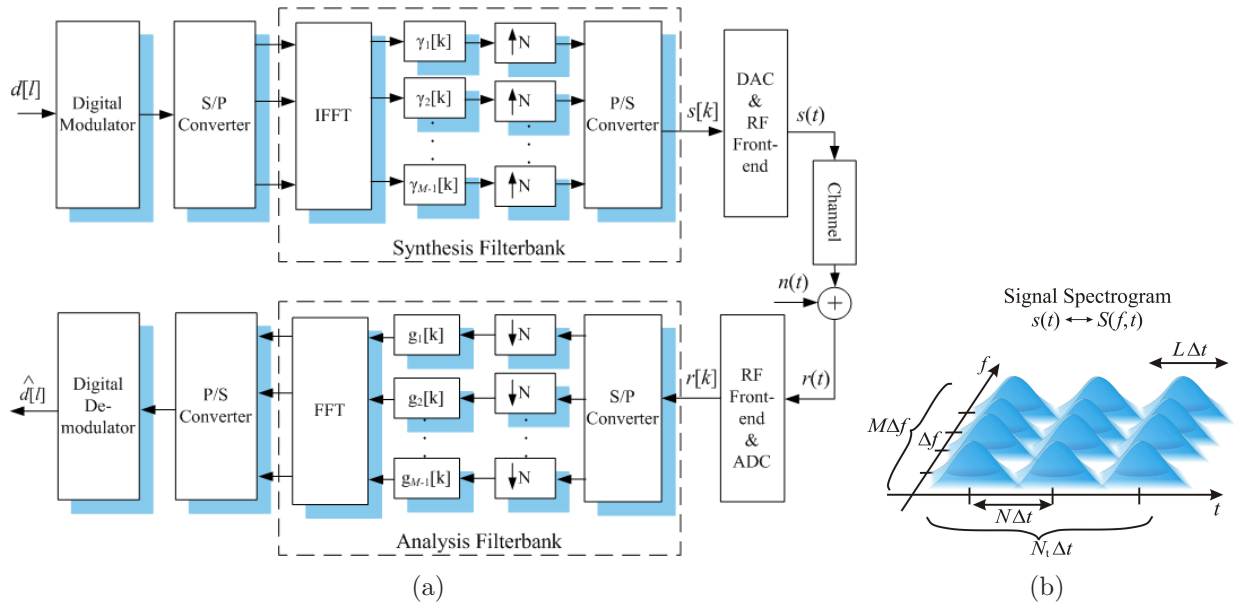


Fig. 5.1 Signal processing and representation in GMC transmission link (a) and the time-frequency (T-F) representation of the transmit signal $s(t)$ (b); Δf - subcarriers distance, Δt - sampling period. L, N, M, N_t denote: the duration of the pulse-shaping filter impulse response $\gamma[k]$ in samples (equal to the duration of the dual-filter impulse response $g[k]$ at the receiver), the oversampling rate, the number of subcarriers, and the number of pulses in time, respectively [4]

5.2 Multicarrier Transmission Techniques for Opportunistic Communications

Multicarrier modulation is a form of *frequency division multiplexing* (FDM), where data is transmitted using several simultaneous narrowband signals located at different carrier frequencies (i.e., *subcarriers*). However, unlike conventional FDM systems, where the narrowband subcarriers are separated by guard bands, multicarrier modulation allows for the overlapping adjacent subcarriers when a certain set of conditions are satisfied. As shown in Fig. 5.1(a), both the GMC transmitter and receiver can be readily implemented by means of an FFT and an inverse FFT (IFFT) pair combined with polyphase filter banks² (or alternatively, via short-time Fourier transforms or Gabor transforms), which implement the

²A polyphase filter bank splits an input signal into a given number M of equidistant sub-band signals and implements filtering of these subband signals.

subcarrier filtering (employing specific digital prototype filters at the transmitter and at the receiver, denoted as $\gamma_m[k]$ and $g_m[k]$ in Fig. 5.1(a)) and multicarrier modulation. In the time-frequency (T-F) representation of a GMC signal presented in Fig. 5.1(b), we can observe T-F blocks of size $N_t \times M$, where N_t and M denote the number of pulses in time and frequency domain, respectively. In this figure, it can be readily observed that depending on the relation between the number of subcarriers M , the pulse-shape duration in samples L and upsampling factor N the information-bearing subcarrier pulses are overlapping in the T-F plane to a smaller or larger extent.

Within the context of spectrally opportunistic wireless access, a secondary wireless transceiver employing multicarrier modulation is well-suited for this situation since it does not require a contiguous frequency band in order to transmit information. This is due to the fact that each subcarrier operates independently of each other, which means deactivating those subcarriers located in the vicinity of primary user signals will not impact the remaining active subcarriers. Moreover, the aggregate data rates available from the remaining active subcarriers may still be significant if there is a substantial amount of unoccupied (potentially fragmented) wireless spectrum. Two approaches for implementing non-contiguous multicarrier modulation will now be presented in the following subsections.

5.2.1 Non-Orthogonal Frequency Division Multiplexing

The mathematical representation of a discrete NOFDM signal $s[k]$ can be expressed as follows [77]:

$$s[k] = \sum_{n \in \mathbb{Z}} \sum_{m=0}^{M-1} c_{n,m} \cdot \gamma_{n,m}[k], \quad (5.1)$$

where $s[k], k \in \mathbb{Z}$ is the discrete-time signal belonging to the complex Hilbert space of square-summable sequences l_2 , $\{c_{n,m}\}$ are the so-called frame coefficients, M is the number of subcarriers, \mathbb{Z} is the set of integers, and $\{\gamma_{n,m}[k]\}$ is a sequence of basis functions, defined as [77]:

$$\gamma_{n,m}[k] = \gamma[k - nN] \cdot \exp\{2\pi j m(k - nN)/M\}. \quad (5.2)$$

For these expressions, N denotes the time spacing between M parallel symbols (in samples) modulating M subcarriers while $\gamma[k]$ is the pulse shape, i.e., synthesis window, used for the synthesis of signal $s[k]$ as described by Eq. (5.1). In fact, Eq. (5.1) is the Gabor discrete signal expansion (synthesis) of $s[k]$. Consequently, the Gabor-frames theory can

be employed as a useful tool in analyzing NOFDM signals as we are defining them. The basis functions $\{\gamma_{n,m}[k]\}$ are referred to as the Gabor atoms, and they constitute the frame if the so-called frame condition holds, i.e.:

$$A\|s[k]\|^2 \leq |\langle s[k], \gamma_{n,m}[k] \rangle| \leq B\|s[k]\|^2, \forall s[k] \in l_2(\mathbb{Z}), \quad (5.3)$$

where A and B are real values called the frame bounds. The necessary (but not sufficient) condition for $\{\gamma_{n,m}[k]\}$ to be a Gabor frame is that $N/M \leq 1$, which corresponds to the overcritical sampling scenario. In this case, $\{\gamma_{n,m}[k]\}$ are sufficiently densely placed in the time-frequency (TF) plane, and that the dual Gabor frame $\{g_{n,m}[k]\}$ exists [77], which means that we can obtain the inverse formula to Eq. (5.1) and calculate the frame coefficients $\{c_{n,m}\}$ for a given $s[k]$. The frame coefficients $\{c_{n,m}\}$ constitute the TF representation of the signal $s[k]$, with this inverse operation called the Gabor-analysis of the $s[k]$ signal. We define this process as:

$$c_{n,m} = \sum_{k \in \mathbb{Z}} s[k] \cdot g_{n,m}^*, \quad (5.4)$$

where:

$$g_{n,m}[k] = g[k - nN] \cdot \exp\{2\pi jm(k - nN)/M\} \quad (5.5)$$

is referred to as the analysis window, and $*$ denotes the complex conjugate. The existence of the dual frame allows for the restoration of the data symbols at the NOFDM receiver. Based on the Balian-Low theorem, adequate TF localization of the atoms (concentrated around the (n, m) coordinates on the discrete TF plane) will yield a reduction in the inter-symbol interference (ISI) and inter-carrier interference (ICI), and allow for the omission of the guard periods necessary in the case of OFDM [75, 77].

It has been shown that Eq. (5.1) describes the operation of the discrete Fourier transform (DFT) synthesis-filter bank, which can be efficiently implemented by the means of an inverse fast Fourier transform (IFFT) and a polyphase filter bank as long as M is a power of 2, which is the case we are considering in this paper. The polyphase filtering is implemented after the IFFT stage, which possesses a lower complexity relative to when pulse-shaping is performed in every subcarrier at the input of the IFFT.

When considering the ideal channel scenario, Eq. (5.4) describes the projection of the received signal onto the set of functions defined by Eq. (5.5). Under these conditions, the

so-called perfect (i.e., complete) reconstruction of the user data symbols is possible only if the biorthogonality condition is held, namely:

$$\langle \gamma_{n,m}[k], g_{n',m'}[k] \rangle = \delta(n - n', m - m'), \quad (5.6)$$

where $\langle \cdot \rangle$ denotes the inner product, and $\delta(\cdot)$ refers to the two-dimensional Kronecker delta function. As a result, Eq. (5.6) reduces into the well-known orthogonality constraint when $N = M$ and $g[k] = \gamma[k]$, which corresponds to OFDM transmission. However, if $N \leq M$ the dual functions for a given synthesis function $\gamma[k]$ are not unique. This implies that it is impossible to recover the user data from the received signal in a reliable manner. The interested reader on this topic is encouraged to research the literature on Weyl-Heisenberg frame-based transmissions, as well as some of the recent achievements in this area [77]. Furthermore, several efficient procedures for performing the dual window calculation are also available in the open literature [78, 79].

5.2.2 Orthogonal Frequency Division Multiplexing

Orthogonal frequency division multiplexing (OFDM) is a widely used data transmission approach, employed in numerous modern wireless communication systems. Together with *orthogonal frequency division multiple access* (OFDMA), it is considered to be both flexible and scalable, and it can be easily optimized, thus making it well suited for future high data-rate wireless communication systems and standards. Moreover, when implementing an OFDM transceiver in hardware, the IFFT/FFT algorithm can be employed to make modulation and demodulation highly efficient in terms of hardware and computational complexity. In fact, it has been shown that a radix-2 FFT/IFFT pair possesses $\mathcal{O}(M \log(M))$ complexity for M subcarriers, thus making it an attractive option for multicarrier-based communication systems. Finally, the hardware implementation of a non-contiguous version of OFDM (i.e., NC-OFDM) can be further streamlined by performing *FFT pruning* on the FFT/IFFT pair, especially if the baseband transceiver modules are constructed on a programmable or software-defined communication system or a cognitive radio.

With respect to the mathematical formulation of OFDM, the same framework described in the previous subsection involving NOFDM can be employed here, except that the pulse shape for OFDM is chosen to be rectangular in Eq. (5.1), where $N = M$, $\{c_{n,m}\}$ are Fourier

coefficients. That is, in Eq. (5.2), $\gamma[k] = \text{rect}_{[0, N-1]}[k]$ with:

$$\text{rect}_{[0, N-1]}[k] = \begin{cases} 1 & n = 0, 1, \dots, N-1 \\ 0 & \text{else} \end{cases} . \quad (5.7)$$

5.3 Non-contiguous Data Transmission

Given the locations in frequency of the wireless spectrum occupied by incumbent primary signals, the goal of a secondary wireless access device such as a cognitive radio employing a non-contiguous version of multicarrier modulation, e.g., the two approaches described above, is to deactivate subcarriers that could potentially interfere with the primary users and transmit over the remaining active subcarriers. Consequently, subcarriers located within the same frequency vicinity as the incumbent primary signals are deactivated, i.e., “turned off”, resulting in the non-contiguous spectral characteristic of the secondary multicarrier signal. In the following section, we examine an important challenge posed by employing non-contiguous orthogonal multicarrier-modulation-based data transmission systems, namely, the mitigation of high out-of-band interference. This issue is not as significant for the case of NOFDM signals due to the fact that the pulses employed are expected to have smoother transitions. On the other hand, the discussion on the resulting implementation complexity for NOFDM will be conducted in Section 5.4. This is illustrated in Fig. 5.2, where the NC-NOFDM waveform employs a larger number of subcarriers and possesses higher spectral selectivity relative to the NC-OFDM waveform. Overall, both of these challenges become especially apparent when dealing with fragmented bands of unoccupied wireless spectrum. Although there does not exist a single non-contiguous multicarrier solution that possesses both low out-of-band interference and low implementation complexity, we will study these non-contiguous variants of multicarrier modulation in order to provide the reader with some insights into the design trade-offs associated with the implementation of these spectrally agile transmission systems.

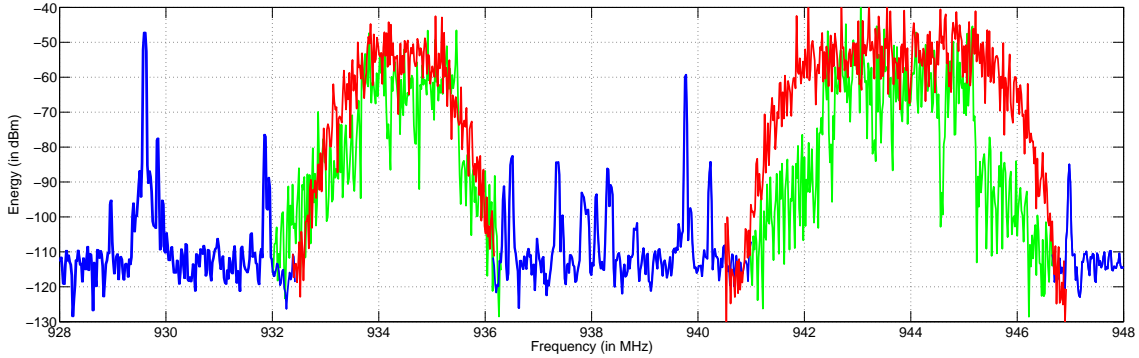


Fig. 5.2 An illustration of the non-contiguous OFDM (shown in green) and non-contiguous NOFDM (shown in red) transmissions in the paging band (928 MHz - 948 MHz). Paging transmission is shown in blue [4].

5.3.1 Frequency-Domain Cancellation Carrier Technique for OFDM Transmissions

Let us consider the DFT operation of the symbols shown in Eq. (5.1) for the case of one OFDM symbol³ transmission. As mentioned earlier in this paper, the temporal pulse shape for each symbol is defined to be rectangular. As a result, the frequency response for each subcarrier will be a sinc-type pulse with large sidelobe levels. Therefore, the frequency response of each subcarrier is given by:

$$s_m(y) = c_m \frac{\sin(\pi(y - y_m))}{\pi(y - y_m)}, \quad m = 0, 1, \dots, M - 1, \quad (5.8)$$

where $y = (f - f_0)T_0$ and $y_m = (f_m - f_0)T_0$. Since each OFDM symbol vector in frequency consists of the superposition of individual subcarrier spectra, this yields the OFDM pulse shape:

$$S_n(y) = \sum_{m=0}^{M-1} s_m(y) \quad n \in \mathbb{Z}. \quad (5.9)$$

Depending on the symbols transmitted across each of the subcarriers, it can be observed that the resulting sidelobes from each of the *sinc* pulses may add either constructively or destructively, leading to different power values over the sidelobes near the edges of the composite signal. By reserving several subcarrier locations on either side of a contiguous

³We refer to each IDFT block for a certain value of n as an OFDM “symbol”.

group of active subcarriers, non data-bearing *cancellation subcarriers* (CCs) can be inserted, whose amplitude and phase values are computed such that the out-of-band (OOB) spectral spillage is reduced.

Suppose we define the total number of subcarriers that can be transmitted by a secondary user in a spectral white space as $M = M_A + M_{CC}$, where M_A is the number of active subcarriers used for signal transmission, and M_{CC} is the total number of subcarriers reserved for inserting cancellation subcarriers. As a result, Eqs. (5.8) and (5.9) can be expressed as:

$$s_{m_a}(y) = c_{m_a} \frac{\sin(\pi(y - y_{m_a}))}{\pi(y - y_{m_a})},$$

$$m_a = M_{CC}/2 + 1, M_A/2 + 1, \dots, M - M_{CC}/2, \quad (5.10)$$

and:

$$\hat{S}_n(y) = \sum_{m_a=M_{CC}/2+1}^{M-M_{CC}/2} s_{m_a}(y) \quad n \in \mathbb{Z}. \quad (5.11)$$

Since the frequency response of an OFDM subcarrier can be represented by the *sinc* function, the sidelobe power levels of the composite signal, at any frequency location can be algebraically computed as the sum of the sidelobe powers of each of *sinc* function at that location given the input sequence. Therefore, if $I(p)$ represents the sidelobe amplitude level at the p^{th} frequency index in the OOB region normalized to the subcarrier bandwidth, we then have the following expression:

$$I(p) = \sum_{m_a=M_{CC}/2+1}^{M-M_{CC}/2} s_{m_a}(p)$$

$$= \sum_{m_a=M_{CC}/2+1}^{M-M_{CC}/2} c_{m_a} \frac{\sin(\pi(y - y_{m_a}))}{\pi(y - y_{m_a})}. \quad (5.12)$$

The idea here is to scale $c_{CC}(j)$, the amplitude of the cancellation subcarrier at j^{th} frequency location, in such a way that at the frequency location of the intended sidelobe cancellation, p , has the same amplitude but opposite phase to the existing sidelobe. i.e.:

$$C(j) = \frac{I(p)}{C_{CC}(p)} \cdot \frac{\sin(\pi(j - y_{m_a}))}{\pi(j - y_{m_a})}. \quad (5.13)$$

The time-domain version of the cancellation carrier from the above expressions is obtained by taking the IDFT of $c_{cc}(j)$. Notice that the frequency location j is a frequency originally intended for the transmission of data carriers by the secondary user, but used for inserting cancellation carriers whereas the frequency location p is in the out-of-band region. Also, both j and p appear on the same side of the frequency axis. Thus, for the case of the first cancellation carrier on the right side of the OFDM spectrum, $j = M - M_A/2$ and $p = M + 1$. Similarly, for the case of the second cancellation carrier on the same side of the OFDM spectrum, $j = M - M_A/2 + 1$ and $p = M + 2$. The procedure can be continued for a given number of cancellation subcarriers until the desired sidelobe power levels is achieved⁴. Significant sidelobe power suppression can be achieved with a small number of CCs, such as one or two subcarriers on each side of a contiguous group of subcarriers, resulting in a reasonable trade-off between bandwidth reduction and achievable interference suppression. Also, since the proposed algorithm attempts to minimize the amplitude values of the real and imaginary components of the OOB sidelobes, it can be used with any modulation scheme. Several variants of the basic principle described in the above paragraphs can be found in [80, 81].

5.4 Spectral Agility in Real-world Transmission Scenarios

In this section, the interference mitigation and implementation complexity performance for non-contiguous versions of OFDM and NOFDM is presented. Note that for the interference performance analysis conducted in this paper, actual wireless spectrum measurements of several primary user signals have been employed in a computer simulation environment to provide a more realistic transmission environment when evaluating both non-contiguous multicarrier modulation approaches.

The process of quantifying the amount of interference experienced by both primary and secondary transmissions located within the same frequency vicinity was based on 125 spectrum measurement sweeps of the paging band (928 MHz - 948 MHz) taken in Worcester, MA, USA on July 27, 2008 at location N42°17.829', W071°50.3607' [82]. The frequency resolution for these time sweeps is 20 kHz. These real-world spectrum measurements were then employed in an emulation environment, where 25,000 BPSK symbols were simulated,

⁴Both M_A and M_{CC} are assumed to be even

and the number of subcarriers transmitting these symbols were based on the primary user spectrum occupancy characteristics observed. For the non-contiguous NOFDMA case, a Gaussian window was applied for shaping the subband pulses. The duration of the pulse-shaping filter impulse-response in samples L was equal to the oversampling rate N in the time domain ($L = N = 1024$). Otsu's algorithm [62] was employed to classify the channels as either "occupied" or "available" ⁵.

In order to apply Otsu's algorithm, a matrix $\mathbf{M}(t_j, f_i)$ is formed from the collected data points where the row t_j contains data points over all the frequency locations in the band of interest during one particular time instant and the column f_i represents the data points observed in that frequency bin over all time sweeps during the measurement process. The next step is to transform the contents of this matrix into gray scale values by applying the procedure given by:

$$\mathbf{I}(t_j, f_i) = \frac{1.0 - 0.0}{\max\{\mathbf{M}(t_j, f_i)\} - \min\{\mathbf{M}(t_j, f_i)\}} \times (\mathbf{M}(t_j, f_i) - \min\{\mathbf{M}(t_j, f_i)\}) \quad (5.14)$$

Applying Otsu's algorithm to the matrix, $\mathbf{I}(t_j, f_i)$ gives the required optimum threshold that can be used to classify all values above this threshold as signal while the rest is classified as noise. The information symbols are now transmitted across the available channels such that the interference levels affecting the neighboring licensed transmissions are below a set power-level.

5.4.1 Interference Analysis

The Parks-McClellan optimal equiripple FIR filter, $h_{PM}[k]$, was employed at the receiver front-end to eliminate the interference from the neighboring licensed or unlicensed signals. In our analysis of the impact of secondary user on the paging band primary user, we study the ESD characteristics of the signal:

$$y[k] = h_{PM}[k] * h[k] * s[k] + v[k], \quad (5.15)$$

⁵Otsu's method is used to calculate the optimum threshold, which is the maximum inter-class variance separating two classes of data, e.g., the foreground pixels and background pixels in image processing research. In this work, we employed Otsu's method in order to separate the occupied portions of the paging bands from the spectrum holes.

where $h[k]$ is the unknown multipath channel affecting the transmitted signal, $s[k]$ and $v[k]$ is the additive noise. Note that in Eq. (5.1), although the summation is over all M , several zeros have been inserted in the modulated data in order to reflect the fact that the paging band spectrum usage is known to the secondary receiver, and hence it is being used in a non-contiguous fashion. The interference suppressing filters were also designed such that there are multiple filters, with each possessing a different pass-band tailored to the bandwidth of each non-contiguous block. Note that the filtering operation performed in Eq. (5.15) will result in the noise affecting the received signal to be colored. However, without loss of generality, we assume that the noise power is known and hence a whitening filter can be applied to obtain the above equation with uncorrelated noise.

The following assumptions were made in performing our simulation-based analysis in order to understand the interference characteristics under certain basic conditions:

- The primary user spectrum occupancy profile observed by the secondary user transmitter and the intended secondary user receiver is the same. That is, the secondary transmitter and the receiver are closely located.
- The primary user spectrum occupancy profile does not change between the scanning time and the transmission time of the secondary user transmitter.

Interference as a Function of Filter Order

Referring to Fig. 5.3, the interference experienced by the primary and secondary users as a function of the filter order used at the receiver end is presented, where the y-axis displays the “normalized interference power”. In other words, the y-axis represents the ratio of the total undesired signal power observed at the receiver to the sum of the undesired and desired signal powers. In Fig. 5.3, the red dotted line indicates the application of Kaiser window, the red dashed indicates the application of Hanning window and the red solid indicates the application of Gaussian window to the secondary transmissions that employ NOFDM.

On the other hand, no windowing is applied to NC-OFDM transmissions and the only interference minimization is due to cancellation carriers as described in the previous section. This figure highlights the constraints on the receive filter in order to minimize the amount of interference in an NC-OFDM scenario. In contrast, since the non-contiguous NOFDM

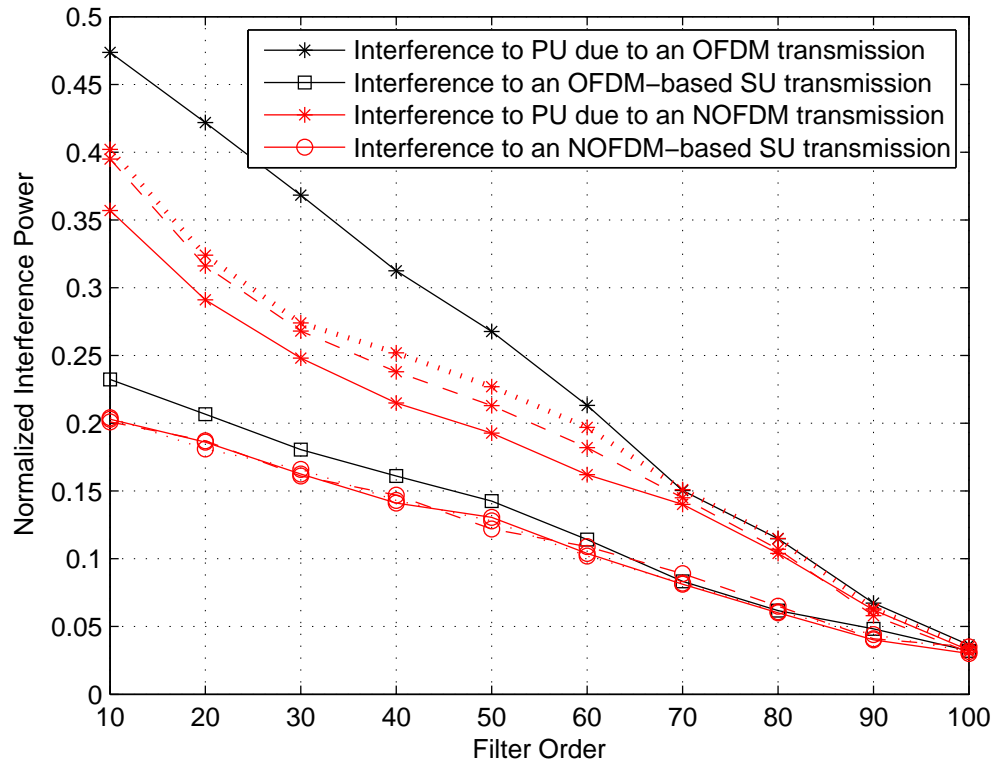


Fig. 5.3 Normalized interference as a function of the filter order [5].

pulse contains smoother edges when compared to an OFDM-based signal with a rectangular pulse, the non-contiguous NOFDM performs better relative to non-contiguous OFDM and causes less interference to the neighboring band primary user when an interference-suppressing filter of the same order is applied. Also note how in Fig. 5.3 that by employing a Gaussian filter function in Eq. (5.1), the interference caused to the primary transmission is the lowest of all the filter functions studied in this simulation.

Interference as a Function of Signal Threshold

A Parks-McClellan FIR receive filter of order 25 is used in Fig. 5.4, where the threshold used in Otsu's algorithm is varied such that the interference caused by the OFDM sidelobes at the primary users' frequency location is above the optimum threshold. The same color conventions as in Fig. 5.3 are employed for this figure. Using this convention, the blue lines

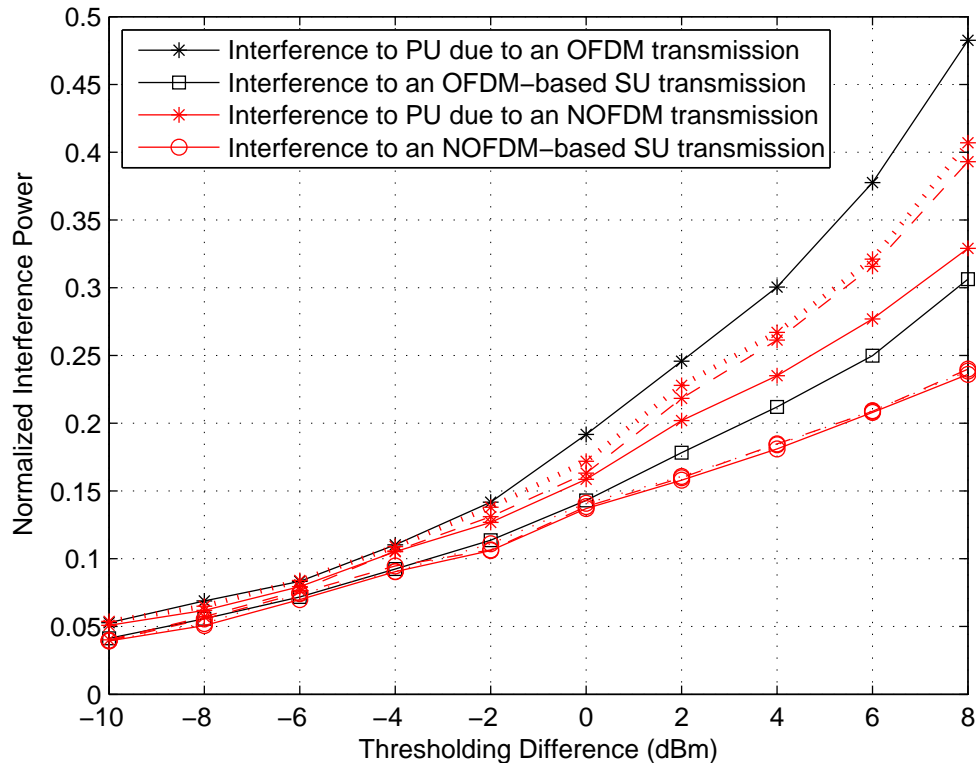


Fig. 5.4 Normalized interference as a function of the threshold difference [5].

are for the case of SUs that employ OFDM transmissions. The x-axis in Fig. 5.4 represents the difference between the optimum value of the threshold, assuming the secondary user transmitter and receiver pair observe the same spectral occupancy profile, and the actual threshold used in inserting the subcarriers is within a few decibels of this value. When the threshold difference is well below the optimum value (i.e., 0 dBm), the resulting interference will be minimal since only a few subcarriers will be inserted due to an overly conservative interpretation of the primary user profile. As the threshold increases beyond the optimum value, the interference power quickly rises to very high values. In this scenario, NOFDM will achieve better performance relative to non-contiguous OFDM in terms of interference mitigation, with the Gaussian pulse shape achieving the best results.

Interference as a Function of Filter Order in the event of false detection of PU

Although the adverse effects of false detection of primary transmissions on the interference performance of these non-contiguous multicarrier approaches can be displayed either as a function of filter order or as a function of the signal threshold, we chose the former option for the purposes of brevity. The primary intention of the analysis in this subsection is to understand the effect of false alarms on the channels occupied by the primary user.

During an incorrect decision on the presence of a primary transmission, certain channels that are purely noise and hence vacant are classified as occupied and hence no information-bearing signals are transmitted. As a result, several potentially usable channels are not utilized and hence the secondary users might be forced to transmit across several fragmented blocks of spectrum even though it is not necessary. Consequently, this is an undesirable scenario for a secondary transmission approach. However, it is observed that due to the false alarm probability being high, the amount of interference resulting channels located in close proximity to the primary transmissions are no longer used by the SU, thus yielding low interference levels. This hypothesis corresponds to the simulated results shown in Fig. 5.5. Using the same color conventions employed previously in Figs. 5.3 and 5.4, it is observed that as the filter order increases, the amount of interference affecting the primary transmissions as well as suffered by the secondary transmissions is relatively small. However, as mentioned before, this occurrence is a result of false alarms alone leading to reduced efficiency of the secondary wireless access receiver.

5.4.2 Complexity Evaluation

When assessing the performance of either non-continuous OFDM or NOFDM approaches, it is very important to understand the impact of computational complexity associated with each approach since it can significantly affect the construction of a practical wireless transceiver implementation. For instance, when the number of deactivated subcarriers used in NC-OFDM is very large, pruning mechanisms can be applied to the IFFT/FFT modules employed in the transceiver in order to minimize hardware usage, reduce power consumption, and increase the overall execution time. On the other hand, this enhancement in hardware utilization and associated benefits comes at the cost of lower spectral efficiency and interference mitigation capabilities. Thus, there is a non-contiguous multicarrier transceiver design trade-off between interference mitigation performance and reduced

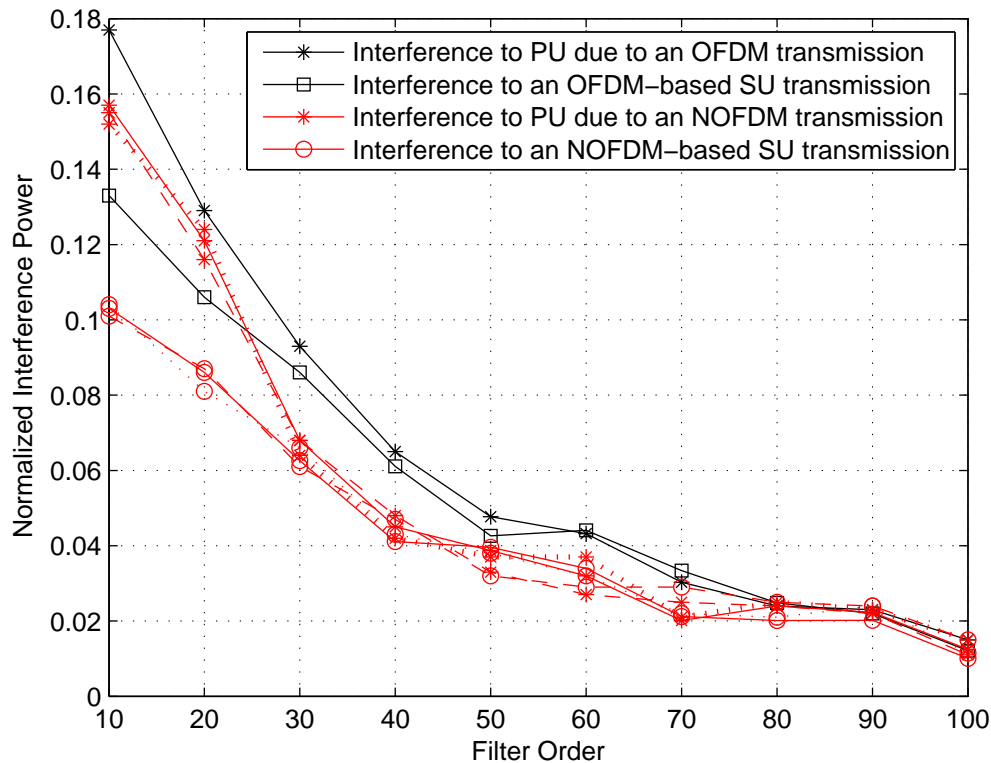


Fig. 5.5 Normalized interference as a function of the filter order in the event of false detection of PU [5].

computational complexity. In the NOFDM case, the additional filtering operations result in a better interference mitigation performance outcome but at the expense of additional computation complexity relative to the OFDM case. Moreover, in both NC-OFDM and NC-NOFDM systems, the subcarriers located in the frequency vicinity of the primary user signal coupled with several guard subcarriers should be excluded from the modulation process, where pruning can be applied to the IFFT/FFT operations in order to reduce complexity.

Derivations conducted in [5] have resulted in a closed form expression for the number of required complex multiplications computed at the transmitter per sampling period, i.e., at the input to the analysis filter bank. First, the IFFT operation, which is performed at a rate that is N times lower relative to the sampling rate, requires $\frac{(M \cdot \log_2 M)}{(2N)}$ complex multiplication per unit time, where $\lceil x \rceil$ denotes the lowest integer that is not lower than

x. Furthermore, each polyphase filter with the corresponding decimator requires $\lceil \frac{L}{M} \rceil / N$ complex multiplications, where L is the length of the synthesis pulse $\gamma_{n,m}[k]$ expressed in samples. For the sake of simplicity, the length of the analysis pulse $g[k]$ is assumed to be equal to L . In such a case, the number of required operation at the transmitter and at the receiver side will be identical. Thus, the final number of required complex multiplications, denoted as N_{CM} , in the whole transceiver in one sampling period at the transmitter input can be expressed as:

$$N_{CM} = \frac{M}{N} \cdot \left(2 \cdot \left\lceil \frac{L}{M} \right\rceil + \log_2 M \right). \quad (5.16)$$

In Fig. 5.6, the number of required operations employed at the transmitter (resp. modulator) and at the receiver (resp. demodulator) per sampling period versus the number of subcarriers is presented for the worst-case scenario, i.e., when no simplifications in the IFFT/FFT implementation is possible. It can be observed that the NC-OFDM transceiver consistently achieves the best performance relative to the NOFDM-system transceiver in terms of computational complexity. This is due to the application of filterbanks with respect to NOFDM transmission. Note that in practice, various techniques can be used to reduce the number of operations needed for modulation and demodulation of NC-OFDM and NC-NOFDM signals, with one example being the pruning of the IFFF/FFT operations. Moreover, several of the algorithms employed at the receiver working in conjunction with the demodulator can be simplified due to some of the features associated with NOFDM waveforms, e.g., frequency-offset correction.

5.5 Chapter Summary

Wireless communication systems such as cognitive radio require a high level of spectral agility when performing opportunistic wireless access. As a result, multicarrier modulation has been identified as a possible candidate for spectrally agile data transmission, especially when the wireless communication system is operating across several non-contiguous unoccupied frequency bands. The challenges posed by employing non-contiguous multicarrier-modulation-based data transmission systems include high out-of-band interference and implementation complexity, which become especially apparent when dealing with fragmented bands of unoccupied wireless spectrum. Although there does not exist a single non-contiguous multicarrier solution that possesses both low out-of-band interference and

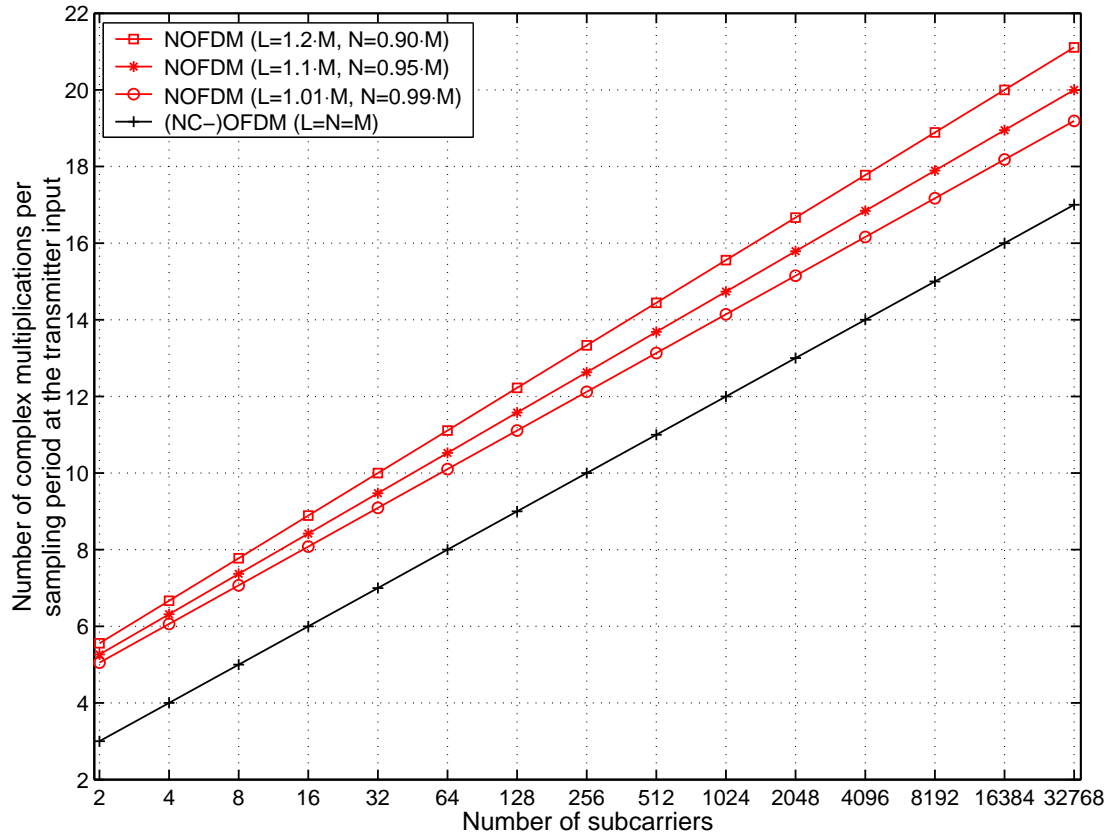


Fig. 5.6 Complexity of NOFDM and NC-OFDM transmissions as a function of the number of subcarriers. L, N, M denote: length of the pulse $\gamma[k]$ or $g[k]$ in samples, oversampling rate and the number of subcarriers, respectively [5].

low implementation complexity, it is possible to assess the performance trade-offs for several possible multicarrier solutions in order to select the solution that is most suitable for the application.

Chapter 6

Time-Selective MIMO-OFDM Channel Tracking in Low-Mobility Scenarios¹

6.1 Introduction

In the presence of a rich scattering environment, multiple-input, multiple-output (MIMO) systems enable a linear increase in capacity with no increase in bandwidth or transmit power compared to single-input, single-output (SISO) systems. However, the seminal work of [84] is based on the assumption that the channel is perfectly known to the receiver. In practical systems, the estimated channel using training sequences can be imperfect. As a result, there is potentially a mutual information loss between the input and the output of the channel. Given a power budget and a desired data-rate, the time and power spent on training versus information symbols has to be judiciously selected since there is an interesting interplay involving information throughput and the quality of the channel estimates. If a large fraction of the time and/or power is spent on training, excellent channel estimates can be obtained at the expense of poor information throughput. Conversely, expending too little time and/or power on training results in poor channel estimates that lead to error-prone information symbol transmission. Receivers that rely on channel estimates to

¹The work included in this chapter has been funded by the Office of Naval Research via grant N00014-10-1-0065. It has been partly published in the 2011 IEEE Pacific Rim Conference on Communications, Computers and Signal Processing [83]

perform information symbol decoding are termed as “mismatched” receivers [85–88].

The problem of channel estimation has been studied in numerous contexts. Here, we list a few relevant studies. For an exhaustive survey of the area of channel estimation using known pilot sequences, see [40]. One of the earliest works in formulating training designs to obtain channel estimates for OFDM systems was [89]. In [90], optimal training designs have been designed for single-carrier and orthogonal frequency division multiplexing (OFDM) systems by maximizing a tight lower bound on the ergodic training-based independent and identically distributed (i.i.d.) capacity. Optimal pilot symbol design and their placement in a packet were addressed for both SISO and MIMO systems in [91] by minimizing the Bayesian Cramer-Rao Bound (CRB) of a semi-blind channel estimator. In [92], a general affine-precoding framework [93] is considered and it was shown that decoupling channel estimation from symbol detection and optimizing a least-squares channel estimator naturally leads to an OFDM system with information and training symbols on disjoint subcarriers. Considering the same framework, [94] provides a link between optimal training designs and maximizing the channel capacity lower bound similar to [90]. This work was extended in [95] to include a MIMO communications setup. Furthermore, by considering block-processing of transmitted symbols with a cyclic-prefix or zero-padding, optimal training designs are provided that maximize the channel capacity lower bound when a linear minimum mean square error (LMMSE) estimator is employed.

The impact of receiver estimation error from an information theoretic viewpoint has also been extensively studied. The first study was conducted in [87] where the relationship between lower and upper bounds on the mutual information between transmitted and estimated Gaussian symbols is derived by modeling a time-varying frequency-selective channel as a random component with a known mean and a covariance that accounts for the channel estimation error. Specifically, it was shown that signal-to-noise ratio in the mutual information lower bound is lowered as a result of imperfect channel knowledge. In [96], the achievable data-rate of a flat-fading interleaved MIMO channel is related to the linear minimum mean squared error (LMMSE) covariance matrix. In [88], the transmission of Gaussian symbols through a flat-fading channel is considered and it was demonstrated that when the Gaussianity assumption on the additive noise is rendered invalid due to channel estimation errors, scaled nearest neighbor detection is suboptimal. In [97], a lower bound on the capacity of a time-multiplexed training scheme in the presence of a flat-fading channel is studied and related to the variance of a LMMSE channel estimator. In [98], two

pilot arrangement schemes are considered and the impact of the receiver estimation error is analyzed when channel state information (CSI) is available only at the receiver and when it is also feedback to the transmitter. In both cases, maximum-likelihood channel estimation is considered. The relationship between the symbol Bayesian CRB and the mutual information between estimated and transmitted symbols was shown in [99]. In this work, two strategies are considered. One, when the receiver obtains joint Bayesian channel and symbol estimates and two, when the receiver computes channel estimates followed by their utilization in obtaining symbol estimates. The model presented in [97] was generalized in [100] by considering a superimposed training scheme of which time multiplexed training can be termed as a special case. Based on the mutual information bounds derived, a comparison between the superimposed training and the conventional time multiplexed training is performed by optimizing over training design, number of transmit antennas and a training/information symbol power budget. While [97] provides the optimal noise covariance matrix that maximizes a tight lower bound on the mutual information between the input and the output when both the transmitter and the receiver have imperfect CSI, [101] provides the optimal signal covariance matrix and shows that the uniform power allocation scheme is suboptimal.

In this chapter, we extend the discussion in [97] and [100] by considering a “slowly” time-varying frequency-selective channel. We start from first principles and derive the Bayesian CRB of a general MIMO communications system that employs affine precoding at the transmitter. We then show that in order to decouple channel estimation from data detection, an orthogonality constraint has to be met between the training and linear precoder matrices. A solution to the orthogonality constraint is the MIMO-OFDM system with FDM training symbols. Consequently, we formulate a scheme where during the training phase, the OFDM symbol contains training and information symbols, whereas in the data transmission phase, only information symbols are transmitted. We consider a MIMO channel that undergoes block-wise variations according to a first-order autoregressive (AR) model. Therefore, we consider a scheme wherein during the training phase, channel tracking is performed by a Kalman filter followed by the estimation of information symbols during the data phase based on channel state prediction. In this setup, we derive the capacity upper and lower bounds based on a training scheme that has been derived in an MMSE minimizing sense. We then provide simulation examples to support the theoretical results.

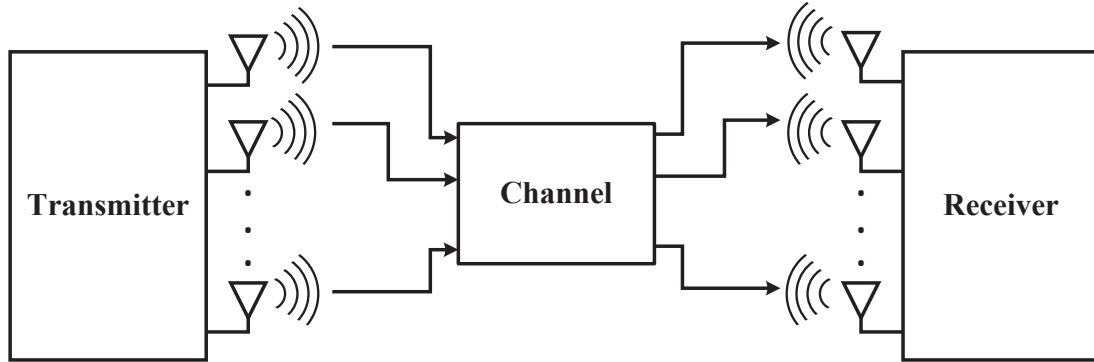


Fig. 6.1 Block diagram of a digital MIMO communications system

6.2 System Model

In our analysis, we consider a MIMO communications system consisting of K transmit antennas that transmit N training and information symbols over a time-varying frequency-selective block fading channel. We design super-imposed training symbols optimally such that the channel estimates from N_t consecutive blocks of training symbols are utilized in the data detection of the following N_d information symbol blocks. We assume that the receiver also has K receive antennas without loss of generality. The maximum order of the discrete-time complex baseband wireless channels, L is assumed to be known. An illustration diagram depicting a MIMO communication system is shown in Fig. 6.1.

Training Phase In the training phase, training symbols and information symbols are *affinely*-pre-coded [93] and transmitted over K antennas. A matrix formulation of this system for an arbitrary time index, n is as follows. Assuming that the information symbol vector at each antenna is of size M , we stack the symbols transmitted across K transmit antennas as shown below:

$$\tilde{\mathbf{x}}_n \triangleq \text{vec}([\tilde{\mathbf{x}}_{n,1} \ \tilde{\mathbf{x}}_{n,2} \ \dots \ \tilde{\mathbf{x}}_{n,K}]) \quad (6.1)$$

where the n th block of M symbols from k th transmit antenna is represented as:

$$\tilde{\mathbf{x}}_{n,k} \triangleq [\tilde{x}_{n,k}(n) \ \tilde{x}_{n,k}(1) \ \dots \ \tilde{x}_{n,k}(M-1)]^T \quad (6.2)$$

The affine-precoder output vector is similarly arranged as,

$$\mathbf{x}_n \triangleq \text{vec}([\mathbf{x}_{n,1} \ \mathbf{x}_{n,2} \ \dots \ \mathbf{x}_{n,K}]) \quad (6.3a)$$

$$\mathbf{x}_{n,k} \triangleq [x_{n,k}(0) \ x_{n,k}(1) \ \dots \ x_{n,k}(P-1)]^T \quad (6.4)$$

Denoting the precoder matrix of size $KP \times KM$ as \mathbf{Q} and the additive pilot-symbol vector of size $KP \times 1$ as \mathbf{t} , we can now write the equation for the transmitted symbol vector during the training mode as follows:

$$\mathbf{x}_n = \mathbf{t} + \mathbf{Q} \tilde{\mathbf{x}}_n \quad (6.5)$$

where $\mathbf{t} \triangleq \text{vec}([\mathbf{t}_1 \ \mathbf{t}_2 \ \dots \ \mathbf{t}_K])$. Furthermore, the matrix \mathbf{Q} is such that the data stream transmitted from an antenna is precoded independently of the data-streams from the other antennas. In other words, \mathbf{Q} has a block diagonal structure and hence $\mathbf{Q} \triangleq \text{diag}([\mathbf{Q}_1 \ \mathbf{Q}_2 \ \dots \ \mathbf{Q}_K])$. Despite this restriction on the structure of \mathbf{Q} , it is still general enough to encapsulate not only a MIMO system employing K antennas but also a multi-user system *e.g.*, K_U users utilizing K antennas in total and communicating with a base-station equipped with K antennas. Also, restricting the structure of \mathbf{Q} to be block diagonal simplifies an orthogonality condition (cf., Theorem 6.2) that helps in the design of the linear precoder and the training vector.

After pre-multiplying the above vector by $\mathbf{I}_K \otimes \mathbf{C}_T$ (cf. Section 2.4), the $K\bar{P} \times 1$ vector ($\bar{P} = P + L$) undergoes a digital-to-analog conversion followed by pulse-shaping to yield a continuous-time signal. Assuming perfect timing and carrier synchronization at the receiver, the signal is sampled to obtain the received symbol vector. Subsequently, the cyclic-prefix is removed by a pre-multiplication operation with $\mathbf{I}_K \otimes \mathbf{C}_R$ and an ISI-free received vector of size $KP \times 1$ is available for processing:

$$\mathbf{y}_n = \mathcal{H}_n \mathbf{t} + \mathcal{H}_n \mathbf{x}_n + \mathbf{z}_n \quad (6.6)$$

where the channel matrix \mathcal{H}_n is:

$$\mathcal{H}_n \triangleq \begin{bmatrix} \mathbf{H}_{1,1}^{(n)} & \mathbf{H}_{1,2}^{(n)} & \cdots & \mathbf{H}_{1,K}^{(n)} \\ \mathbf{H}_{2,1}^{(n)} & \mathbf{H}_{2,2}^{(n)} & \cdots & \mathbf{H}_{2,K}^{(n)} \\ \vdots & \vdots & \ddots & \vdots \\ \mathbf{H}_{K,1}^{(n)} & \mathbf{H}_{K,2}^{(n)} & \cdots & \mathbf{H}_{K,K}^{(n)} \end{bmatrix} \quad (6.7)$$

Each matrix in the set, $\{\mathbf{H}_{i,j}^{(n)}\}$ for $1 \leq i \leq K$, $1 \leq j \leq K$ is circulant with the first column, $[h_{i,k}^{(n)}[0] \dots h_{i,k}^{(n)}[L] \mathbf{0}]^\top$ and first row, $[h_{i,k}^{(n)}[0] \mathbf{0} h_{i,k}^{(n)}[L] \dots h_{i,k}^{(n)}[1]]$. We now define a channel vector \mathbf{h}_n such that,

$$\mathbf{h}_n \triangleq \text{vec}([\mathbf{h}_{n,1} \ \mathbf{h}_{n,2} \ \dots \ \mathbf{h}_{n,K}]) \quad (6.8a)$$

$$\mathbf{h}_{n,i} \triangleq \text{vec}([\mathbf{h}_{i,1}^{(n)} \ \mathbf{h}_{i,2}^{(n)} \ \dots \ \mathbf{h}_{i,K}^{(n)}]) \quad (6.8b)$$

$$\mathbf{h}_{i,k}^{(n)} \triangleq [h_{i,k}^{(n)}[0] \ \dots \ h_{i,k}^{(n)}[L]]^\top \quad (6.8c)$$

By exploiting the commutativity property of discrete convolution, (6.6) can now be written in a different form in terms of the MIMO channel vector, \mathbf{h}_n and the pilot symbol matrix, $\mathbf{T} \triangleq [\mathbf{T}_1 \ \mathbf{T}_2 \ \dots \ \mathbf{T}_K]$ as,

$$\mathbf{y}_n = (\mathbf{I}_K \otimes \mathbf{T}) \mathbf{h}_n + \mathcal{H}_n \mathbf{x}_n + \mathbf{z}_n \quad (6.9)$$

where the circulant matrices, $\{\mathbf{T}_k\}$ are constructed such that $[t_k[0] \dots t_k[P-1]]^\top$ is the first column and $[t_k[0] \ t_k[P-L] \dots t_k[P-1]]$ is the first row. In (6.6) and (6.9), we use the subscript n in \mathcal{H}_n and \mathbf{h}_n to indicate the time-dependance of the random channel. The system model described above needs to satisfy the following conditions.

- (C1) The $KP \times KM$ dimensional linear-precoder matrix, \mathbf{Q} is of full column-rank and strictly-tall, *i.e.*, $P > M$. Also, $V \triangleq P - M$.
- (C2) The $P \times K(L+1)$ dimensional training matrix, \mathbf{T} is a tall matrix, *i.e.*, $P \geq K(L+1)$.
- (C3) The matrix, \mathbf{T} is of full column-rank, *i.e.*, $\text{rank}(\mathbf{T}) = K(L+1)$.

Remark: Condition (C1) is enforced as a simple way of introducing redundancy in the precoding process [35, 102]. Condition (C2) ensures that enough dimensions are available for the identification of the unknown channel coefficients in a linear least-squares sense. As we shall show in Theorem 6.2, the extra dimensions that are available as a result of

employing a full-column rank, strictly-tall precoding matrix are useful in designing the training vector. Condition (C2) also suggests that given the knowledge of the channel order and for a fixed number of transmit antennas, the data-block size has to be at least equal to the product of the number of channel taps and the number of transmit antennas. Condition (C3) which complements (C2) implies that each element of the set, $\{\mathbf{T}_k\}$ is also of full column-rank.

Data Transmission Phase Due to the fact that no training symbols are available in the data transmission phase, we can write the system model as follows:

$$\mathbf{r}_n = \mathcal{H}_n \mathbf{s}_n + \mathbf{z}_n \quad (6.10)$$

where $\mathbf{s}_n = \bar{\mathbf{Q}} \tilde{\mathbf{s}}_n$ and $\tilde{\mathbf{s}}_n$ is obtained in a manner similar to (6.1).

A few assumptions on the system model shown in (6.9) and (6.10) are now in order.

(A1) The channel vector, \mathbf{h}_n is zero-mean, independent and identically distributed (i.i.d) complex Gaussian with variance σ_h^2 , *i.e.*, $\mathbf{h}_n \sim \mathcal{CN}(\mathbf{0}, \sigma_h^2 \mathbf{I}_{K^2(L+1)})$. Moreover, each channel tap gain is assumed to be an independent AR process (cf. Section 2.2.3). We only consider a first-order AR model for each tap gain so that

$$\mathbf{h}_n = a\mathbf{h}_{n-1} + \mathbf{u}_n \quad (6.11)$$

where $a \in [0, 1]$ is the AR coefficient for the l th channel tap gain and the excitation noise, $\mathbf{u}_n \sim \mathcal{CN}(\mathbf{0}, \sigma_u^2 \mathbf{I}_{K^2(L+1)})$. In order to match the correlation functions at lags 0 and 1 and thus make the random process WSS for $n \geq 0$, we select $\sigma_u^2 = (1 - a^2) \sigma_h^2$.

(A2) The transmitted symbol vectors, $\tilde{\mathbf{x}}_n$ and $\tilde{\mathbf{s}}_n$ are independent and identically distributed (i.i.d) complex Gaussian with variance σ_x^2 and σ_s^2 , *i.e.*, $\tilde{\mathbf{x}}_n \sim \mathcal{CN}(\mathbf{0}, \sigma_x^2 \mathbf{I}_{KP})$ and $\tilde{\mathbf{s}}_n \sim \mathcal{CN}(\mathbf{0}, \sigma_s^2 \mathbf{I}_{KP})$ respectively.

(A3) The additive noise vector, \mathbf{z}_n is zero-mean, circularly-symmetric i.i.d complex Gaussian noise with variance σ_z^2 , *i.e.*, $\mathbf{z}_n \sim \mathcal{CN}(\mathbf{0}, \sigma_z^2 \mathbf{I}_{KP})$.

Remark: Assumption (A1) indicates that the channel is modeled as Rayleigh-fading random vector. This assumption represents a standard model for a rich scattering environment in the absence of line-of-sight. An expression for a in terms of the channel Doppler

spread and the transmission bandwidth was shown in [87]. However, the first-order AR model possibly incurs considerable estimation error and results in numerous erroneous symbol decisions [103, 104]. One reason for making assumption (A2) is to satisfy the regularity conditions related to the evaluation of the Bayesian FIM described below. They require that the joint distribution of $p(\mathbf{y}_n, \tilde{\mathbf{x}}_n, \mathbf{h}_n)$ be absolutely continuous with respect to $x_{n,k}(p)$. A data vector modeled as Gaussian meets this criterion. For those transmit symbol vectors modeled on other distributions, the Theorem 6.1 gives an approximation. Another reason for making this assumption lies in the fact that a signal that is a zero-mean uncorrelated complex Gaussian distributed maximizes the lower bound (which is given with respect to a zero-mean uncorrelated complex Gaussian noise vector) on the mutual information between the input and the output for MIMO channels [97, 105]. Moreover, for a block transmission scheme such as an OFDM system with large number of subcarriers, the transmit symbol vector obtained by linear-precoding the information-symbol vector with an IDFT matrix can be claimed to be Gaussian by an appeal to the central limit theorem [106, Figure 4.21]. Hence, (A2) is not a particularly restrictive assumption.

6.3 Decoupled Channel and Symbol Estimation

An observation of (6.9) reveals that the knowledge of the MIMO channel vector is contained not only in the known training symbols, but also in the unknown information symbols. However, the joint estimation of the channel vector and the detection of the information symbol vector is a non-linear problem, and its solution may not exist in certain cases [92]. On the other hand, a sub-optimal approach is to decouple the channel estimation problem from the data detection process. In order to do so, we may consider the channel vector to be a deterministic unknown within the classical approach to statistical estimation or as a random vector by adapting the Bayesian viewpoint. In this work, we consider the latter approach and derive the FIM of the channel vector based on the (6.9). That is, we derive the Bayesian FIM concerning the estimation of the channel vector using $KP \times 1$ observations gathered from all the receive antennas at an arbitrary time instant, n . We then maximize the Bayesian FIM, which is equivalent to minimizing the Bayesian Cramer-Rao Lower Bound (CRLB) and obtain an orthogonality criterion. Finally, we formulate an affine precoder scheme that meets this condition.

6.3.1 Strategy: Bayesian FIM Maximization

Theorem 6.1. *Assuming that the likelihood function of $p(\mathbf{y}_n; \mathbf{h}_n)$ for the system model given in (6.9) satisfies the regularity condition, the complex FIM for estimating the MIMO channel is,*

$$\mathcal{I}(\mathbf{h}_n) = \sigma_z^{-2}(\mathbf{I}_K \otimes \mathbf{T}^H \mathbf{T}) - \sigma_z^{-4} \sigma_x^2 \Xi(\mathbf{t}, \mathbf{Q}) + \sigma_x^4 \Xi(\mathbf{Q}) + \sigma_h^{-2} \mathbf{I}_{K^2(L+1)} \quad (6.12)$$

where,

$$\Xi(\mathbf{t}, \mathbf{Q}) \triangleq \mathbb{E}_h \{ (\mathbf{I}_K \otimes \mathbf{T})^H \mathcal{H}_n \mathbf{Q} \mathbf{G} \mathbf{Q}^H \mathcal{H}_n^H (\mathbf{I}_K \otimes \mathbf{T}) \} \quad (6.13a)$$

$$\Xi(\mathbf{Q}) \triangleq \mathbb{E}_h \left\{ \sum_{n=0}^{KM-1} (\mathcal{Q}_n^H \otimes \mathbf{h}_n^T \mathcal{Q}_n^T) (\mathbf{R}_{y_n}^{-1} \otimes \mathbf{R}_{y_n}^{-T}) \sum_{n=0}^{KM-1} (\mathcal{Q}_n^* \otimes \mathcal{Q}_n \mathbf{h}_n) \right\} \quad (6.13b)$$

$$\mathbf{G} \triangleq (\mathbf{I}_{KM} + \sigma_z^{-2} \sigma_x^2 \mathbf{Q}^H \mathcal{H}_n^H \mathcal{H}_n \mathbf{Q})^{-1} \quad (6.13c)$$

$$\mathcal{Q}_n \triangleq \mathbf{I}_K \otimes [\mathcal{Q}_{n,1} \ \mathcal{Q}_{n,2} \ \cdots \ \mathcal{Q}_{n,K}] \quad (6.13d)$$

Proof. See Appendix C. □

Remark: The term, $\Xi(\mathbf{Q})$ represents the loss that is incurred due to the non-utilization of the information carried by the information symbols regarding the channel coefficients in a non decision-aided setup. Consequently, as it is independent of \mathbf{t} , the maximization of $\mathcal{I}(\mathbf{h}_n)$ in such a scenario is possible by working with $\Xi(\mathbf{t}, \mathbf{Q})$ alone. The maximization of $\mathcal{I}(\mathbf{h}_n)$ leads us to the the orthogonality condition shown in Theorem (6.2).

Theorem 6.2. *If the affine precoder scheme, (\mathbf{t}, \mathbf{Q}) satisfies conditions, (C1) and (C2), then the following orthogonality condition is necessary and sufficient for a non decision-aided training-only estimator to maximize the Bayesian FIM, $\mathcal{I}(\mathbf{h}_n)$ obtained in (6.12):*

$$\mathbf{T}_i^H \mathbf{Q}_{j,m} = \mathbf{0} \quad 1 \leq i, j \leq K \quad 0 \leq m \leq M-1 \quad (6.14)$$

Proof. See Appendix D. □

The expression for the Bayesian FIM that we have obtained in Theorem 6.1 is analogous to the result provided in [107, Lemma 1]. However, unlike in [107], the expression shown in (6.12) is in closed form. Moreover, as shown in Appendix C, we have not based this result on the block-diagonal structure of \mathbf{Q} . Hence the result in Theorem 6.1 is a general one. Also, the result that we derived in Theorem 6.2 was showed previously in [92] for SISO systems and in [108] for MIMO OFDM systems using minimum least-squares estimation error variance arguments. In [95] and [107], the orthogonality condition was derived within a Bayesian framework with the former relying on a LMMSE channel estimator while the latter uses a Bayesian FIM expression similar to our work. However, while we focus on a block diagonal structure of the linear precoder, [107] focuses on a general linear precoder matrix.

6.3.2 OFDM with FDM Training: An Orthogonal Affine Precoder Scheme

We see from [92, Theorem 1] for the case of a SISO system that the affine precoder scheme which uses linearly precoded OFDM along with an FDM training sequence that modulates a disjoint set of tones not used for data transmission, meets the orthogonality criterion. In other words, Theorem (6.3) establishes that although the the training symbols and information-bearing symbols overlap in time domain, orthogonality between the subcarriers in frequency domain satisfies (6.14).

Theorem 6.3. *The affine precoder scheme, (\mathbf{t}, \mathbf{Q}) that satisfies the orthogonality condition given in (6.14) irrespective of the FIR channel provides a non data-aided channel estimator if it is selected from the class*

$$\mathbf{Q}_k = \mathbf{W}^H \mathbf{P}^{(\mathbf{Q})} \begin{bmatrix} \boldsymbol{\Theta}_{M \times M} \\ \mathbf{0}_{V \times M} \end{bmatrix} \quad (6.15a)$$

$$\mathbf{t}_k = \mathbf{W}^H \mathbf{P}^{(\mathbf{t})} \begin{bmatrix} \tilde{\mathbf{t}}_k \\ \mathbf{0} \end{bmatrix} \quad (6.15b)$$

In the above equations, $\boldsymbol{\Theta}_{M \times M}$ is any full-rank matrix and $\mathbf{P}^{(\mathbf{t})}$ is a permutation matrix that places the $L + 1$ possible non-zero entries of $\tilde{\mathbf{t}}_k$ on non data-bearing subcarriers.

Proof. The proof is a straight-forward generalization of [92, Appendix I]. □

In the subsequent sections, we focus our analysis on a MIMO-OFDM communication system. That is, we assume $\tilde{\mathbf{x}}_{n,\bar{k}}$ to be the result of a linear-precoding operation involving a general full-rank matrix, $\Theta_{M \times M}$ before it is IDFT-modulated. Moreover, the same set of subcarriers are used for transmitting training symbols across all the antennas.

Training Phase By substituting the result of Theorem 6.3 in (6.6), and considering the signal at an arbitrary receive antenna, k , we write the following equation:

$$\begin{aligned} \mathbf{y}_{n,k} &= \sum_{\bar{k}=1}^K \mathbf{H}_{k,\bar{k}}^{(n)} \mathbf{t}_{\bar{k}} + \sum_{\bar{k}=1}^K \mathbf{H}_{k,\bar{k}}^{(n)} \mathbf{Q}_{\bar{k}} \tilde{\mathbf{x}}_{n,\bar{k}} + \mathbf{z}_{n,k} \\ &= \sum_{\bar{k}=1}^K \mathbf{H}_{k,\bar{k}}^{(n)} \mathcal{W}^H \mathbf{P}^{(t)} \begin{bmatrix} \tilde{\mathbf{t}}_{\bar{k}} \\ \mathbf{0} \end{bmatrix} + \sum_{\bar{k}=1}^K \mathbf{H}_{k,\bar{k}}^{(n)} \mathcal{W}^H \mathbf{P}^{(Q)} \begin{bmatrix} \mathbf{I}_{M \times M} \\ \mathbf{0}_{V \times M} \end{bmatrix} \tilde{\mathbf{x}}_{n,\bar{k}} + \mathbf{z}_{n,k} \end{aligned} \quad (6.16)$$

By multiplying the above equation with $\mathbf{P}_{0:V-1}^{(t)\top} \mathcal{W}$, we notice that the channel estimation is decoupled from data detection so that the following expression is obtained

$$\mathbf{P}_{0:V-1}^{(t)\top} \mathcal{W} \mathbf{y}_{n,k} = \sum_{\bar{k}=1}^K \mathbf{P}_{0:V-1}^{(t)\top} \tilde{\mathbf{H}}_{k,\bar{k}}^{(n)} \mathbf{P}_{0:V-1}^{(t)} \tilde{\mathbf{t}}_{\bar{k}} + \mathbf{P}_{0:V-1}^{(t)\top} \mathcal{W} \mathbf{z}_{n,k} \quad (6.17)$$

where $\tilde{\mathbf{H}}_{k,\bar{k}}^{(n)} \triangleq \mathcal{W} \mathbf{H}_{k,\bar{k}}^{(n)} \mathcal{W}^H$ is a diagonal matrix (cf., Section 2.4) and $\mathbf{P}_{0:V-1}^{(t)}$ is the result of disregarding the zero entries in $[\tilde{\mathbf{t}}_{\bar{k}}^H \mathbf{0}^H]^H$. Moreover, we have utilized the fact that $\mathbf{P}_{0:V-1}^{(t)\top} \mathbf{P}_{0:M}^{(Q)} = \mathbf{0}$ *i.e.*, the submatrices, $\mathbf{P}_{0:V-1}^{(t)}$ and $\mathbf{P}_{0:M}^{(Q)}$ are orthogonal to each other. We also recognize that the following relationship holds due to the diagonal nature of $\tilde{\mathbf{H}}_{k,\bar{k}}^{(n)}$:

$$\mathbf{P}_{0:V-1}^{(t)\top} \tilde{\mathbf{H}}_{k,\bar{k}}^{(n)} \mathbf{P}_{0:V-1}^{(t)} \tilde{\mathbf{t}}_{\bar{k}} = \sqrt{P} \tilde{\mathbf{T}}_{\bar{k}} \mathbf{P}_{0:V-1}^{(t)\top} \mathcal{W}_{0:L} \mathbf{h}_{k,\bar{k}}^{(n)} = \tilde{\mathbf{T}}_{\bar{k}} \hat{\mathcal{W}}_{0:L} \mathbf{h}_{k,\bar{k}}^{(n)} \quad (6.18)$$

where $\tilde{\mathbf{T}}_{\bar{k}} \triangleq \text{diag}(\tilde{\mathbf{t}}_{\bar{k}})$ and $\hat{\mathcal{W}}_{0:L} \triangleq \sqrt{P} \mathbf{P}_{0:V-1}^{(t)\top} \mathcal{W}_{0:L}$. As a result, (6.17) can be written as:

$$\tilde{\mathbf{y}}_{n,k}^{(t)} = \tilde{\mathbf{T}} \mathbf{h}_{n,k} + \tilde{\mathbf{z}}_{n,k} \quad (6.19)$$

where $\tilde{\mathbf{y}}_{n,k}^{(t)} \triangleq \hat{\mathcal{W}}_{0:L} \mathbf{y}_{n,k}$ and

$$\tilde{\mathbf{T}} \triangleq [\tilde{\mathbf{T}}_1 \hat{\mathcal{W}}_{0:L} \quad \tilde{\mathbf{T}}_2 \hat{\mathcal{W}}_{0:L} \quad \dots \quad \tilde{\mathbf{T}}_K \hat{\mathcal{W}}_{0:L}] \quad (6.20)$$

Also, it can be showed that $\mathbf{T}_k^H \mathbf{T}_k = \hat{\mathbf{W}}_{0:L}^H \tilde{\mathbf{T}}_k^* \tilde{\mathbf{T}}_k \hat{\mathbf{W}}_{0:L}$. By defining the vector, $\tilde{\mathbf{y}}_n^{(t)} \triangleq \text{vec}([\tilde{\mathbf{y}}_{n,1}^{(t)} \tilde{\mathbf{y}}_{n,2}^{(t)} \dots \tilde{\mathbf{y}}_{n,K}^{(t)}])$, we can write the MIMO system model for the measured signal across all receive antennas due to the pilot tones as follows:

$$\tilde{\mathbf{y}}_n^{(t)} = (\mathbf{I}_K \otimes \tilde{\mathbf{T}}) \mathbf{h}_n + \tilde{\mathbf{z}}_n \quad (6.21)$$

We can now enforce two more standard conditions regarding the structure of $\tilde{\mathbf{T}}$ to satisfy the dimensionality of (6.21).

(C4) The $V \times K(L+1)$ dimensional training matrix, $\tilde{\mathbf{T}}$ is a tall matrix, *i.e.*, $V \geq K(L+1)$.

(C5) The matrix, $\tilde{\mathbf{T}}$ is of full column-rank, *i.e.*, $\text{rank}(\tilde{\mathbf{T}}) = K(L+1)$.

By employing operations similar to those that helped in obtaining (6.21), the equation for the observation vector affected by the information symbols alone is as follows:

$$\tilde{\mathbf{y}}_n^{(dt)} = \tilde{\mathcal{H}}_n \tilde{\mathbf{x}}_n + \tilde{\mathbf{z}}_n \quad (6.22)$$

where the $KM \times KM$ channel matrix, $\tilde{\mathcal{H}}_n$ is as follows:

$$\tilde{\mathcal{H}}_n \triangleq \begin{bmatrix} \tilde{\mathbf{H}}_{1,1}^{(n)} & \tilde{\mathbf{H}}_{1,2}^{(n)} & \cdots & \tilde{\mathbf{H}}_{1,K}^{(n)} \\ \tilde{\mathbf{H}}_{2,1}^{(n)} & \tilde{\mathbf{H}}_{2,2}^{(n)} & \cdots & \tilde{\mathbf{H}}_{2,K}^{(n)} \\ \vdots & \vdots & \ddots & \vdots \\ \tilde{\mathbf{H}}_{K,1}^{(n)} & \tilde{\mathbf{H}}_{K,2}^{(n)} & \cdots & \tilde{\mathbf{H}}_{K,K}^{(n)} \end{bmatrix} \quad (6.23)$$

Each matrix in the set, $\{\tilde{\mathbf{H}}_{i,j}^{(n)}\}$ for $1 \leq i \leq K$, $1 \leq j \leq K$ is a diagonal matrix and is obtained by performing the operation,

$$\tilde{\mathbf{H}}_{i,k}^{(n)} = \mathbf{P}_{0:M-1}^{(\mathbf{Q})\top} \bar{\mathbf{H}}_{i,k}^{(n)} \mathbf{P}_{0:M-1}^{(\mathbf{Q})} \quad (6.24)$$

Data Transmission Phase Although the linear precoder matrix, $\bar{\mathbf{Q}}$ can be any full-column rank matrix in general, we focus on a block diagonal structure. We consider each element in the set, $\{\bar{\mathbf{Q}}_k\}$ to be a $P \times P$ IDFT matrix that modulates an information symbol vector which has been linearly precoded by a general full-rank matrix, $\bar{\Theta}_{P \times P}$.

$$\tilde{\mathbf{r}}_n = \bar{\mathcal{H}}_n \tilde{\mathbf{s}}_n + \tilde{\mathbf{z}}_n \quad (6.25)$$

where $\tilde{\mathbf{r}}_n \triangleq \mathbf{W} \mathbf{r}_n$ and the $KP \times KP$ channel matrix, $\overline{\mathcal{H}}_n$ is defined as follows:

$$\overline{\mathcal{H}}_n \triangleq \begin{bmatrix} \bar{\mathbf{H}}_{1,1}^{(n)} & \bar{\mathbf{H}}_{1,2}^{(n)} & \cdots & \bar{\mathbf{H}}_{1,K}^{(n)} \\ \bar{\mathbf{H}}_{2,1}^{(n)} & \bar{\mathbf{H}}_{2,2}^{(n)} & \cdots & \bar{\mathbf{H}}_{2,K}^{(n)} \\ \vdots & \vdots & \ddots & \vdots \\ \bar{\mathbf{H}}_{K,1}^{(n)} & \bar{\mathbf{H}}_{K,2}^{(n)} & \cdots & \bar{\mathbf{H}}_{K,K}^{(n)} \end{bmatrix} \quad (6.26)$$

Remark: By enforcing the orthogonality condition and by choosing MIMO-OFDM with FDM training symbols as the affine precoder scheme, we have broken down (6.9) into (6.21) and (6.22). As a result, the impact of overlapping data-bearing symbols on the channel estimator has been circumvented. Moreover, we carryover the linear precoder from the training phase to the data transmission phase by introducing a simple modification on the structure of the IDFT matrix. A different problem which deals with transmit and receiver precoder design under the assumption that CSI is available at the transmitter has been studied extensively in the published literature *e.g.*, see [35, 109, 110].

Before we study the MMSE characteristics during training and data transmission phases when a Kalman filter is employed to track the time-varying channel vector, \mathbf{h}_n we note that the following time and power budget constraints are enforced over (6.21), (6.22) and (6.25),

$$N = N_t + N_d \quad (6.27a)$$

$$\mathcal{P} N = (\mathcal{P}_t + \mathcal{P}_{dt}) N_t + \mathcal{P}_d N_d \quad (6.27b)$$

where \mathcal{P} is the total average transmit power that is split into \mathcal{P}_t , the average power allocated for training, \mathcal{P}_{dt} , the average power allocated for information symbols in the training phase, and \mathcal{P}_d , the average power allocated for information symbols in the data transmission phase. Additionally, \mathcal{P}_t is distributed equally among the transmit antennas *i.e.*,

$$\mathcal{P}_t = \|\mathbf{t}\|^2 = \sum_{k=1}^K \|\mathbf{t}_k\|^2 \quad (6.28)$$

where $\|\mathbf{t}_k\|^2 = \sum_{v=0}^{V-1} |\tilde{\mathbf{T}}_k[v]|^2 = \mathcal{P}_t/K$, $\forall 1 \leq k \leq K$.

6.4 Blockwise Kalman Tracking

Due to the AR(1) random process model for time-variations on the channel vector, in order to compute the channel estimator in the MMSE sense, we have to utilize the past and the current observations, $\{\tilde{\mathbf{y}}_{nN+k}^{(t)} : k \in [0, N_t - 1], n = 1, 2, \dots\}$. An MMSE channel estimator can then be given as,

$$\hat{\mathbf{h}}_{nN+k} = \mathbb{E} \{ \mathbf{h}_{nN+k} \mid \{ \tilde{\mathbf{y}}_{nN+j}^{(t)} : j \leq k, j \in [0, N_t - 1] \}, \{ \tilde{\mathbf{y}}_{(n-m)N+j}^{(t)} : j \in [0, N_t - 1], m = 1, 2, \dots \} \} \quad (6.29)$$

However, a batch processing approach would necessitate the use of large datasets. A natural choice is the sequential MMSE approach and is implemented by a Kalman filter. A Kalman filter is well-known for its computationally efficiency which results from the fact that only the most recent estimate need to be stored in order to refine the MMSE estimate of the unknown parameter of interest based on the new observations. For the current problem at hand, we compute the channel estimate during the training phase based on (6.21) and utilize the predicted channel vector in the data transmission phase. The Kalman filter recursion algorithm for estimating a vector parameter based on vector observations is summarized in (6.30a)–(6.30e) [111].

6.4.1 Kalman Filter Recursion

It can be noticed that when the system converges to a steady state, the MMSE of the channel estimator is not stationary during each cycle of N blocks. In the data transmission phase, the MMSE associated with the channel estimator's predicted state increases monotonically from the N_t th block to the $(N - 1)$ th block. Thus, the maximum steady state MMSE in the data transmission phase occurs at the last information symbol block of each cycle. On the other hand, since the channel estimator computed based on the observations of the 0th block in n th cycle refines the predicted channel state at the end of the last information symbol block of $(n - 1)$ th cycle, the steady state MMSE decreases monotonically from the 0th training block to the $(N_t - 1)$ th training block. Before we derive the steady state MMSE expressions for the two cases described above, we derive the steady state MMSE when all the blocks are training symbols and make an interesting observation. The steady state MMSE when all blocks are training symbols is given by the

Prediction:

$$\hat{\mathbf{h}}_{n|n-1} = a\hat{\mathbf{h}}_{n-1|n-1} \quad (6.30a)$$

Minimum Prediction MSE Matrix:

$$\mathbf{M}_{n|n-1} = a^2\mathbf{M}_{n-1|n-1} + (1 - a^2)\sigma_h^2\mathbf{I}_{K^2(L+1)} \quad (6.30b)$$

Kalman Gain Matrix:

$$\mathbf{K}_n = \mathbf{M}_{n|n-1} (\mathbf{I}_K \otimes \tilde{\mathbf{T}}^H) (\sigma_z^2\mathbf{I}_{KP} + (\mathbf{I}_K \otimes \tilde{\mathbf{T}}) \mathbf{M}_{n|n-1} (\mathbf{I}_K \otimes \tilde{\mathbf{T}}^H))^{-1} \quad (6.30c)$$

Correction:

$$\hat{\mathbf{h}}_{n|n} = \hat{\mathbf{h}}_{n|n-1} + \mathbf{K}_n (\tilde{\mathbf{y}}_n^{(t)} - (\mathbf{I}_K \otimes \tilde{\mathbf{T}}) \hat{\mathbf{h}}_{n|n-1}) \quad (6.30d)$$

Minimum MSE Matrix:

$$\mathbf{M}_{n|n} = (\mathbf{I} - \mathbf{K}_n (\mathbf{I}_K \otimes \tilde{\mathbf{T}})) \mathbf{M}_{n|n-1} \quad (6.30e)$$

solution to the Ricatti equation,

$$\mathbf{M}^{(\infty)} = (\mathbf{I} - \mathbf{K}^{(\infty)} (\mathbf{I}_K \otimes \tilde{\mathbf{T}})) \mathbf{M}_1^{(\infty)} \quad (6.31)$$

where $\mathbf{M}^{(\infty)} \triangleq \lim_{n \rightarrow \infty} \mathbf{M}_{n|n}$, $\mathbf{M}_1^{(\infty)} \triangleq \lim_{n \rightarrow \infty} \mathbf{M}_{n|n-1}$, and $\mathbf{K}^{(\infty)} \triangleq \lim_{n \rightarrow \infty} \mathbf{K}_n$. Although several techniques have been proposed in the published literature to solve the system of equations obtained in (6.31) such as eigenvector solutions [112], Schur vector approaches [113], iterative solving for scalar polynomials [114] etc., we will show that by utilizing the following lemma describing the optimal design of the training symbols in the MMSE sense, the above system of equations is greatly simplified.

Lemma 6.1. *For the system model shown in (6.21), the minimum error variance of the MMSE channel estimator is,*

$$\sigma_{\Delta \mathbf{h}_n}^2 = \frac{K^3(L+1)\sigma_z^2\sigma_h^2}{K\sigma_z^2 + \sigma_h^2\mathcal{P}_t} \quad (6.32)$$

The optimal $\tilde{\mathbf{T}}$, $\tilde{\mathbf{T}}^{(opt)}$ that attains this error variance is,

$$\tilde{\mathbf{T}}^{(opt)} = [(\boldsymbol{\mathcal{E}}_1 \boldsymbol{\phi}(V))^T \dots (\boldsymbol{\mathcal{E}}_K \boldsymbol{\phi}(V))^T]^T \quad (6.33)$$

where,

$$[\boldsymbol{\mathcal{E}}_k]_{v,v} = \exp \left[\frac{j2\pi v f_k}{V} \right] \quad (6.34a)$$

$$\forall \quad 0 \leq v \leq V-1, \quad 1 \leq k \leq K$$

$$\boldsymbol{\phi}(V) = \sqrt{\frac{\mathcal{P}_t}{KV}} [\exp(j\phi_0) \quad \exp(j\phi_1) \quad \dots \quad \exp(j\phi_{V-1})]^T \quad (6.34b)$$

$$f_k = k(V-L-1) \quad (6.34c)$$

$$\{\phi_v\} \in [-\pi, \pi] \quad (6.35)$$

Proof. See Appendix E. □

Remark: By employing the training design described in (6.33), $\tilde{\mathbf{T}}^H \tilde{\mathbf{T}}$ in (E.7) is diagonal and the MMSE of (6.32) is attained. The time-domain training sequences can be obtained from (6.15b) in a straight-forward manner by using the relation, $\mathbf{t} = (\mathbf{I}_K \otimes \boldsymbol{\mathcal{W}}^H \mathbf{P}_{0:V-1}^{(t)}) \tilde{\mathbf{T}}$. It can be noticed that a simple way of making the term, $\tilde{\mathbf{T}}_{k_1}^*[v, v] \tilde{\mathbf{T}}_{k_2}[v, v]$ in (E.13) equal to zero is to allow only $(L+1)$ out of V subcarriers dedicated for training symbols to be used at any given antenna. These equispaced and equipowered training symbols occupy disjoint sets of subcarriers at each transmit antenna. Clearly, such a scheme utilizes only $(L+1)$ out of V subcarriers dedicated for training symbols at any given antenna. On the other hand, a general training scheme design described in (6.33) uses all non data-bearing subcarriers, *i.e.*, V for channel estimation purposes.

In [95], disjoint sets of subcarriers were considered to reduce the MMSE channel estimation error. Training designs similar to ours were shown in [108] by minimizing the least-squares channel estimation error and in [99] by minimizing the MSE of the LMMSE channel estimate. In [115], several classes of training schemes are derived by minimizing the least-squares channel estimation error. In this work, the disjoint allocation of subcarriers for training symbols from different antennas is referred to as a *frequency domain multiplexing* (FDM) scheme and the phase-shift orthogonal design as a *code-division multiplexing in the frequency domain* (CDM(F)) scheme.

Remark: If we were to initialize the Kalman recursion by substituting the scaled identity covariance matrix of \mathbf{h}_n for $\mathbf{M}_{-1|-1}$, the one-step prediction error matrix, $\mathbf{M}_{n|n-1}$ is always a scaled identity matrix. Consequently, the matrix $\tilde{\mathbf{K}}_n \triangleq \mathbf{K}_n (\mathbf{I}_K \otimes \tilde{\mathbf{T}})$ is also a scaled identity matrix since $(\mathbf{I}_K \otimes \tilde{\mathbf{T}}^H \tilde{\mathbf{T}})$ is designed to be a scaled identity matrix. This is better understood by writing the alternative version of the Kalman gain matrix using the matrix inversion lemma²:

$$\begin{aligned} \mathbf{K}_n &= \sigma_z^{-2} \mathbf{M}_{n|n-1} (\mathbf{I}_K \otimes \tilde{\mathbf{T}}^H) \\ &\quad - \sigma_z^{-4} \mathbf{M}_{n|n-1} (\mathbf{I}_K \otimes \tilde{\mathbf{T}}^H \tilde{\mathbf{T}}) (\mathbf{M}_{n|n-1}^{-1} + (\mathbf{I}_K \otimes \tilde{\mathbf{T}}^H \tilde{\mathbf{T}}))^{-1} (\mathbf{I}_K \otimes \tilde{\mathbf{T}}^H) \end{aligned} \quad (6.36)$$

As an extension of the above remark, due to assumption, (A1) and the optimal training design described by Lemma 6.1, $\mathbf{M}^{(\infty)}$ is also a scaled identity matrix. It can be showed that an arbitrary diagonal element, $\mathbf{m}^{(\infty)} \triangleq \mathbf{M}^{(\infty)}[l, l]$, $0 \leq l \leq K^2(L+1) - 1$ is given as follows:

$$\begin{aligned} \mathbf{m}^{(\infty)} &= \frac{\sigma_z^2 (a^2 \mathbf{m}^{(\infty)} + \sigma_u^2)}{\sigma_z^2 + \frac{\mathcal{P}_t}{K} (a^2 \mathbf{m}^{(\infty)} + \sigma_u^2)} \\ &= \frac{\sigma_h^2}{\frac{1}{2} \left(1 + \frac{\sigma_h^2 \mathcal{P}_t}{\sigma_z^2 K} \right) + \sqrt{\frac{1}{4} \left(1 + \frac{\sigma_h^2 \mathcal{P}_t}{\sigma_z^2 K} \right)^2 + \frac{a^2}{1-a^2} \frac{\sigma_h^2 \mathcal{P}_t}{\sigma_z^2 K}}} \end{aligned} \quad (6.37)$$

This steady-state Ricatti solution is the lower bound on the MMSE for estimating any of the $K^2(L+1)$ channel filter taps, irrespective of the particular phase being considered. To compute the steady state MMSE characteristics, we let $n \rightarrow \infty$, and define,

$$\mathbf{M}_j^{(\infty)} \triangleq \lim_{n \rightarrow \infty} \mathbf{M}_{nN+j|nN+j} \quad (6.38)$$

for $j \in [0, N-1]$. We can now review the closed-form expressions for steady state channel MMSEs in training and data transmission phases based on [116].

Lemma 6.2. *When the training vectors are designed according to (6.33) and a Kalman filter is employed to perform channel tracking, the steady state channel MMSEs for the*

$${}^2(\mathbf{A} + \mathbf{B} \mathbf{C} \mathbf{D})^{-1} = \mathbf{A}^{-1} - \mathbf{A}^{-1} \mathbf{B} (\mathbf{C}^{-1} + \mathbf{D} \mathbf{A}^{-1} \mathbf{B})^{-1} \mathbf{D} \mathbf{A}^{-1}$$

system model corresponding to (6.21), (6.22) and (6.25) are given as follows:

$$\mathbf{m}_{N-1}^{(\infty)} = \delta_{N-1}^{(\infty)}[l, l] + \mathbf{m}^{(\infty)} \quad (6.39a)$$

Training Phase ($j \in [0, N_t - 1]$):

$$\mathbf{m}_j^{(\infty)} = \mathbf{m}^{(\infty)} + \frac{(1 - \alpha) \delta_{N-1}^{(\infty)}[l, l]}{\beta (1 - \alpha^j) \delta_{N-1}^{(\infty)}[l, l] + \alpha^j (1 - \alpha)} \quad (6.39b)$$

Data Transmission Phase ($j \in [N_t, N - 1]$):

$$\mathbf{m}_j^{(\infty)} = \frac{\mathbf{m}_{N-1}^{(\infty)} - \sigma_h^2 (1 - a^{2(N-j)})}{a^{2(N-j)}} \quad (6.39c)$$

where $\mathbf{m}_j^{(\infty)} \triangleq \mathbf{M}_j^{(\infty)}[l, l]$ and $\delta_{N-1}^{(\infty)}[l, l]$ is computed as follows:

$$\delta_{N-1}^{(\infty)}[l, l] = -b_\infty + \sqrt{b_\infty^2 + c_\infty} \quad (6.40a)$$

$$b_\infty \triangleq \left(\frac{\alpha^{N_t} - a^{2(N-N_t)}}{\alpha^{N-t} - 1} \right) \left(\frac{\alpha - 1}{2\beta} \right) - \left(\frac{1 - a^{2(N-N_t)}}{2} \right) (\sigma_h^2 - \mathbf{m}^{(\infty)}) \quad (6.40b)$$

$$c_\infty \triangleq \alpha^{N_t} \left(\frac{1 - a^{2(N-N_t)}}{\alpha^{N_t} - 1} \right) \left(\frac{\alpha - 1}{\beta} \right) (\sigma_h^2 - \mathbf{m}^{(\infty)}) \quad (6.40c)$$

$$\alpha \triangleq \frac{1}{a^2} \left(1 + (\sigma_h^2 - a^2(\sigma_h^2 - \mathbf{m}^{(\infty)})) \frac{\mathcal{P}_t}{K} \right)^2 \quad (6.40d)$$

$$\beta \triangleq \frac{\mathcal{P}_t}{K} \left(1 + (\sigma_h^2 - a^2(\sigma_h^2 - \mathbf{m}^{(\infty)})) \frac{\mathcal{P}_t}{K} \right) \quad (6.40e)$$

Proof. See proof of Lemma 1 in [116]. □

6.5 Capacity Bounds with Sequential MMSE Channel Estimation

Similar to [97], we consider the capacity in bits per channel use to be the maximum over the distribution of the transmit signal of the mutual information between the known training symbols and the observations and the unknown transmitted signal. In other words, for the system model shown in (6.21), (6.22) and (6.25), the channel capacity averaged over

the random channel is defined as follows:

$$\begin{aligned}
C &= \frac{1}{N} \times \frac{M}{P} \sum_{n=0}^{N_t-1} \mathbb{E} \left[\max_{p_x(\cdot), \mathbb{E}[\|\tilde{\mathbf{x}}_n\|^2]=\mathcal{P}_{dt}} \mathbf{I}(\tilde{\mathbf{y}}_n^{(dt)}; \tilde{\mathbf{x}}_n | \widehat{\mathcal{H}}_n) \right] \\
&+ \frac{1}{N} \sum_{n=N_t}^{N-1} \mathbb{E} \left[\max_{p_s(\cdot), \mathbb{E}[\|\tilde{\mathbf{s}}_n\|^2]=\mathcal{P}_d} \mathbf{I}(\tilde{\mathbf{r}}_n; \tilde{\mathbf{s}}_n | \widehat{\mathcal{H}}_n) \right] \quad \text{bits/channel use} \quad (6.41)
\end{aligned}$$

6.5.1 Upper Bound on the Channel Capacity

To benchmark the maximum achievable capacity, we consider the ideal scenario where the channel estimation is perfect. We also utilize the Gaussianity assumption on the distribution of the information symbol vectors, $\tilde{\mathbf{x}}_n$ and $\tilde{\mathbf{s}}_n$ due to (A2) in the channel capacity expression. We now have the following result:

Theorem 6.4. *The upper bound on the channel capacity for the system model shown in (6.21), (6.22) and (6.25) is obtained when the information symbol vectors, $\tilde{\mathbf{x}}_n$ and $\tilde{\mathbf{s}}_n$ are Gaussian distributed and is given by the expression:*

$$\begin{aligned}
C_u &= \frac{N_t}{N} \times \frac{M}{P} \mathbb{E} \left[\max_{p_x(\cdot), \mathbb{E}[\|\tilde{\mathbf{x}}_n\|^2]=\mathcal{P}_{dt}} \mathbf{I}(\tilde{\mathbf{y}}_0^{(dt)}; \tilde{\mathbf{x}}_0 | \tilde{\mathcal{H}}_0) \right] \\
&+ \frac{N_d}{N} \mathbb{E} \left[\max_{p_s(\cdot), \mathbb{E}[\|\tilde{\mathbf{s}}_n\|^2]=\mathcal{P}_d} \mathbf{I}(\tilde{\mathbf{r}}_{N_t}; \tilde{\mathbf{s}}_{N_t} | \overline{\mathcal{H}}_{N_t}) \right] \quad \text{bits/channel use} \\
&= \frac{N_t}{N} \times \frac{M}{P} \mathbb{E} \left[\log \det \left(\mathbf{I}_{KM} + \frac{\mathcal{P}_{dt}}{\sigma_z^2} \tilde{\mathcal{H}}_0 \tilde{\mathcal{H}}_0^H \right) \right] \\
&+ \frac{N_d}{N} \mathbb{E} \left[\log \det \left(\mathbf{I}_{KP} + \frac{\mathcal{P}_d}{\sigma_z^2} \overline{\mathcal{H}}_{N_t} \overline{\mathcal{H}}_{N_t}^H \right) \right] \quad \text{bits/channel use} \quad (6.42)
\end{aligned}$$

Proof. See Appendix F. □

6.5.2 Lower Bound on the Channel Capacity

From [87] and [97, Theorem 1], we know that the lower bound on the mutual information between the channel input and its output is obtained when the additive noise is Gaussian distributed. In other words, when imperfect channel estimates are employed for estimating information symbols, a zero-mean uncorrelated complex Gaussian noise vector minimizes the upper bound over the distribution of the information symbol vector of the mutual

information between the transmitted and observed information symbols. For the problem under consideration, the following signal model can be written by expressing the estimated channel matrix, as a sum of the conditional mean, and the random error component,

$$\tilde{\mathbf{y}}_n^{(d)} = \widehat{\mathcal{H}}_n \tilde{\mathbf{x}}_n + \check{\mathcal{H}}_n \tilde{\mathbf{x}}_n + \tilde{\mathbf{z}}_n = \widehat{\mathcal{H}}_n \tilde{\mathbf{x}}_n + (\mathbf{I}_K \otimes \tilde{\mathbf{X}}_n) \check{\mathbf{h}}_n + \tilde{\mathbf{z}}_n \quad (6.43a)$$

$$\tilde{\mathbf{r}}_n = \widehat{\mathcal{H}}_n \tilde{\mathbf{s}}_n + \check{\mathcal{H}}_n \tilde{\mathbf{s}}_n + \tilde{\mathbf{z}}_n = \widehat{\mathcal{H}}_n \tilde{\mathbf{s}}_n + (\mathbf{I}_K \otimes \tilde{\mathbf{S}}_n) \check{\mathbf{h}}_n + \tilde{\mathbf{z}}_n \quad (6.43b)$$

In (6.43a), we made use of the following relationship,

$$\mathbf{P}_{0:M-1}^{(Q)\top} \bar{\mathbf{H}}_{k,\bar{k}}^{(n)} \mathbf{P}_{0:M-1}^{(Q)} \tilde{\mathbf{x}}_{n,\bar{k}} = \sqrt{P} \tilde{\mathbf{X}}_{n,\bar{k}} \mathbf{P}_{0:M-1}^{(Q)\top} \mathcal{W}_{0:L} \mathbf{h}_{k,\bar{k}}^{(n)} = \tilde{\mathbf{X}}_{n,\bar{k}} \check{\mathcal{W}}_{0:L} \mathbf{h}_{k,\bar{k}}^{(n)} \quad (6.44)$$

where $\tilde{\mathbf{X}}_{n,\bar{k}} \triangleq \text{diag}(\tilde{\mathbf{x}}_{n,\bar{k}})$, $\check{\mathcal{W}}_{0:L} \triangleq \sqrt{P} \mathbf{P}_{0:M-1}^{(Q)\top} \mathcal{W}_{0:L}$ and

$$\tilde{\mathbf{X}}_n \triangleq [\tilde{\mathbf{X}}_{n,1} \check{\mathcal{W}}_{0:L} \quad \tilde{\mathbf{X}}_{n,2} \check{\mathcal{W}}_{0:L} \quad \dots \quad \tilde{\mathbf{X}}_{n,K} \check{\mathcal{W}}_{0:L}] \quad (6.45)$$

Similarly, in (6.43b), we made use of the following relationship,

$$\bar{\mathbf{H}}_{k,\bar{k}}^{(n)} \tilde{\mathbf{s}}_{n,\bar{k}} = \sqrt{P} \tilde{\mathbf{S}}_{n,\bar{k}} \mathcal{W}_{0:L} \mathbf{h}_{k,\bar{k}}^{(n)} \quad (6.46)$$

where $\tilde{\mathbf{S}}_{n,\bar{k}} \triangleq \text{diag}(\tilde{\mathbf{s}}_{n,\bar{k}})$ and

$$\tilde{\mathbf{S}}_n \triangleq [\sqrt{P} \tilde{\mathbf{S}}_{n,1} \mathcal{W}_{0:L} \quad \sqrt{P} \tilde{\mathbf{S}}_{n,2} \mathcal{W}_{0:L} \quad \dots \quad \sqrt{P} \tilde{\mathbf{S}}_{n,K} \mathcal{W}_{0:L}] \quad (6.47)$$

It should be observed that in (6.22) and (6.25), the channel is unknown whereas in (6.43a) and (6.43b), the channel is known. Furthermore, the additive noise in the former two equations is Gaussian and independent of the information symbols whereas in the latter two, it is possibly neither. This is due to the fact that each of the effective additive noise vectors, $\tilde{\mathbf{z}}_n^{(dt)} \triangleq (\mathbf{I}_K \otimes \tilde{\mathbf{X}}_n) \check{\mathbf{h}}_n + \tilde{\mathbf{z}}_n$ and $\tilde{\mathbf{z}}_n^{(d)} \triangleq (\mathbf{I}_K \otimes \tilde{\mathbf{S}}_n) \check{\mathbf{h}}_n + \tilde{\mathbf{z}}_n$ appear to be a sum of a Gaussian vector and a vector whose elements are obtained by summing products of Gaussian random variables. As a result, we will merely derive the lower bound by replacing the effective noise vectors, with Gaussian noise vectors that possess the same average powers. The expressions for the average noise powers in each phase are as shown below.

Training Phase

$$\begin{aligned}
\sigma_{z^{(dt)}}^2(n) &= \frac{1}{KM} \mathbb{E}\{ \text{trace}\{ \tilde{\mathbf{z}}_n^{(dt)} \tilde{\mathbf{z}}_n^{(dt)\text{H}} \} \} \\
&= \frac{1}{M} \mathbf{m}_k^{(\infty)} \mathbb{E}\{ \text{trace}\{ \tilde{\mathbf{X}}_n \tilde{\mathbf{X}}_n^{\text{H}} \} \} + \sigma_z^2 \\
&= \frac{1}{M} \mathbf{m}_n^{(\infty)} \sum_{k=1}^K \mathbb{E}\{ \text{trace}\{ \tilde{\mathbf{X}}_{n,k} \check{\mathbf{W}}_{0:L} \check{\mathbf{W}}_{0:L}^{\text{H}} \tilde{\mathbf{X}}_{n,k}^{\text{H}} \} \} + \sigma_z^2 \\
&= \frac{L+1}{M} \mathbf{m}_n^{(\infty)} \sum_{k=1}^K \sum_{m=0}^{M-1} \mathbb{E}\{ |\tilde{\mathbf{X}}_{n,k}[m, m]|^2 \} + \sigma_z^2 \\
&= \frac{L+1}{M} \mathbf{m}_n^{(\infty)} M \sigma_x^2 + \sigma_z^2 \\
&= (L+1) \mathcal{P}_{dt} \mathbf{m}_n^{(\infty)} + \sigma_z^2 \quad n \in [0, N_t - 1]
\end{aligned} \tag{6.48}$$

where we substituted, $\sigma_x^2 = \mathcal{P}_{dt}$ to account for the power budget on the transmit symbols in the training phase.

Data Transmission Phase

$$\begin{aligned}
\sigma_{z^{(d)}}^2(n) &= \frac{1}{KP} \mathbb{E}\{ \text{trace}\{ \tilde{\mathbf{z}}_n^{(d)} \tilde{\mathbf{z}}_n^{(d)\text{H}} \} \} \\
&= \frac{1}{P} \mathbf{m}_n^{(\infty)} \mathbb{E}\{ \text{trace}\{ \tilde{\mathbf{S}}_n \tilde{\mathbf{S}}_n^{\text{H}} \} \} + \sigma_z^2 \\
&= \frac{1}{P} \mathbf{m}_n^{(\infty)} \sum_{k=1}^K \mathbb{E}\{ \text{trace}\{ P \tilde{\mathbf{S}}_{n,k} \check{\mathbf{W}}_{0:L} \check{\mathbf{W}}_{0:L}^{\text{H}} \tilde{\mathbf{S}}_{n,k}^{\text{H}} \} \} + \sigma_z^2 \\
&= \frac{L+1}{P} \mathbf{m}_n^{(\infty)} \sum_{k=1}^K \sum_{p=0}^{P-1} \mathbb{E}\{ |\tilde{\mathbf{S}}_{n,k}[p, p]|^2 \} + \sigma_z^2 \\
&= \frac{L+1}{P} \mathbf{m}_n^{(\infty)} K \sigma_s^2 + \sigma_z^2 \\
&= (L+1) \mathcal{P}_d \mathbf{m}_n^{(\infty)} + \sigma_z^2 \quad n \in [N_t, N - 1]
\end{aligned} \tag{6.49}$$

where we substituted, $\sigma_s^2 = \mathcal{P}_d$ to account for the power budget on the transmit symbols in the data transmission phase.

The lower bound on the channel capacity when the estimated MIMO channels are taken to be the true channels is now given by the following result.

Theorem 6.5. *The worst-case lower bound on the channel capacity for the system model*

shown in (6.21), (6.22) and (6.25) is obtained when the additive noise is Gaussian distributed and is maximized when the information symbol vectors, $\tilde{\mathbf{x}}_n$ and $\tilde{\mathbf{s}}_n$ are Gaussian distributed. It is given by the expression:

$$\begin{aligned}
C &= \frac{1}{N} \times \frac{M}{P} \sum_{n=0}^{N_t-1} \mathbb{E} \left[\max_{p_x(\cdot), \mathbb{E}[\|\tilde{\mathbf{x}}_n\|^2]=\mathcal{P}_{dt}} \mathbf{I}(\tilde{\mathbf{y}}_n^{(dt)}; \tilde{\mathbf{x}}_n | \widehat{\mathcal{H}}_n) \right] \\
&+ \frac{1}{N} \sum_{n=N_t}^{N-1} \mathbb{E} \left[\max_{p_s(\cdot), \mathbb{E}[\|\tilde{\mathbf{s}}_n\|^2]=\mathcal{P}_d} \mathbf{I}(\tilde{\mathbf{r}}_n; \tilde{\mathbf{s}}_n | \widehat{\mathcal{H}}_n) \right] \quad \text{bits/channel use} \\
&\geq \frac{1}{N} \times \frac{M}{P} \sum_{n=0}^{N_t-1} \log \det (\mathbf{I}_{KM} + \mathcal{P}_{dt} \sigma_{z^{(dt)}}^2(n) \widehat{\mathcal{H}}_n^H \widehat{\mathcal{H}}_n) \\
&+ \frac{1}{N} \sum_{n=N_t}^{N-1} \log \det (\mathbf{I}_{KP} + \mathcal{P}_d \sigma_{z^{(d)}}^2(n) \widehat{\mathcal{H}}_n^H \widehat{\mathcal{H}}_n). \tag{6.50}
\end{aligned}$$

Proof. See Appendix G. □

6.6 Simulation Results

In our simulation, we set $K = 2$, $P = 32$ and $L = 3$. We also selected $\mathcal{P} = 1$, so that the SNR is defined as: $SNR \triangleq -10 \log_{10} \sigma_z^2$. We selected the Rayleigh channel variance to be $\sigma_h^2 = 1/(L + 1)$. Moreover, we normalized the Bayesian CRB and the channel variance values by the number of MIMO channel coefficients, *i.e.*, $K^2(L + 1)$. Moreover, we averaged the results over 500 randomly generated MIMO channel vectors.

6.6.1 MMSE of the Channel Estimator

In this subsection, we have not generated the Rayleigh channels such that there is a correlation between successive block indices. In other words, each MIMO channel vector of any index is assumed to be independent of the MIMO channel vector of any other index. Moreover, we consider each block to contain training and information symbols such that channel tracking is not performed. That is each block is represented by (6.21) and (6.22) alone. This also implies that $\mathcal{P}_{dt} + \lceil = 1$ and $\mathcal{P}_d = 0$ is assumed. Furthermore, we distribute the power equally among the training symbols and the information symbols. We generate

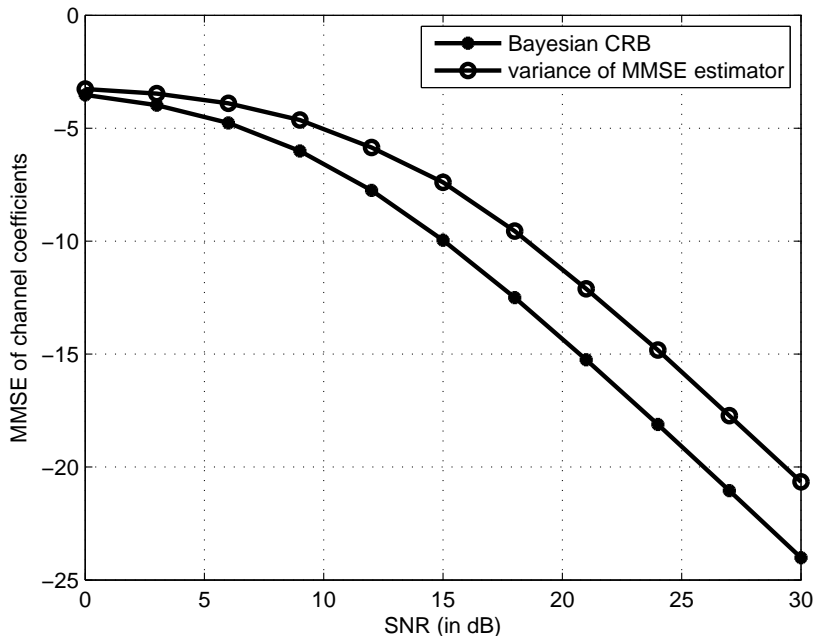


Fig. 6.2 MMSE of channel coefficients

the training vectors according to 6.33. We simulate the input vector such that the elements are drawn from a Gaussian distribution. The result of MMSE channel estimation and the MMSE estimation of information symbols is shown in Figs 6.2 and 6.3. The primary goal of this exercise is only to test the MMSE nature of the training sequences.

6.6.2 Capacity Bounds

In this subsection, we selected the MIMO channel vectors such that they are correlated with $a = 0.95$. We also selected the excitation noise with the appropriate variance so that the channel vectors are WSS. Given the fact that the channel capacity lower bound given by 6.50 is quite involved, we do not attempt to provide an analytical result for the optimal power allocation. Consequently, we resort to numerical optimization to optimally allocate power between the training and data transmission phases. For comparison purposes, we provide the upper and lower bounds when power is equally distributed between training and information symbols. The plot is shown in Fig. 6.4. It can be noticed that at a high SNR of 30 dB, the capacity lower bound is approximately 5 dB higher when optimal power

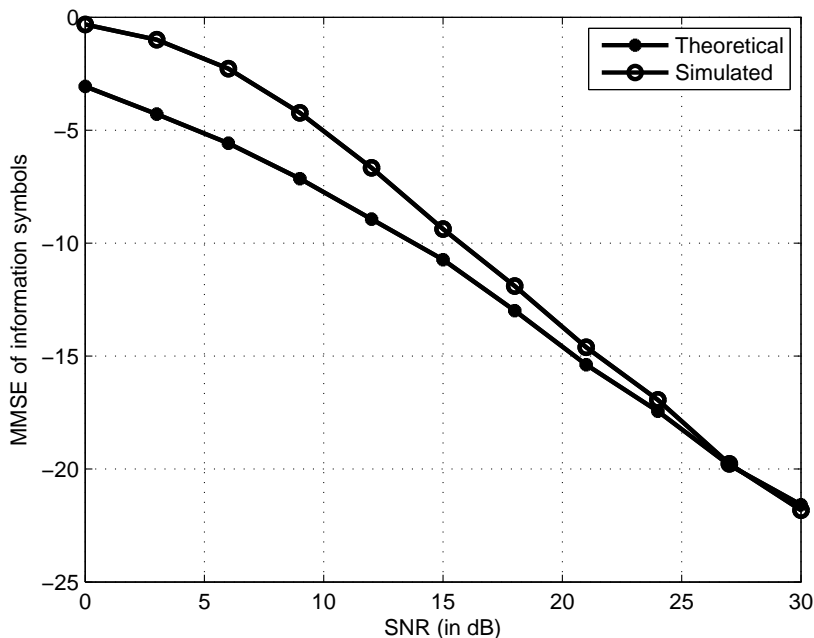


Fig. 6.3 MMSE of information symbols

allocation is performed compared to the equi-powered case.

Additionally, we provide the variance of the MMSE estimates of the information symbols in Fig. 6.5. As expected based on the results of Fig. 6.4, we see that the optimal allocation of power results in a characteristics that is closer to the case where the channel is perfectly known compared to an equi-powered scheme.

6.7 Chapter Summary

In this chapter, we have shown that similar to a SISO case, an OFDM linear precoder with an FDM training sequence satisfies the orthogonality condition and results in decoupled channel estimation and symbol detection. Furthermore, we have derived optimal training sequences such that the FDM training sequences between different antennas are phase-shift orthogonal to each other. Based on the structure of the training matrices, the Kalman filter recursion was simplified to a scalar recursion. Eventually, the upper and lower bounds on the channel capacity were obtained by utilizing the Kalman filter's MMSE expressions to account for imperfect channel estimates. Also, the simulation results shown

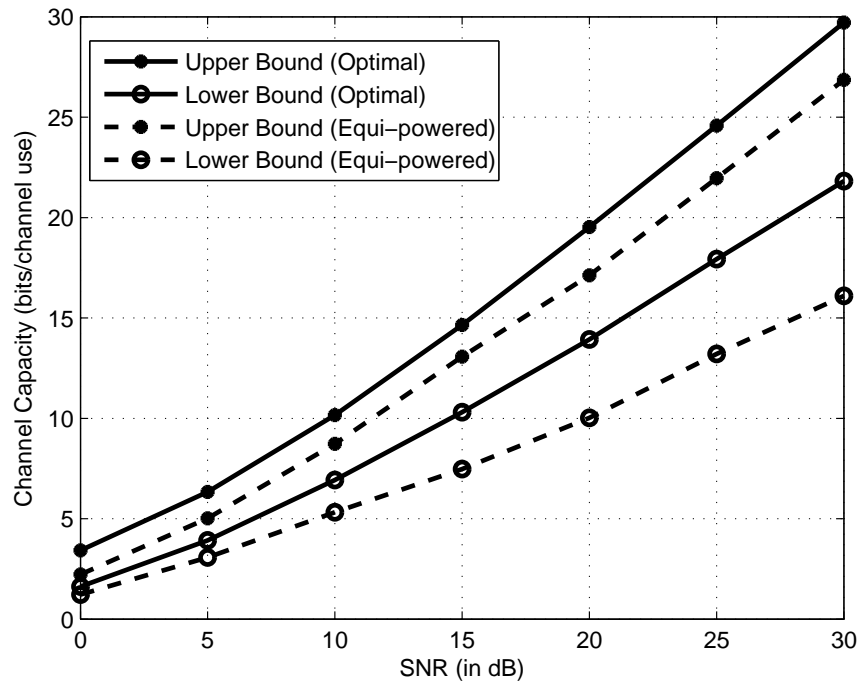


Fig. 6.4 Capacity bounds for optimal Power allocation versus equi-powered allocation.

have confirmed the theoretical results.

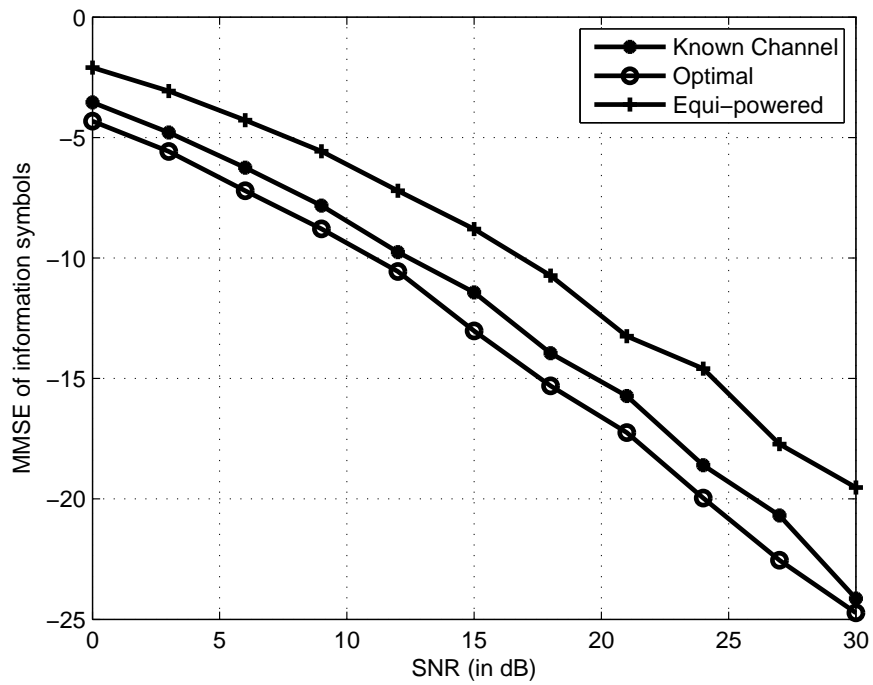


Fig. 6.5 MMSE of information symbols for optimal Power allocation versus equi-powered allocation.

Chapter 7

Conclusions and Future Work

In this dissertation, we have shown that:

- Wireless spectrum occupancy in average case urban environments, which is the more interesting one compared to the worst case urban scenarios exhibit spatial, temporal and frequency-wise variations in spectrum occupancy. Furthermore, we have modeled the variations corresponding to a few bands using a linear mixed effects model and have drawn quantifiable results on the percentage spectrum occupancy and the activity period of the licensed transmissions.
- We then extended this analysis to vehicular settings. Due to an increased demand for high-speed vehicle-to-vehicle and/or vehicle-to-infrastructure communications, the vacant UHF DTV band which became available following to analog-to-digital switchover is seen as a means for secondary access. We conducted a feasibility analysis based on the directives of the FCC and the IEEE 802.22 draft standard to create a geo-location database that identifies vacant channels in a given area.
- Although the identification of vacant channels is an important component of achieving secondary access, interference-free coexistence with a neighboring band licensed user dictates the amount of bandwidth that can be utilized. We looked into these mutual interference issues under two schemes, namely, non-contiguous OFDM and non-contiguous NOFDM.
- Finally, due to the capacity gains offered by MIMO-OFDM systems, we studied the impact of receiver estimation error on the lower bound of channel capacity. We

derived MMSE optimal training sequences and simplified Kalman recursion in matrix variables to a Kalman recursion in scalar variables. Based on the MMSE expressions obtained, we formulated the lower bound on the channel capacity.

The list of publications both resulting from the work submitted in this dissertation and other related results not submitted in this dissertation is as follows:

Book Chapter

1. S. Pagadarai, R. Rajbanshi, and A. Wyglinski, *Cognitive Radio Communications and Networks: Principles and Practice* (A. M. Wyglinski, M. Nekovee, and Y. T. Hou, Eds.), Ch. 6. Agile Transmission Techniques. Academic Press, 2009.

List of Journal Papers

6. S. Pagadarai, B. Lessard, A. Wyglinski, R. Vuyyuru, and O. Altintas, “Dynamic Spectrum Access for Vehicular Communications,” under review for publication in the *IEEE Vehicular Technology Magazine*, 2011.
5. S. Chen, A. Wyglinski, S. Pagadarai, R. Vuyyuru and O. Altintas “Feasibility Analysis of Vehicular Dynamic Spectrum Access via Queuing Theory Model,” accepted for publication in the *IEEE Communications Magazine*, November 2011.
4. S. Pagadarai, A. Kliks, H. Bogucka, and A. Wyglinski, “Non-contiguous Multicarrier Waveforms in Practical Opportunistic Wireless Systems,” *IET Radar, Sonar, and Navigation Journal*, vol. 5, no. 6, pp. 674-680, July 2011.
3. H. Bogucka, A. Wyglinski, S. Pagadarai, and A. Kliks, “Spectrally Agile Multi-Carrier Waveforms for Opportunistic Wireless Access,” *IEEE Communications Magazine*, vol. 49, no. 6, pp. 108-115, June 2011.
2. S. Pagadarai and A. Wyglinski, “A Linear Mixed-Effects Model of Wireless Spectrum Occupancy,” *EURASIP Journal on Wireless Communications and Networking*, vol. 2010, pp. 14:1–14:13, April 2010.
1. C. Ghosh, S. Pagadarai, D. Agrawal, and A. M. Wyglinski, “A Framework for Statistical Wireless Spectrum Occupancy Modeling,” *IEEE Transactions on Wireless Communications*, vol. 9, no. 1, pp. 38–44, 2010.

List of Conference Papers

9. S. Pagadarai, A. Wyglinski, and C. Anderson, “An Evaluation of the Bayesian CRLB for Time-Varying MIMO Channel Estimation Using Complex-Valued Differentials,” in proceedings of the 2011 *IEEE Pacific Rim Conference on Communications, Computers, and Signal Processing*, August 2011.
8. S. Pagadarai, A. Kliks, H. Bogucka, and A. Wyglinski, “On Non-Contiguous Multi-carrier Waveforms for Spectrally Opportunistic Cognitive Radio Systems,” in 2010 *International Waveform Diversity and Design Conference (WDDC)*, pp. 177–181, 2010.
7. C. Ghosh, S. Pagadarai, D. Agrawal, and A. Wyglinski, “Queueing Theory Representation and Modeling of Spectrum Occupancy Employing Radio Frequency Measurements,” in *IEEE 70th Vehicular Technology Conference Fall (VTC 2009-Fall) 2009*, pp. 1–5, 2009.
6. S. Pagadarai, A. Wyglinski, and R. Vuyyuru, “Characterization of Vacant UHF TV Channels for Vehicular Dynamic Spectrum Access,” in *IEEE Vehicular Networking Conference (VNC)*, 2009, pp. 1–8, 2009.
5. Z. Yuan, S. Pagadarai, and A. Wyglinski, “Feasibility of NC-OFDM Transmission in Dynamic Spectrum Access Networks,” in *IEEE Military Communications Conference (MILCOM) 2009*, pp. 1–5, 2009.
4. S. Pagadarai and A. Wyglinski, “A Quantitative Assessment of Wireless Spectrum Measurements for Dynamic Spectrum Access,” in *4th International Conference on Cognitive Radio Oriented Wireless Networks and Communications (CROWNCOM) 2009.*, pp. 1–5, 2009.
3. Z. Yuan, S. Pagadarai, and A. Wyglinski, “Cancellation Carrier Technique Using Genetic Algorithm for OFDM Sidelobe Suppression,” in *IEEE Military Communications Conference (MILCOM) 2008.*, pp. 1–5, 2008.
2. S. Pagadarai, A. Wyglinski, and R. Rajbanshi, “A Novel Sidelobe Suppression Technique for OFDM-Based Cognitive Radio Transmission,” in *3rd IEEE Symposium on New Frontiers in Dynamic Spectrum Access Networks (DySPAN) 2008.*, pp. 1–7, 2008.

1. S. Pagadarai, A. Wyglinski, and R. Rajbanshi, "A Sub-Optimal Sidelobe Suppression Technique for OFDM-Based Cognitive Radios," in *IEEE Military Communications Conference (MILCOM) 2008.*, pp. 1–6, 2008.

7.1 Future Work

Based on the work presented in this dissertation, there are several directions in which the results can be extended. The following is a short list.

- We have used linear mixed-effects model to characterize the influence of several regressor variables on a variable of interest. However, we have not conducted a comparative analysis on other statistical models that perhaps provide a better fit to the observations with respect to the same regressor variables. Another possible study involves the correlation that would exist between the data points collected in the same city and between sites that are not separated by a great distance. It is possible that exploiting this correlation gives further insight into the occupancy of the licensed channels.
- As mentioned previously, in vehicular DSA, the availability of vacant channels is a function of distance with respect to the nearby DTV transmitters as well as the velocity at which the mobile unit is traveling. As a result, switching over from an occupied channel to a vacant one when it becomes unavailable requires a sensing mechanism that is accurate and fast. In other words, standard approaches such as energy detection which are not particularly known to yield a high probability of detection with reasonably low probability of false alarm may not work. Similarly, cyclostationary approaches that require large datasets also fail to meet the above condition. Identifying the appropriate sensing technique in vehicular environments where the channel vacancy characteristics change rapidly is of great significance.
- The mutual interference analysis that we have conducted can be extended to analyze the bit error rates of primary and secondary users as a function of the signal-to-interference-plus-noise ratio. Such an analysis would provide further insight into quantifying the data-rate that is possible in such an impaired channel environment. Furthermore, capacity considerations in cognitive radio networks has attracted a good deal of attention from the wireless research community.

- While the problem of optimal training design for a MIMO-OFDM communication system is comparatively easy to solve, a harder problem is training design when there are within-block variations of the channel where orthogonality between subcarriers is destroyed. In other words, by considering blockwise time-variations of the channel vector, the problem is more manageable compared to the case where the channel vector's time-variations occur shorter than the duration of the block. Although training designs have been provided when all the symbols in the block are known [117], it is not known what the optimal training and placement is. However, it has been suggested that grouping pilot symbols in clusters across subcarriers leads to lower channel MSE for fast time-varying channels than equispaced placed which is known to be optimal for time-invariant channels [118].

Appendix A

Linear Mixed Effects Model

In this chapter, we provide details on the linear mixed-effects that we employ to describe spectrum occupancy characteristics. The normal linear model given by the equation:

$$y_i = \beta_1 x_{1i} + \beta_2 x_{2i} + \dots + \beta_p x_{pi} + \varepsilon_i, \quad (\text{A.1})$$

explains the relationship between one or more independent variables, called *regressor variables*, and a dependent variable, called the *response variable*. The parameters of the model are called the *regression coefficients*, specified as $\beta_1, \beta_2, \dots, \beta_p$, and the *error variance*, defined as σ^2 . The above model has one *random effect* term, the error term ε_i given by:

$$\varepsilon_i \sim N(0, \sigma^2), \quad (\text{A.2})$$

which is assumed to be independent and identically distributed (i.i.d.). Another important assumption is that the sample is drawn randomly from the population of interest. Usually, we set $x_{1i} = 1$ while β_1 is either a constant or an intercept. Therefore, rewriting the model in matrix form yields:

$$\mathbf{y} = \mathbf{X}\beta + \varepsilon, \quad (\text{A.3})$$

$$\varepsilon \sim N_n(0, \sigma^2 \mathbf{I}_n), \quad (\text{A.4})$$

where we define the following variables:

- $\mathbf{y} = [y_1, y_2, \dots, y_n]^T$, is the response vector,
- \mathbf{X} is the model matrix

- $\beta = [\beta_1, \beta_2, \dots, \beta_n]^T$, is the vector of regression coefficients,
- $\varepsilon = [\varepsilon_1, \varepsilon_2, \dots, \varepsilon_n]^T$, is the vector of errors, and
- \mathbf{N}_n represents the n -variable multivariate-normal distribution.

Estimating the parameters of the above model is a well known *linear least squares problem*. The estimate of the regression coefficient vector is given by the expression:

$$\hat{\beta} = (\mathbf{X}^T \mathbf{X})^{-1} \mathbf{X}^T y. \quad (\text{A.5})$$

Several variants of the basic linear regression model of Eq. (A.1) are widely used in various areas of science. One such variant is the *mixed effect model*. These models include additional random effect terms and are appropriate in representing clustered, and therefore, dependent data arising when data are collected over time on the same entities. That is, these *repeated measures data* are generated by observing a number of entities repeatedly under differing experimental conditions, where the entities are assumed to constitute a random sample from a population of interest. Longitudinal data constitute a common type of repeated measures data, where the observations are ordered by time or position in space. In general, longitudinal data can be defined as repeated measures data where the observations within entities could not have been randomly assigned to the levels of a “treatment” of interest (usually time or position in space). Hence, serial correlation results.

Writing the linear mixed effect model of the form shown in Eq. (A.1) yields:

$$\begin{aligned} y_i &= \beta_1 x_{1i} + \beta_2 x_{2i} + \dots + \beta_p x_{pi} \\ &+ b_1 z_{1i} + b_2 z_{2i} + \dots + b_q z_{qi} + \varepsilon_i \end{aligned} \quad (\text{A.6})$$

where

$$b_i \sim \text{N}(0, \sigma^2 \mathbf{D})$$

and

$$\varepsilon_{ij} \sim \text{N}(0, \sigma^2 \Lambda)$$

Alternately, but equivalently, the above model can be written in matrix form as:

$$y_i = X_i \beta + Z_i b + \varepsilon_i \quad (\text{A.7})$$

$$b \sim N_q(0, \sigma^2 \mathbf{D})$$

$$\varepsilon_i \sim N_{n_i}(0, \sigma^2 \Lambda)$$

where we define the following variables:

- y_i is the $n_i \times 1$ response variable for observations in the i^{th} group,
- X_i is the $n_i \times p$ model vector for the fixed effects for observations in the i^{th} group,
- β is the $p \times 1$ vector of fixed-effects coefficients for the i^{th} group,
- Z_i is the $n_i \times q$ model matrix for the random effects for observations in the i^{th} group,
- b_i is the $q \times 1$ vector of random-effects coefficients for the i^{th} group,
- ε_i is the $n_i \times 1$ variable of error for the i^{th} group,
- $\sigma^2 \mathbf{D}$ is the $q \times q$ covariance matrix for the random-effects, and
- $\sigma^2 \Lambda$ is the $n_i \times n_i$ covariance matrix for the errors in the i^{th} group.

From the above representation, define $\mathbf{X} = [\mathbf{X}_1^T, \mathbf{X}_2^T, \dots, \mathbf{X}_M^T]^T$, $\tilde{\mathbf{D}} = \text{diag}(\mathbf{D}_1, \mathbf{D}_2, \dots, \mathbf{D}_M)$ and $\mathbf{Z} = \text{diag}(\mathbf{Z}_1, \mathbf{Z}_2, \dots, \mathbf{Z}_M)$. When the variance components Λ and \mathbf{D} are known, the standard estimators for β and \mathbf{b} are the generalized linear estimator $\hat{\beta}_{lin} = (\mathbf{X}^T \mathbf{V}^{-1} \mathbf{X})^{-1} \mathbf{X}^T \mathbf{V}^{-1} \mathbf{y}$ where $\mathbf{V} = \Lambda + \mathbf{Z} \mathbf{D} \mathbf{Z}^T$ and the posterior mean, $\hat{b}_{lin} = \mathbf{D} \mathbf{Z}^T \mathbf{V}^{-1} (\mathbf{y} - \mathbf{X} \hat{\beta})$. The estimates $\hat{\beta}_{lin}$ and \hat{b}_{lin} jointly maximize the function [119]:

$$g_{lin}(\beta, b|y) = -\frac{1}{2} \sigma^{-2} (\mathbf{y} - \mathbf{X}\beta - \mathbf{Z}\mathbf{b})^T \Lambda^{-1} (\mathbf{y} - \mathbf{X}\beta - \mathbf{Z}\mathbf{b}) - \frac{1}{2} \sigma^{-2} \mathbf{b}^T \tilde{\mathbf{D}} \mathbf{b}. \quad (\text{A.8})$$

The above function is the logarithm of the posterior density of b (up to a constant) for fixed β and for fixed b is the log-likelihood for β (up to a constant). Eq. (A.8) has two terms, a sum of squares term and a quadratic term in \mathbf{b} . By transforming the quadratic term in \mathbf{b} to an equivalent sum of squares term, the optimization can be treated purely as a least squares problem. Then it is straightforward to translate it into the nonlinear setting.

Appendix B

An Overview of Complex-Valued Matrix Differentiation

In order to evaluate the partial derivatives involved in identifying the FIMs of the likelihood functions shown in eq.s () w.r.t the unknown parameters, we apply the chain rule for finding partial derivatives of a complex-valued vector as outlined in [120, Theorem 1]. The statement of the theorem and a brief discussion is provided here for reference. For a detailed introduction to the framework on determining the derivatives of a general complex-valued matrix function using complex differentials, see [120].

Theorem (Chain Rule [120]). *Let $(S_0, S_1, S_2) \subseteq \mathbb{R}^{K \times L} \times \mathbb{C}^{N \times Q} \times \mathbb{C}^{N \times Q}$, and let $\mathbf{F} : S_0 \times S_1 \times S_2 \rightarrow \mathbb{C}^{M \times P}$ be differentiable w.r.t its first, second and third argument at an interior point $(\mathbf{X}, \mathbf{Z}, \mathbf{Z}^*)$ in the set $S_0 \times S_1 \times S_2$. Let $T_0 \times T_1 \subseteq \mathbb{C}^{M \times P} \times \mathbb{C}^{M \times P}$ be such that $(\mathbf{F}(\mathbf{X}, \mathbf{Z}, \mathbf{Z}^*), \mathbf{F}^*(\mathbf{X}, \mathbf{Z}, \mathbf{Z}^*)) \in T_0 \times T_1$ for all $(\mathbf{X}, \mathbf{Z}, \mathbf{Z}^*) \in S_0 \times S_1 \times S_2$.*

Assume that $\mathbf{G} : T_0 \times T_1 \rightarrow \mathbb{C}^{R \times S}$ is differentiable at an interior point $(\mathbf{F}(\mathbf{X}, \mathbf{Z}, \mathbf{Z}^), \mathbf{F}^*(\mathbf{X}, \mathbf{Z}, \mathbf{Z}^*)) \in T_0 \times T_1$. Define the composite function $\mathbf{H} : S_0 \times S_1 \times S_2 \rightarrow \mathbb{C}^{R \times S}$ by $\mathbf{H}(\mathbf{X}, \mathbf{Z}, \mathbf{Z}^*) \triangleq \mathbf{G}(\mathbf{F}(\mathbf{X}, \mathbf{Z}, \mathbf{Z}^*), \mathbf{F}^*(\mathbf{X}, \mathbf{Z}, \mathbf{Z}^*))$. The derivatives $\mathcal{D}_{\mathbf{X}} \mathbf{H}$, $\mathcal{D}_{\mathbf{Z}} \mathbf{H}$ and $\mathcal{D}_{\mathbf{Z}^*} \mathbf{H}$ are:*

$$\mathcal{D}_{\mathbf{X}} \mathbf{H} = (\mathcal{D}_{\mathbf{F}} \mathbf{G}) \mathcal{D}_{\mathbf{X}} \mathbf{F} + (\mathcal{D}_{\mathbf{F}^*} \mathbf{G}) \mathcal{D}_{\mathbf{X}} \mathbf{F}^* \quad (\text{B.1a})$$

$$\mathcal{D}_{\mathbf{Z}} \mathbf{H} = (\mathcal{D}_{\mathbf{F}} \mathbf{G}) \mathcal{D}_{\mathbf{Z}} \mathbf{F} + (\mathcal{D}_{\mathbf{F}^*} \mathbf{G}) \mathcal{D}_{\mathbf{Z}} \mathbf{F}^* \quad (\text{B.1b})$$

$$\mathcal{D}_{\mathbf{Z}^*} \mathbf{H} = (\mathcal{D}_{\mathbf{F}} \mathbf{G}) \mathcal{D}_{\mathbf{Z}^*} \mathbf{F} + (\mathcal{D}_{\mathbf{F}^*} \mathbf{G}) \mathcal{D}_{\mathbf{Z}^*} \mathbf{F}^* \quad (\text{B.1c})$$

Following the notational convention of [120], the set of patterned matrices is denoted as, $\mathcal{W} \subseteq \mathbb{C}^{M \times P}$ and a particular patterned matrix as, $\mathbf{W} \in \mathcal{W}$, \mathbf{W} is parameterized by the matrices, \mathbf{X} and \mathbf{Z} through the relation, $\mathbf{W} = \mathbf{F}(\mathbf{X}, \mathbf{Z}, \mathbf{Z}^*)$, where \mathbf{F} is referred to as *pattern producing function*. In order to apply the chain rule, the matrix functions \mathbf{F} and \mathbf{G} must be differentiable which is possible when these functions do not contain patterns. Therefore, we let the domain of the matrix function \mathbf{G} , to be the elements that belong to the larger set of unpatterned matrices, $\tilde{\mathcal{W}}$ such that when $\mathbf{G}(\tilde{\mathbf{W}}, \tilde{\mathbf{W}}^*)$ is restricted to the patterned matrices \mathbf{W} and \mathbf{W}^* , we obtain the function whose derivative we want to find. In other words,

$$\begin{aligned} \mathbf{G}(\mathbf{W}, \mathbf{W}^*) &= \mathbf{G}(\tilde{\mathbf{W}}, \tilde{\mathbf{W}}^*)|_{\tilde{\mathbf{W}}=\mathbf{W}=\mathbf{F}(\mathbf{X}, \mathbf{Z}, \mathbf{Z}^*)} \\ &= \mathbf{G}(\mathbf{F}(\mathbf{X}, \mathbf{Z}, \mathbf{Z}^*), \mathbf{F}^*(\mathbf{X}, \mathbf{Z}, \mathbf{Z}^*)) \\ &\triangleq \mathbf{H}(\mathbf{X}, \mathbf{Z}, \mathbf{Z}^*) \end{aligned} \quad (\text{B.2})$$

Hence, the derivative of $\mathbf{H}(\mathbf{X}, \mathbf{Z}, \mathbf{Z}^*)$ w.r.t \mathbf{X} , \mathbf{Z} and \mathbf{Z}^* can be written using the chain rule shown in eq.s (B.1a), (B.1b) and (B.1c) in the form of eq.s (B.3a), (B.3b) and (B.3c).

$$\begin{aligned} \mathcal{D}_{\mathbf{X}} \mathbf{H}(\mathbf{X}, \mathbf{Z}, \mathbf{Z}^*) &= (\mathcal{D}_{\mathbf{F}} \mathbf{G}(\tilde{\mathbf{W}}, \tilde{\mathbf{W}}^*)|_{\tilde{\mathbf{W}}=\mathbf{W}=\mathbf{F}(\mathbf{X}, \mathbf{Z}, \mathbf{Z}^*)}) \mathcal{D}_{\mathbf{X}} \mathbf{F}(\mathbf{X}, \mathbf{Z}, \mathbf{Z}^*) \\ &\quad + (\mathcal{D}_{\mathbf{F}^*} \mathbf{G}(\tilde{\mathbf{W}}, \tilde{\mathbf{W}}^*)|_{\tilde{\mathbf{W}}=\mathbf{W}=\mathbf{F}(\mathbf{X}, \mathbf{Z}, \mathbf{Z}^*)}) \mathcal{D}_{\mathbf{X}} \mathbf{F}^*(\mathbf{X}, \mathbf{Z}, \mathbf{Z}^*) \end{aligned} \quad (\text{B.3a})$$

$$\begin{aligned} \mathcal{D}_{\mathbf{Z}} \mathbf{H}(\mathbf{X}, \mathbf{Z}, \mathbf{Z}^*) &= (\mathcal{D}_{\mathbf{F}} \mathbf{G}(\tilde{\mathbf{W}}, \tilde{\mathbf{W}}^*)|_{\tilde{\mathbf{W}}=\mathbf{W}=\mathbf{F}(\mathbf{X}, \mathbf{Z}, \mathbf{Z}^*)}) \mathcal{D}_{\mathbf{Z}} \mathbf{F}(\mathbf{X}, \mathbf{Z}, \mathbf{Z}^*) \\ &\quad + (\mathcal{D}_{\mathbf{F}^*} \mathbf{G}(\tilde{\mathbf{W}}, \tilde{\mathbf{W}}^*)|_{\tilde{\mathbf{W}}=\mathbf{W}=\mathbf{F}(\mathbf{X}, \mathbf{Z}, \mathbf{Z}^*)}) \mathcal{D}_{\mathbf{Z}} \mathbf{F}^*(\mathbf{X}, \mathbf{Z}, \mathbf{Z}^*) \end{aligned} \quad (\text{B.3b})$$

$$\begin{aligned} \mathcal{D}_{\mathbf{Z}^*} \mathbf{H}(\mathbf{X}, \mathbf{Z}, \mathbf{Z}^*) &= (\mathcal{D}_{\mathbf{F}} \mathbf{G}(\tilde{\mathbf{W}}, \tilde{\mathbf{W}}^*)|_{\tilde{\mathbf{W}}=\mathbf{W}=\mathbf{F}(\mathbf{X}, \mathbf{Z}, \mathbf{Z}^*)}) \mathcal{D}_{\mathbf{Z}^*} \mathbf{F}(\mathbf{X}, \mathbf{Z}, \mathbf{Z}^*) \\ &\quad + (\mathcal{D}_{\mathbf{F}^*} \mathbf{G}(\tilde{\mathbf{W}}, \tilde{\mathbf{W}}^*)|_{\tilde{\mathbf{W}}=\mathbf{W}=\mathbf{F}(\mathbf{X}, \mathbf{Z}, \mathbf{Z}^*)}) \mathcal{D}_{\mathbf{Z}^*} \mathbf{F}^*(\mathbf{X}, \mathbf{Z}, \mathbf{Z}^*) \end{aligned} \quad (\text{B.3c})$$

Appendix C

Proof of Theorem 6.1

From [121], we know that the complex FIM is given by the equation,

$$\begin{aligned}
& \mathbb{E} \left\{ \left(\frac{\partial \ln p(\mathbf{y}_n; \mathbf{h}_n)}{\partial \mathbf{h}_n^*} \right) \left(\frac{\partial \ln p(\mathbf{y}_n; \mathbf{h}_n)}{\partial \mathbf{h}_n^*} \right)^H \right\} \\
&= \mathbb{E} \left\{ \mathbb{E} \left[\left(\frac{\partial \ln p(\mathbf{y}_n | \mathbf{h}_n)}{\partial \mathbf{h}_n^*} \right) \left(\frac{\partial \ln p(\mathbf{y}_n | \mathbf{h}_n)}{\partial \mathbf{h}_n^*} \right)^H \middle| \mathbf{h}_n \right] \right\} \\
&+ \mathbb{E} \left\{ \left(\frac{\partial \ln p(\mathbf{h}_n)}{\partial \mathbf{h}_n^*} \right) \left(\frac{\partial \ln p(\mathbf{h}_n)}{\partial \mathbf{h}_n^*} \right)^H \right\} \tag{C.1}
\end{aligned}$$

In the second equality of the above equation, the inner expectation in the first term is w.r.t \mathbf{y}_n , whereas the outer expectation is w.r.t \mathbf{h}_n . The log-likelihood function of the probability density function, $p(\mathbf{y}_n | \mathbf{h}_n)$ in (C.1) and its derivative are as follows:

$$\ln p(\mathbf{y}_n | \mathbf{h}_n) = \text{constant} - \ln(|\mathbf{R}_{\mathbf{y}_n}|) - \mathbf{u}^H \mathbf{R}_{\mathbf{y}_n}^{-1} \mathbf{u} \tag{C.2a}$$

$$\frac{\partial \ln p(\mathbf{y}_n | \mathbf{h}_n)}{\partial \mathbf{h}_n^*} = -\frac{\partial \ln |\mathbf{R}_{\mathbf{y}_n}|}{\partial \mathbf{h}_n^*} - \frac{\partial \mathbf{u}^H \mathbf{R}_{\mathbf{y}_n}^{-1} \mathbf{u}}{\partial \mathbf{h}_n^*} \tag{C.2b}$$

where, $\mathbf{u} \triangleq (\mathbf{y}_n - (\mathbf{I}_K \otimes \mathbf{T}) \mathbf{h}_n)$ and

$$\begin{aligned} \mathbf{R}_{\mathbf{y}_n} &= \sigma_x^2 \mathcal{H}_n \mathbf{Q} \mathbf{Q}^H \mathcal{H}_n^H + \sigma_z^2 \mathbf{I}_{KP} \\ &= \sigma_x^2 \sum_{n=0}^{KM-1} \mathcal{Q}_n \mathbf{h}_n \mathbf{h}_n^H \mathcal{Q}_n^H + \sigma_z^2 \mathbf{I}_{KP} \end{aligned} \quad (\text{C.3a})$$

$$\begin{aligned} \mathbf{R}_{\mathbf{y}_n}^{-1} &= \sigma_z^{-2} \mathbf{I}_{KP} - \sigma_z^{-4} \sigma_x^2 \mathcal{H}_n \mathbf{Q} (\mathbf{I}_{KM} + \sigma_z^{-2} \sigma_x^2 \mathbf{Q}^H \mathcal{H}_n^H \mathcal{H}_n \mathbf{Q})^{-1} \mathbf{Q}^H \mathcal{H}_n^H \\ &= \sigma_z^{-2} \mathbf{I}_{KP} - \sigma_z^{-4} \sigma_x^2 \mathcal{H}_n \mathbf{Q} \mathbf{G} \mathbf{Q}^H \mathcal{H}_n^H \end{aligned} \quad (\text{C.3b})$$

and $\mathcal{Q}_n \triangleq \mathbf{I}_K \otimes [\mathcal{Q}_{n,1} \mathcal{Q}_{n,2} \dots \mathcal{Q}_{n,K}]$ are obtained from each of the KM columns of \mathbf{Q} . The matrices $\{\mathcal{Q}_{n,k}\}$ are a result of applying the commutativity property of convolution. It should be noted we have not utilized the block-diagonal structure of \mathbf{Q} in obtaining $\{\mathcal{Q}_{n,k}\}$. In other words, the matrices $\{\mathcal{Q}_{n,k}\}$ are constructed without explicit consideration of the fact that $(K-1)P$ out of KP elements in each column of \mathbf{Q} are zeros. We have utilized the matrix inversion lemma in obtaining (C.3b) where $\mathbf{G} \triangleq (\mathbf{I}_{KM} + \sigma_z^{-2} \sigma_x^2 \mathbf{Q}^H \mathcal{H}_n^H \mathcal{H}_n \mathbf{Q})^{-1}$. We now evaluate the two partial derivatives in (C.2b) separately.

(i) $\frac{\partial \ln |\mathbf{R}_{\mathbf{y}_n}|}{\partial \mathbf{h}_n^*}$: Using (B.1c), we note that

$$\begin{aligned} \frac{\partial \ln |\mathbf{R}_{\mathbf{y}_n}|}{\partial \mathbf{h}_n^*} &= \mathcal{D}_{\mathbf{h}_n^*} \ln |\mathbf{R}_{\mathbf{y}_n}| \\ &= (\mathcal{D}_{\mathbf{R}_{\mathbf{y}_n}} \ln |\mathbf{R}_{\mathbf{y}_n}|) \mathcal{D}_{\mathbf{h}_n^*} \mathbf{R}_{\mathbf{y}_n} + (\mathcal{D}_{\mathbf{R}_{\mathbf{y}_n}^*} \ln |\mathbf{R}_{\mathbf{y}_n}|) \mathcal{D}_{\mathbf{h}_n^*} \mathbf{R}_{\mathbf{y}_n}^* \end{aligned} \quad (\text{C.4})$$

Here, $\mathcal{D}_{\mathbf{R}_{\mathbf{y}_n}} \ln |\mathbf{R}_{\mathbf{y}_n}| = \mathbf{R}_{\mathbf{y}_n}^{-\text{T}}$ and $\mathcal{D}_{\mathbf{R}_{\mathbf{y}_n}^*} \ln |\mathbf{R}_{\mathbf{y}_n}| = 0$ [122, Table II]. Moreover, from (C.3a), we see that,

$$d\mathbf{R}_{\mathbf{y}_n} = \sigma_x^2 \sum_{n=0}^{KM-1} \mathcal{Q}_n \mathbf{h}_n d\mathbf{h}_n^H \mathcal{Q}_n^H + \sigma_x^2 \sum_{n=0}^{KM-1} \mathcal{Q}_n d\mathbf{h}_n \mathbf{h}_n^H \mathcal{Q}_n^H \quad (\text{C.5a})$$

$$\begin{aligned} d\text{vec} \mathbf{R}_{\mathbf{y}_n} &= \sigma_x^2 \sum_{n=0}^{KM-1} (\mathcal{Q}_n^* \otimes \mathcal{Q}_n \mathbf{h}_n) d\text{vec}(\mathbf{h}_n^*) \\ &\quad + \sigma_x^2 \sum_{n=0}^{KM-1} (\mathcal{Q}_n^* \mathbf{h}_n^* \otimes \mathcal{Q}_n) d\text{vec}(\mathbf{h}_n) \end{aligned} \quad (\text{C.5b})$$

From the above equations and [120, Table III], we notice that, $\mathcal{D}_{\mathbf{h}_n^*} \mathbf{R}_{\mathbf{y}_n} = \sigma_x^2 \sum_{n=0}^{KM-1} (\mathcal{Q}_n^* \otimes \mathcal{Q}_n \mathbf{h}_n)$. It should be noted that the definition of the partial derivative for the case of a scalar function w.r.t a column vector adopted by Hjörungnes *et al*, results in a row vector [120, Table III]. For the problem under consideration, we consider this definition to lead to transposed derivative. Therefore, we perform a transpose operation of the results obtained based on (B.3a), (B.3b) and (B.3c) in order to obtain the FIM with appropriate dimensions. As a result,

$$\begin{aligned}
& \frac{\partial \ln |\mathbf{R}_{\mathbf{y}_n}|}{\partial \mathbf{h}_n^*} \\
&= (\mathcal{D}_{\mathbf{R}_{\mathbf{y}_n}} \ln |\mathbf{R}_{\mathbf{y}_n}|) \mathcal{D}_{\mathbf{h}_n^*} \mathbf{R}_{\mathbf{y}_n} \\
&= \left(\text{vec}^\top \left[\frac{\partial \ln |\mathbf{R}_{\mathbf{y}_n}|}{\partial \mathbf{R}_{\mathbf{y}_n}} \right] \left[\frac{\partial \text{vec} \mathbf{R}_{\mathbf{y}_n}}{\partial \mathbf{h}_n^*} \right] \right)^\top \\
&= \sigma_x^2 \sum_{n=0}^{KM-1} (\mathcal{Q}_n^H \otimes \mathbf{h}_n^\top \mathcal{Q}_n^\top) \text{vec}(\mathbf{R}_{\mathbf{y}_n}^{-\top})
\end{aligned} \tag{C.6}$$

(ii) $\frac{\partial \mathbf{u}^H \mathbf{R}_{\mathbf{y}_n}^{-1} \mathbf{u}}{\partial \mathbf{h}_n^*}$: Using (B.1c), we can similarly show that

$$\begin{aligned}
\frac{\partial \mathbf{u}^H \mathbf{R}_{\mathbf{y}_n}^{-1} \mathbf{u}}{\partial \mathbf{h}_n^*} &= -\sigma_x^2 \sum_{n=0}^{KM-1} (\mathcal{Q}_n^H \otimes \mathbf{h}_n^\top \mathcal{Q}_n^\top) (\mathbf{R}_{\mathbf{y}_n}^{-1} \otimes \mathbf{R}_{\mathbf{y}_n}^{-\top}) (\mathbf{u} \otimes \mathbf{u}^*) \\
&\quad - (\mathbf{I}_K \otimes \mathbf{T})^H \mathbf{R}_{\mathbf{y}_n}^{-1} \mathbf{u}
\end{aligned} \tag{C.7}$$

Hence, from (C.2b),

$$\begin{aligned}
\frac{\partial \ln p(\mathbf{y}|\mathbf{h}_n)}{\partial \mathbf{h}_n^*} &= \sigma_x^2 \sum_{n=0}^{KM-1} (\mathcal{Q}_n^H \otimes \mathbf{h}_n^\top \mathcal{Q}_n^\top) [(\mathbf{R}_{\mathbf{y}_n}^{-1} \otimes \mathbf{R}_{\mathbf{y}_n}^{-\top}) (\mathbf{u} \otimes \mathbf{u}^*) - \text{vec}(\mathbf{R}_{\mathbf{y}_n}^{-\top})] \\
&\quad + (\mathbf{I}_K \otimes \mathbf{T})^H \mathbf{R}_{\mathbf{y}_n}^{-1} \mathbf{u}
\end{aligned} \tag{C.8}$$

Before we evaluate the inner expectation in the first term of the second equality of (C.1), we notice that,

$$\mathbb{E}[\mathbf{u} \otimes \mathbf{u}^*] = \mathbb{E}[\text{vec}(\mathbf{u}^* \mathbf{u}^\top)] = \text{vec}(\mathbb{E}[\mathbf{u}^* \mathbf{u}^\top]) = \text{vec}(\mathbf{R}_{\mathbf{y}_n}^\top) \tag{C.9}$$

Incidentally, by utilizing the above result, we can see that $\mathbb{E} \left[\frac{\partial \ln p(\mathbf{y}_n | \mathbf{h}_n)}{\partial \mathbf{h}_n^*} \right] = 0$ indicating that the regularity condition is satisfied. Employing (C.8) and (C.9), we can show that

$$\begin{aligned} & \mathbb{E} \left[\left(\frac{\partial \ln p(\mathbf{y} | \mathbf{h}_n)}{\partial \mathbf{h}_n^*} \right) \left(\frac{\partial \ln p(\mathbf{y} | \mathbf{h}_n)}{\partial \mathbf{h}_n^*} \right)^H \middle| \mathbf{h}_n \right] \\ &= (\mathbf{I}_K \otimes \mathbf{T})^H \mathbf{R}_{\mathbf{y}_n}^{-1} (\mathbf{I}_K \otimes \mathbf{T}) + \sigma_x^4 \sum_{n=0}^{KM-1} (\mathbf{Q}_n^H \otimes \mathbf{h}_n^T \mathbf{Q}_n^T) (\mathbf{R}_{\mathbf{y}_n}^{-1} \otimes \mathbf{R}_{\mathbf{y}_n}^{-T}) \\ & \quad \times \sum_{n=0}^{KM-1} (\mathbf{Q}_n^* \otimes \mathbf{Q}_n \mathbf{h}_n) \end{aligned} \quad (\text{C.10})$$

Moreover, we observe that $\mathbb{E} \left\{ \left(\frac{\partial \ln p(\mathbf{h}_n)}{\partial \mathbf{h}_n^*} \right) \left(\frac{\partial \ln p(\mathbf{h}_n)}{\partial \mathbf{h}_n^*} \right)^H \right\} = \sigma_h^{-2} \mathbf{I}_{K^2(L+1)}$. Substituting this result along with (C.10) and (C.3b) in (C.1) gives:

$$\begin{aligned} \mathcal{I}(\mathbf{h}_n) &= \mathbb{E}_h \{ (\mathbf{I}_K \otimes \mathbf{T})^H \mathbf{R}_{\mathbf{y}_n}^{-1} (\mathbf{I}_K \otimes \mathbf{T}) \} + \sigma_x^4 \Xi(\mathbf{Q}) + \sigma_h^{-2} \mathbf{I}_{K^2(L+1)} \\ &= \sigma_z^{-2} (\mathbf{I}_K \otimes \mathbf{T})^H (\mathbf{I}_K \otimes \mathbf{T}) - \sigma_z^{-4} \sigma_x^2 \mathbb{E}_h \{ (\mathbf{I}_K \otimes \mathbf{T})^H \mathcal{H}_n \mathbf{Q} \mathbf{G} \mathbf{Q}^H \mathcal{H}_n^H (\mathbf{I}_K \otimes \mathbf{T}) \} \\ & \quad + \sigma_x^4 \Xi(\mathbf{Q}) + \sigma_h^{-2} \mathbf{I}_{K^2(L+1)} \\ &= \sigma_z^{-2} (\mathbf{I}_K \otimes \mathbf{T})^H (\mathbf{I}_K \otimes \mathbf{T}) - \sigma_z^{-4} \sigma_x^2 \Xi(\mathbf{t}, \mathbf{Q}) + \sigma_x^4 \Xi(\mathbf{Q}) + \sigma_h^{-2} \mathbf{I}_{K^2(L+1)} \end{aligned} \quad (\text{C.11})$$

Appendix D

Proof of Theorem 6.2

From (6.13c), we see that \mathbf{G} is the inverse of sum of two full-rank positive-definite matrices. This is because, \mathcal{H}_n is a Rayleigh-fading channel matrix of full rank (with probability 1) due to (A1) and (C1) stipulates that \mathbf{Q} be a full column-rank matrix. Hence, $\mathbf{Q}^H \mathcal{H}_n^H \mathcal{H}_n \mathbf{Q}$ is a matrix with strictly-positive eigenvalues. Together with the fact that \mathbf{I}_{KM} is also a matrix with strictly-positive eigen-values, we arrive at the result that $\mathbf{G} \succ \mathbf{0}$. By making a similar argument, we can show that $\mathbf{R}_{\mathbf{y}_n}^{-1} \succ \mathbf{0}$. As a result of the above statements, we can claim that $\mathbf{\Xi}(\mathbf{t}, \mathbf{Q}) \succeq \mathbf{0}$ and $\mathbf{\Xi}(\mathbf{t}) \succeq \mathbf{0}$. Combining the above results with (C1) leads us to conclude that $\mathcal{I}(\mathbf{h}_n) \succ \mathbf{0}$. Now, based on a previous observation that only $\mathbf{\Xi}(\mathbf{t}, \mathbf{Q})$ is the term under the designer's control, we see that $\mathcal{I}^{(opt)}(\mathbf{h}_n) \succeq \mathcal{I}(\mathbf{h}_n)$ where the optimal Bayesian FIM for a training-based channel estimator is as follows:

$$\mathcal{I}^{(opt)}(\mathbf{h}_n) = \sigma_z^{-2}(\mathbf{I}_K \otimes \mathbf{T})^H (\mathbf{I}_K \otimes \mathbf{T}) + \sigma_x^4 \mathbf{\Xi}(\mathbf{Q}) + \sigma_h^{-2} \mathbf{I}_{K^2(L+1)} \quad (\text{D.1})$$

It should be noticed that for any $\mathbf{A}, \mathbf{B} \succ \mathbf{0}$ such that $\mathbf{A} \succeq \mathbf{B}$, we have $\mathbf{B}^{-1} \preceq \mathbf{A}^{-1}$ and therefore, $\text{tr}(\mathbf{B}^{-1}) \preceq \text{tr}(\mathbf{A}^{-1})$. Hence, finding the conditions under which $\mathcal{I}^{(opt)}(\mathbf{h}_n) \succeq \mathcal{I}(\mathbf{h}_n)$ is equivalent to finding the conditions under which $\text{tr}(\mathcal{I}^{(opt)}(\mathbf{h}_n)^{-1}) \preceq \text{tr}(\mathcal{I}(\mathbf{h}_n)^{-1})$. where $\text{tr}(\mathcal{I}^{(opt)}(\mathbf{h}_n)^{-1})$ is the Bayesian CRB of a non decision-aided channel estimator for the system model described in (6.9). We can now see that $\mathcal{I}^{(opt)}(\mathbf{h}_n)$ is obtained by making

$\Xi(\mathbf{t}, \mathbf{Q}) = 0$ which in turn is possible by enforcing the condition:

$$(\mathbf{I}_K \otimes \mathbf{T})^H \mathcal{H}_n \mathbf{Q} = \begin{bmatrix} \mathbf{T}^H \mathbf{H}_{1,1}^{(n)} \mathbf{Q}_1 & \mathbf{T}^H \mathbf{H}_{1,2}^{(n)} \mathbf{Q}_2 & \dots & \mathbf{T}^H \mathbf{H}_{1,K}^{(n)} \mathbf{Q}_K \\ \mathbf{T}^H \mathbf{H}_{2,1}^{(n)} \mathbf{Q}_1 & \mathbf{T}^H \mathbf{H}_{2,2}^{(n)} \mathbf{Q}_2 & \dots & \mathbf{T}^H \mathbf{H}_{2,K}^{(n)} \mathbf{Q}_K \\ \vdots & \vdots & \ddots & \vdots \\ \mathbf{T}^H \mathbf{H}_{K,1}^{(n)} \mathbf{Q}_1 & \mathbf{T}^H \mathbf{H}_{K,2}^{(n)} \mathbf{Q}_2 & \dots & \mathbf{T}^H \mathbf{H}_{K,K}^{(n)} \mathbf{Q}_K \end{bmatrix} = \mathbf{0} \quad (\text{D.2})$$

In other words,

$$\mathbf{T}^H \mathbf{H}_{i,j}^{(n)} \mathbf{Q}_j = \mathbf{0} \quad 1 \leq i, j \leq K \quad (\text{D.3})$$

We now utilize the commutativity property of convolution and in a manner similar in the construction of the matrices, $\{\mathbf{T}_k\}$, we see that $\mathbf{H}_{i,j}^{(n)} \mathbf{Q}_j = [\mathbf{Q}_{j,1} \mathbf{h}_{i,j}^{(n)} \quad \mathbf{Q}_{j,2} \mathbf{h}_{i,j}^{(n)} \dots \mathbf{Q}_{j,M-1} \mathbf{h}_{i,j}^{(n)}]$ where the circulant matrices, $\{\mathbf{Q}_{j,m}\}$ are constructed such that $[q_{j,m}[0] \dots q_{j,m}[P-1]]^T$ is the first column and $[q_{j,m}[0] \quad t_k[P-L] \dots q_{j,m}[P-1]]$ is the first row. The column vector $q_{j,m}$ is the m th column of the j th linear precoder, \mathbf{Q}_j . Hence,

$$\mathbf{T}_i^H \mathbf{Q}_{j,m} = \mathbf{0} \quad 1 \leq i, j \leq K \quad 0 \leq m \leq M-1 \quad (\text{D.4})$$

Appendix E

Proof of Lemma 6.1

Firstly, it is easy to see that the optimal MMSE estimator coincides with the linear MMSE estimator for the system under consideration *i.e.*, (6.21), due to the joint Gaussian nature of the unknown parameter and the observation vectors. The optimal minimum mean squared-error (MMSE) channel estimator, $\hat{\mathbf{h}}_n$ is now [111, (11.33) and (11.35)]:

$$\hat{\mathbf{h}}_n = \sigma_{\mathbf{z}}^{-2} [\sigma_{\mathbf{h}}^{-2} \mathbf{I}_{K^2(L+1)} + \sigma_{\mathbf{z}}^{-2} (\mathbf{I}_K \otimes \tilde{\mathbf{T}}^H \tilde{\mathbf{T}})]^{-1} (\mathbf{I}_K \otimes \tilde{\mathbf{T}}^H) \tilde{\mathbf{y}}_n \quad (\text{E.1a})$$

$$\mathbf{C}_{\Delta \mathbf{h}_n} = [\sigma_{\mathbf{h}}^{-2} \mathbf{I}_{K^2(L+1)} + \sigma_{\mathbf{z}}^{-2} (\mathbf{I}_K \otimes \tilde{\mathbf{T}}^H \tilde{\mathbf{T}})]^{-1} \quad (\text{E.1b})$$

where, $\Delta \mathbf{h}_n = \mathbf{h}_n - \hat{\mathbf{h}}_n$. The resulting channel estimator error variance is,

$$\begin{aligned} \sigma_{\Delta \mathbf{h}_n}^2 &= \text{trace} \{ \mathbf{C}_{\Delta \mathbf{h}_n} \} \\ &= \text{trace} \{ [\sigma_{\mathbf{h}}^{-2} \mathbf{I}_{K^2(L+1)} + \sigma_{\mathbf{z}}^{-2} (\mathbf{I}_K \otimes \tilde{\mathbf{T}}^H \tilde{\mathbf{T}})]^{-1} \} \end{aligned} \quad (\text{E.2})$$

The optimal $\tilde{\mathbf{T}}$, $\tilde{\mathbf{T}}^{(opt)}$ needs to minimize $\sigma_{\Delta \mathbf{h}_n}^2$ subject to (6.28). An equivalent representation of this pilot power constraint that will be useful for finding $\tilde{\mathbf{T}}^{(opt)}$ is as follows:

$$\text{trace} (\tilde{\mathbf{T}}_k^H \tilde{\mathbf{T}}_k) = \mathcal{P}_t / K \quad (\text{E.3a})$$

$$\text{trace} (\tilde{\mathbf{T}}^H \tilde{\mathbf{T}}) = (L+1) \mathcal{P}_t \quad (\text{E.3b})$$

As a result of (E.3b), we have

$$\tilde{\mathbf{T}}^{(opt)} = \arg_{\tilde{\mathbf{T}}} \min_{\text{trace} (\tilde{\mathbf{T}}^H \tilde{\mathbf{T}}) = (L+1) \mathcal{P}_t} \sigma_{\Delta \mathbf{h}_n}^2 \quad (\text{E.4})$$

From [94, Appendix I], we see that for any $M \times M$ dimensional positive-definite matrix \mathbf{A} ,

$$\text{trace}(\mathbf{A}^{-1}) \geq \sum_{m=0}^{M-1} \frac{1}{a_{m,m}} \quad (\text{E.5})$$

where the equality is attained if and only if \mathbf{A} is diagonal. Therefore, if $\tilde{\mathbf{T}}^{(opt)}$ is employed to perform the MIMO-OFDM channel estimation, the resulting variance of the MMSE channel estimator is as follows:

$$\begin{aligned} \sigma_{\Delta \mathbf{h}_n}^2 &= \text{trace} \{ [\sigma_h^{-2} \mathbf{I}_{K^2(L+1)} + \sigma_z^{-2} (\mathbf{I}_K \otimes \tilde{\mathbf{T}}^H \tilde{\mathbf{T}})]^{-1} \} \\ &\geq \sum_{l=0}^{K^2(L+1)-1} \frac{1}{[\sigma_h^{-2} \mathbf{I}_{K^2(L+1)} + \sigma_z^{-2} (\mathbf{I}_K \otimes \tilde{\mathbf{T}}^H \tilde{\mathbf{T}})]_{l,l}} \\ &= \frac{K^3(L+1) \sigma_z^2 \sigma_h^2}{K \sigma_z^2 + \sigma_h^2 \mathcal{P}_t} \end{aligned} \quad (\text{E.6})$$

and equality in the above equation is attained when $\tilde{\mathbf{T}}^H \tilde{\mathbf{T}}$ is diagonal.

E.0.1 Optimal Training Design

We now design the optimal training design that achieves the minimum MSE variance shown in (E.6). We will see that in order to attain this bound, the pilot sequences of each transmit antenna as well as their relationship with the training sequences emitted from every other transmit antenna need to satisfy certain specific properties. These properties are a direct consequence of (E.3b) and (E.5).

A closer observation of $\tilde{\mathbf{T}}^H \tilde{\mathbf{T}}$ reveals the following:

$$\tilde{\mathbf{T}}^H \tilde{\mathbf{T}} = \begin{bmatrix} \mathbf{R}_{1,1} & \cdots & \mathbf{R}_{1,K} \\ \mathbf{R}_{2,1} & \cdots & \mathbf{R}_{2,K} \\ \vdots & \ddots & \vdots \\ \mathbf{R}_{K,1} & \cdots & \mathbf{R}_{K,K} \end{bmatrix} \quad (\text{E.7})$$

where, the $(L+1) \times (L+1)$ dimensional submatrix \mathbf{R}_{k_1, k_2} is defined based on (6.20) as:

$$\mathbf{R}_{k_1, k_2} \triangleq \hat{\mathbf{W}}_{0:L}^H \tilde{\mathbf{T}}_{k_1}^H \tilde{\mathbf{T}}_{k_2} \hat{\mathbf{W}}_{0:L} \quad (\text{E.8})$$

The minimum variance as shown in (E.6) is therefore attained when

$$\mathbf{R}_{k_1, k_2} = \hat{\mathbf{W}}_{0:L}^H \tilde{\mathbf{T}}_{k_1}^H \tilde{\mathbf{T}}_{k_2} \hat{\mathbf{W}}_{0:L} = \frac{\bar{\mathcal{P}}}{K} \mathbf{I}_{L+1} \delta(k_1 - k_2) \quad (\text{E.9})$$

Case - $k_1 = k_2$: In order to understand the conditions that need to be imposed on the structure of $\tilde{\mathbf{T}}_k$, we examine an arbitrary element of $\mathbf{R}_{k,k}$. From (E.9), we notice that

$$\begin{aligned} [\mathbf{R}_{k,k}]_{l_1, l_2} &= \sum_{v=0}^{V-1} |\tilde{\mathbf{T}}_k[v, v]|^2 \exp\{-j2\pi l_v(l_2 - l_1)/P\} \\ &= \frac{\mathcal{P}_t}{K} \delta(l_1 - l_2) \end{aligned} \quad (\text{E.10})$$

It can be verified that the above expression is true under three conditions:

(C6) $P = VS$ where $S \in \mathbb{Z}^+$.

(C7) $\{l_v\}$, the index set of subcarriers that carry pilot symbols are chosen such that $l_v = l_s + vS$ for $l_s \in [0, S - 1]$ and $0 \leq v \leq V - 1$.

(C8) The pilot tones are all equally powered so that $|\tilde{\mathbf{T}}_k[v, v]|^2 = \frac{\mathcal{P}_t}{KV}$.

The above conditions indicate that the pilot symbols used for channel estimation must be *equispaced* in the subcarrier domain and *equipowered*. Due to (C8), we see that $\tilde{\mathbf{T}}_k^* \tilde{\mathbf{T}}_k = \frac{\mathcal{P}_t}{KV} \mathbf{I}_V$. Combined with the fact that $\hat{\mathbf{W}}_{0:L}^H \hat{\mathbf{W}}_{0:L} = V \mathbf{I}_{L+1}$, we see that $\mathbf{R}_{k,k} = \frac{\mathcal{P}_t}{K} \mathbf{I}_{L+1}$. We now see that when $K = 1$, the following pilot sequence design:

$$\tilde{\mathbf{T}}_k = \boldsymbol{\phi}(V) = \sqrt{\frac{\mathcal{P}_t}{KV}} [\exp(j\phi_0) \quad \exp(j\phi_1) \quad \dots \quad \exp(j\phi_{V-1})]^T \quad (\text{E.11})$$

meets conditions (C6), (C7), and (C8) that mandate the usage of equipowered, equispaced pilots at each transmit antenna. In (E.11), $\{\phi_v\}$ are any arbitrary values in $[-\pi, \pi]$.

Case - $k_1 \neq k_2$: We now incorporate the consequences of imposing the condition, $\mathbf{R}_{k_1, k_2} = 0$ when $k_1 \neq k_2$, in (E.11). We again utilize (E.9) and apply (C7). We see that

$$\begin{aligned} [\mathbf{R}_{k_1, k_2}]_{l_1, l_2} &= \exp\{-j2\pi l_s(l_1 - l_2)/P\} \times \\ &\quad \sum_{v=0}^{V-1} \tilde{\mathbf{T}}_{k_1}^*[v, v] \tilde{\mathbf{T}}_{k_2}[v, v] \exp\{-j2\pi vS(l_1 - l_2)/P\} \end{aligned} \quad (\text{E.12})$$

which equals zero when

$$\begin{aligned} & \sum_{v=0}^{V-1} \tilde{\mathbf{T}}_{k_1}^*[v, v] \tilde{\mathbf{T}}_{k_2}[v, v] \exp\{-j2\pi vS(l_1 - l_2)/P\} = 0 \\ \Leftrightarrow & \sum_{v=0}^{V-1} \tilde{\mathbf{T}}_{k_1}^*[v, v] \tilde{\mathbf{T}}_{k_2}[v, v] \exp\{-j2\pi v(l_1 - l_2)/V\} = 0 \end{aligned} \quad (\text{E.13})$$

$\forall 1 \leq k_1, k_2 \leq K$ and $\forall (l_1 - l_2) \in [0, \pm 1 \dots \pm L]$. This condition clearly suggests that in the frequency-domain, phase-shift orthogonality is required between the pilot sequences of different transmit antennas over the range, $(l_1 - l_2) \in [0, \pm 1 \dots \pm L]$. Equivalently, this translates to circular shift orthogonality in the time-domain. We now define a diagonal $V \times V$ dimensional phase-shifting matrix, \mathcal{E}_k as shown below:

$$[\mathcal{E}_k]_{v,v} = \exp\left[\frac{j2\pi v f_k}{V}\right] \quad (\text{E.14})$$

$\forall 0 \leq v \leq V - 1, 1 \leq k \leq K$ and design the pilot sequence such that

$$\tilde{\mathbf{T}}_k = \mathcal{E}_k \phi(V) \quad (\text{E.15})$$

As a result of substituting (E.14) in (E.13), we see that

$$\sum_{v=0}^{V-1} \exp\{-j2\pi v(f_{k_1} - f_{k_2} + l_1 - l_2)/V\} = 0 \quad (\text{E.16})$$

We selected \mathcal{E}_k as shown in (E.14) so that we can exploit the property of summation of the roots of unity. In order to do so, we require that the term, $(f_{k_1} - f_{k_2} + l_1 - l_2)$ be a non integer-multiple of V . So, we choose $f_k = k(V - L - 1)$. In conclusion, the training design shown in (6.33) meets not only conditions (C6), (C7), and (C8) but also (E.13) so that phase-shift orthogonality is maintained between the pilot sequences of any pair of transmit antennas.

Appendix F

Proof of Theorem 6.4

By denoting the entropy using $H(\cdot)$ and applying the definition of mutual information, we can write the following expression,

$$I(\tilde{\mathbf{y}}_n^{(dt)}; \tilde{\mathbf{x}}_n | \tilde{\mathcal{H}}_n) = H(\tilde{\mathbf{x}}_n | \tilde{\mathcal{H}}_n) - H(\tilde{\mathbf{x}}_n | \tilde{\mathcal{H}}_n, \tilde{\mathbf{y}}_n^{(dt)}), \quad (\text{F.1})$$

for the system model in the training phase. In the above equation, $H(\tilde{\mathbf{x}}_n | \tilde{\mathcal{H}}_n)$ is maximized when $\tilde{\mathbf{x}}_n$ is Gaussian. Hence, with $\mathbf{R}_{\tilde{\mathbf{x}}_n} = \mathcal{P}_{dt} \mathbf{I}_{KM}$,

$$H(\tilde{\mathbf{x}}_n | \tilde{\mathcal{H}}_n) = \log \det(\pi e \mathcal{P}_{dt} \mathbf{I}_{KM}). \quad (\text{F.2})$$

On the other hand,

$$H(\tilde{\mathbf{x}}_n | \tilde{\mathcal{H}}_n, \tilde{\mathbf{y}}_n^{(dt)}) = \log \det(\pi e \mathbf{R}_{\tilde{\mathbf{x}}_n | \tilde{\mathbf{y}}_n^{(dt)}, \tilde{\mathcal{H}}_n}), \quad (\text{F.3})$$

where $\mathbf{R}_{\tilde{\mathbf{x}}_n | \tilde{\mathbf{y}}_n^{(dt)}, \tilde{\mathcal{H}}_n} = ((1/\mathcal{P}_{dt}) \mathbf{I}_{KM} + (1/\sigma_z^2) \tilde{\mathcal{H}}_n^H \tilde{\mathcal{H}}_n)^{-1}$. In writing the covariance matrix of the random vector, $\tilde{\mathbf{x}}_n$ conditioned on $\tilde{\mathbf{y}}_n^{(dt)}$ and $\tilde{\mathcal{H}}_n$, we utilize the fact that $\tilde{\mathbf{z}}_n$ is Gaussian distributed. Consequently,

$$I(\tilde{\mathbf{y}}_n^{(dt)}; \tilde{\mathbf{x}}_n | \tilde{\mathcal{H}}_n) = \log \det \left(\mathbf{I}_{KM} + \frac{\mathcal{P}_{dt}}{\sigma_z^2} \tilde{\mathcal{H}}_n \tilde{\mathcal{H}}_n^H \right). \quad (\text{F.4})$$

By a similar approach, we can show that

$$I(\tilde{\mathbf{r}}_n; \tilde{\mathbf{s}}_n | \overline{\mathcal{H}}_n) = \log \det \left(\mathbf{I}_{KP} + \frac{\mathcal{P}_d}{\sigma_z^2} \overline{\mathcal{H}}_n \overline{\mathcal{H}}_n^H \right), \quad (\text{F.5})$$

in the data transmission phase. Due to the fact that the mutual information between the transmitted and estimated data vectors is independent of the block index, we represent the channel capacity upper bound by choosing the mutual information with respect to an arbitrary block indices as shown in (6.42). It can also be observed that we have included the appropriate normalization factor since only M out of P subcarriers in each OFDM symbol in the training phase, carry information symbols.

Appendix G

Proof of Theorem 6.5

We again apply the definition of mutual information and write the expression,

$$I(\tilde{\mathbf{y}}_n^{(dt)}; \tilde{\mathbf{x}}_n | \widehat{\mathcal{H}}_n) = H(\tilde{\mathbf{x}}_n | \widehat{\mathcal{H}}_n) - H(\tilde{\mathbf{x}}_n | \widehat{\mathcal{H}}_n, \tilde{\mathbf{y}}_n^{(dt)}), \quad (\text{G.1})$$

for the system model in the training phase. Similar to (F.2), we see that

$$H(\tilde{\mathbf{x}}_n | \widehat{\mathcal{H}}_n) = \log \det(\pi e \mathcal{P}_{dt} \mathbf{I}_{KM}), \quad (\text{G.2})$$

whereas,

$$H(\tilde{\mathbf{x}}_n | \widehat{\mathcal{H}}_n, \tilde{\mathbf{y}}_n^{(dt)}) \leq \log \det(\pi e \mathbf{R}_{\tilde{\mathbf{x}}_n | \tilde{\mathbf{y}}_n^{(dt)}, \widehat{\mathcal{H}}_n}), \quad (\text{G.3})$$

with equality if and only if $\tilde{\mathbf{x}}_n$ given $\tilde{\mathbf{y}}_n^{(dt)}$ and $\widehat{\mathcal{H}}_n$ is drawn from a Gaussian distribution with the covariance matrix, $\mathbf{R}_{\tilde{\mathbf{x}}_n | \tilde{\mathbf{y}}_n^{(dt)}, \widehat{\mathcal{H}}_n}$. We can now formulate an expression for $\mathbf{R}_{\tilde{\mathbf{x}}_n | \tilde{\mathbf{y}}_n^{(dt)}, \widehat{\mathcal{H}}_n}$ by assuming that LMMSE estimator¹ has been used to estimate $\tilde{\mathbf{x}}_n$:

$$\mathbf{R}_{\tilde{\mathbf{x}}_n | \tilde{\mathbf{y}}_n^{(dt)}, \widehat{\mathcal{H}}_n} = \mathbf{R}_{\tilde{\mathbf{x}}_n} - \mathbf{R}_{\tilde{\mathbf{x}}_n, \tilde{\mathbf{y}}_n^{(dt)}} \mathbf{R}_{\tilde{\mathbf{y}}_n^{(dt)}}^{-1} \mathbf{R}_{\tilde{\mathbf{y}}_n^{(dt)}, \tilde{\mathbf{x}}_n}, \quad (\text{G.4})$$

¹Notice that when $\tilde{\mathbf{z}}_n^{(dt)}$ is Gaussian, the LMMSE estimator coincides with an MMSE estimator.

where

$$\mathbf{R}_{\tilde{\mathbf{x}}_n, \tilde{\mathbf{y}}_n^{(dt)}} \triangleq \mathbb{E} \{ \tilde{\mathbf{x}}_n \tilde{\mathbf{y}}_n^{(dt)\text{H}} | \widehat{\mathcal{H}}_n \} = \mathcal{P}_{dt} \widehat{\mathcal{H}}_n^{\text{H}}, \quad (\text{G.5a})$$

$$\mathbf{R}_{\tilde{\mathbf{y}}_n^{(dt)}} \triangleq \mathbb{E} \{ \tilde{\mathbf{y}}_n^{(dt)} \tilde{\mathbf{y}}_n^{(dt)\text{H}} | \widehat{\mathcal{H}}_n \} = \mathcal{P}_{dt} \widehat{\mathcal{H}}_n \widehat{\mathcal{H}}_n^{\text{H}} + \sigma_{z^{(dt)}}^2(n) \mathbf{I}_{KM}. \quad (\text{G.5b})$$

In (G.5a) and (G.5b), we have utilized the orthogonality property of LMMSE estimation and eliminated the covariance terms between the information symbol vector, $\tilde{\mathbf{x}}_n$ and the effective noise vector, $\tilde{\mathbf{z}}_n^{(dt)}$. By substituting (G.5a) and (G.5b) in (G.4), we see that:

$$\begin{aligned} \mathbf{R}_{\tilde{\mathbf{x}}_n | \tilde{\mathbf{y}}_n^{(dt)}, \widehat{\mathcal{H}}_n} &= \mathcal{P}_{dt} \mathbf{I}_{KM} - \mathcal{P}_{dt}^2 \widehat{\mathcal{H}}_n^{\text{H}} (\mathcal{P}_{dt} \widehat{\mathcal{H}}_n \widehat{\mathcal{H}}_n^{\text{H}} + \sigma_{z^{(dt)}}^2(n) \mathbf{I}_{KM})^{-1} \widehat{\mathcal{H}}_n \\ &= ((1/\mathcal{P}_{dt}) \mathbf{I}_{KM} + \sigma_{z^{(dt)}}^2(n) \widehat{\mathcal{H}}_n^{\text{H}} \widehat{\mathcal{H}}_n)^{-1}. \end{aligned} \quad (\text{G.6})$$

Finally, from (G.2), (G.3) and (G.6), we have,

$$\mathbb{I}(\tilde{\mathbf{y}}_n^{(dt)}; \tilde{\mathbf{x}}_n | \widehat{\mathcal{H}}_n) \geq \log \det (\mathbf{I}_{KM} + \mathcal{P}_{dt} \sigma_{z^{(dt)}}^2(n) \widehat{\mathcal{H}}_n^{\text{H}} \widehat{\mathcal{H}}_n). \quad (\text{G.7})$$

By a similar approach, we can show that

$$\mathbb{I}(\tilde{\mathbf{r}}_n; \tilde{\mathbf{s}}_n | \widehat{\mathcal{H}}_n) \geq \log \det (\mathbf{I}_{KP} + \mathcal{P}_d \sigma_{z^{(d)}}^2(n) \widehat{\mathcal{H}}_n^{\text{H}} \widehat{\mathcal{H}}_n), \quad (\text{G.8})$$

in the data transmission phase. Therefore, the channel capacity lower bound is obtained by combining (G.7) and (G.8) as shown in (6.50).

References

- [1] “Adapted from the wikimedia commons file “File:Marconi_at_newfoundland.jpg”.” [online]: http://en.wikipedia.org/wiki/File:Marconi_at_newfoundland.jpg.
- [2] S. Pagadarai and A. M. Wyglinski, “A Linear Mixed-Effects Model of Wireless Spectrum Occupancy,” *EURASIP Journal on Wireless Communications and Networking*, vol. 2010, pp. 14:1–14:13, April 2010.
- [3] S. Pagadarai, A. Wyglinski, and R. Vuyyuru, “Characterization of Vacant UHF TV Channels for Vehicular Dynamic Spectrum Access,” in *IEEE Vehicular Networking Conference (VNC), 2009*, pp. 1–8, 2009.
- [4] H. Bogucka, A. Wyglinski, S. Pagadarai, and A. Kliks, “Spectrally Agile Multicarrier Waveforms for Opportunistic Wireless Access,” *IEEE Communications Magazine*, vol. 49, pp. 108–115, June 2011.
- [5] S. Pagadarai, A. Kliks, H. Bogucka, and A. Wyglinski, “Non-Contiguous Multicarrier Waveforms in Practical Opportunistic Wireless Systems,” *IET Radar, Sonar and Navigation Journal*, vol. 5, pp. 674–680, July 2011.
- [6] J. Elvish, “Radio - Its Impact on Shipping,” *Journal of the British Institution of Radio Engineers*, vol. 20, no. 6, pp. 403–407, 1960.
- [7] D. Noble, “The History of Land-Mobile Radio Communications,” *Proceedings of the IRE*, vol. 50, pp. 1405–1414, May 1962.
- [8] J. Hilliard, “The History of Stereophonic Sound Reproduction,” *Proceedings of the IRE*, vol. 50, pp. 776–780, May 1962.
- [9] D. Fink, “Television Broadcasting in the United States, 1927-1950,” *Proceedings of the IRE*, vol. 39, pp. 116–123, Feb. 1951.
- [10] W. R. Young, “Advanced Mobile Phone Service: Introduction, Background and Objectives,” *The Bell System Technical Journal*, vol. 58, pp. 1–14, Jan. 1979. [Online]: <http://www.alcatel-lucent.com/bstj/vol58-1979/articles/bstj58-1-1.pdf>.

-
- [11] J. Schulte, H.J. and W. Cornell, "Multi-Area Mobile Telephone System," *IRE Transactions on Vehicular Communications*, vol. 9, pp. 49 – 53, June 1957.
- [12] W. Lewis, "Coordinated Broadband Mobile Telephone System," *IRE Transactions on Vehicular Communications*, vol. 9, pp. 43 – 48, June 1957.
- [13] H. Nylund and R. Swanson, "An Improved Mobile Dial Telephone System," *IRE Transactions on Vehicular Communications*, vol. 12, pp. 32 – 38, Apr. 1959.
- [14] A. Bailey, "Future Developments in Vehicular Communications," *Proceedings of the IRE*, vol. 50, pp. 1415 – 1420, May 1962.
- [15] J. Engel, "The Effects of Cochannel Interference on the Parameters of a Small-Cell Mobile Telephone System," *IEEE Transactions on Vehicular Technology*, vol. 18, pp. 110 – 116, Nov. 1969.
- [16] R. Frenkiel, "A High-Capacity Mobile Radiotelephone System Model Using a Coordinated Small-Zone Approach," *IEEE Transactions on Vehicular Technology*, vol. 19, pp. 173 – 177, May 1970.
- [17] H. Staras and L. Schiff, "A Dynamic Space Division Multiplex Mobile Radio System," *IEEE Transactions on Vehicular Technology*, vol. 19, pp. 206 – 213, May 1970.
- [18] [Online]: <http://www.alcatel-lucent.com/bstj/vol58-1979/bstj-vol58-issue01.html>.
- [19] S. McConoughey, "New concepts in spectrum usage," *IEEE Transactions on Communications*, vol. 21, pp. 1172 – 1176, Nov. 1973.
- [20] R. Gould, "Regulatory Aspects of Digital Communications (Radio Frequency Considerations)," *IEEE Transactions on Communications*, vol. 24, pp. 118 – 130, Jan. 1976.
- [21] J. Robinson, "Spectrum Allocation and Economic Factors in FCC Spectrum Management," *IEEE Transactions on Electromagnetic Compatibility*, vol. EMC-19, no. 3, pp. 182 – 190, 1977.
- [22] J. Krauss, "Implications of FCC Regulation of Telecommunications Technical Standards," *IEEE Communications Magazine*, vol. 20, pp. 28 – 32, Sept. 1982.
- [23] Communications Act of 1934, "Act of Congress, Pub. Law No. 416-73rd Congress, approved June 19, 1934." [Online]: http://www.fcc.gov/Bureaus/OSEC/library/legislative_histories/47.pdf.
- [24] J. McMahon, "Capability of the FCC Mobile Monitoring Van," *IEEE Transactions on Vehicular Technology*, vol. 23, pp. 139 – 143, Nov. 1974.

-
- [25] R. Matheson, "A Radio Spectrum Measurement System for Frequency Management Data," *IEEE Transactions on Electromagnetic Compatibility*, vol. EMC-19, no. 3, pp. 225–230, 1977.
- [26] G. Hufford and J. Murray, "Television Coverage in the Coterminous United States: Methodology and Results," *Proceedings of the IEEE*, vol. 70, no. 11, pp. 1263–1268, 1982.
- [27] M. A. McHenry, "NSF Spectrum Occupancy Measurements Project Summary," tech. rep., Shared Spectrum Company, August 2005.
- [28] D. A. Roberson, C. S. Hood, J. L. LoCicero, and J. T. MacDonald, "Spectral Occupancy and Interference Studies in Support of Cognitive Radio Technology Deployment," in *Proceedings of IEEE Workshop*, (Boulder, CO, USA), pp. 167–175, March 7–9, 2006.
- [29] J. Mitola III, *Cognitive Radio: An Integrated Agent Architecture for Software Defined Radio*. Ph.D Dissertation, KTH (Royal Institute of Technology), Stockholm, Sweden, 2000.
- [30] Federal Communications Commission, "In the Matter of Unlicensed Operation in the TV Broadcast Bands, Additional Spectrum for Unlicensed Devices Below 900 MHz and in the 3 GHz Band." [Online]: http://hraunfoss.fcc.gov/edocs_public/attachmatch/FCC08260A1.pdf.
- [31] G. J. Foschini and M. J. Gans, "On Limits of Wireless Communications in a Fading Environment When Using Multiple Antennas," *Wireless Personal Communications*, vol. 6, pp. 311–335, 1998.
- [32] U. Madhow, *Fundamentals of Digital Communication*. Cambridge University Press, 2008.
- [33] S. Kay, *Modern Spectral Estimation: Theory and Application*. New Jersey: Prentice-Hall, 1999.
- [34] P. Stoica and R. L. Moses, *Spectral Analysis of Signals*. New Jersey: Prentice-Hall, 2005.
- [35] A. Scaglione, G. Giannakis, and S. Barbarossa, "Redundant Filterbank Precoders and Equalizers. Parts I & II," *IEEE Transactions on Signal Processing*, vol. 47, pp. 1988–2006, July 1999.
- [36] L. Tong and S. Perreau, "Multichannel Blind Identification: From Subspace to Maximum Likelihood Methods," *Proceedings of the IEEE*, vol. 86, pp. 1951–1968, October 1998.

-
- [37] Y. Hua and M. Wax, "Strict Identifiability of Multiple FIR Channels Driven by an Unknown Arbitrary Sequence," *IEEE Transactions on Signal Processing*, vol. 44, pp. 756–759, March 1996.
- [38] A. Liavas, P. Regalia, and J.-P. Delmas, "Robustness of Least-Squares and Subspace Methods for Blind Channel Identification/Equalization With Respect to Effective Channel Undermodeling/Overmodeling," *IEEE Transactions on Signal Processing*, vol. 47, pp. 1636–1645, June 1999.
- [39] R. Johnson Jr., P. Schniter, T. Endres, J. Behm, D. Brown, and R. Casas, "Blind Equalization Using the Constant Modulus Criterion: A Review," *Proceedings of the IEEE*, vol. 86, pp. 1927–1950, October 1998.
- [40] L. Tong, B. Sadler, and M. Dong, "Pilot-Assisted Wireless Transmissions: General Model, Design Criteria, and Signal Processing," *IEEE Signal Processing Magazine*, vol. 21, pp. 12–25, November 2004.
- [41] D. Roberson and W. Webb, *Cognitive Radio Communications and Networks: Principles and Practice*, ch. Radio Frequency Spectrum and Regulation. Academic Press, 2009.
- [42] A. J. Petrin, *Maximizing the Utility of Radio Spectrum: Broadband Spectrum Measurements and Occupancy Model for Use by Cognitive Radio*. Ph.d dissertation, Georgia Institute of Technology, Atlanta, Georgia, USA, August 2005.
- [43] P. F. Marshall, "Closed-Form Analysis of Spectrum Characteristics for Cognitive Radio Performance Analysis," in *Proc. IEEE DySPAN Conf.*, pp. 1–12, Oct 14-17, 2008.
- [44] M. A. McHenry, "NSF Spectrum Occupancy Measurements Project Summary," tech. rep., Shared Spectrum Company, August 2005.
- [45] R. I. C. Chiang, G. B. Rowe, and K. W. Sowerby, "A Quantitative Analysis of Spectral Occupancy Measurements for Cognitive Radio," in *Proc. IEEE Veh. Technol. Conf. - Spring*, pp. 3016–3020, April 22-25, 2007.
- [46] M. Wellens, A. de Baynast, and P. Mahonen, "Exploiting Historical Spectrum Occupancy Information for Adaptive Spectrum Sensing," in *Proc. IEEE Wireless Commn. and Netw. Conf.*, (Las Vegas, NV, USA), pp. 717–722, March 31 - April 3, 2008.
- [47] M. Nekovee, "Quantifying the Availability of TV White Spaces for Cognitive Radio Operation in the UK," in *Proc. IEEE ICC Conf.*, (Dresden, Germany), June 14-18, 2009.

-
- [48] F. C. Commission, "Spectrum Policy Task Force Report: ET Docket No. 02-135, 2002." [online]: http://hraunfoss.fcc.gov/edocs_public/attachmatch/D0C-228542A1.pdf.
- [49] T. A. Weiss and F. K. Jondral, "Spectrum Pooling: An Innovative Strategy for the Enhancement of Spectrum Efficiency," *IEEE Commun. Mag.*, vol. 43, pp. 8–14, March 2004.
- [50] J. Mitola III, "Cognitive radio for flexible mobile multimedia communications," in *Proc. IEEE Int. Wksp. Mobile Multimedia Commun.*, vol. 1, (San Diego, CA, USA), pp. 3–10, Nov. 1999.
- [51] J. Mitola III, "Software Radio Architecture: A Mathematical Perspective," in *Proc. IEEE Journal on selected areas in Commn.*, vol. 17, No. 4, April 1999.
- [52] D. Čabrić and R. W. Brodersen, "Physical layer design issues unique to cognitive radio systems," *IEEE 16th International Symposium on Personal, Indoor and Mobile Radio Commun.*, vol. 2, pp. 759–763, Sept. 2005.
- [53] T. A. Weiss, J. Hillenbrand, A. Krohn and F. K. Jondral, "Mutual interference in OFDM-based spectrum pooling systems," in *Proc. IEEE Veh. Technol. Conf. - Fall*, vol. 4, pp. 1872–1877, May 2004.
- [54] S. Haykin, "Cognitive Radio: Brain-empowered Wireless Communications," *IEEE Journal on Sel. Areas of Commns.*, vol. 23, pp. 201–220, Feb. 2005.
- [55] R. V. Prasad, P. Pawelczak, James A. Hoffmeyer, and H. Steven Berger, "Cognitive Functionality in Next Generation Wireless Networks:Standardization Efforts," *IEEE Commun. Mag.*, pp. 72–78, April 2008.
- [56] U.S. Department of Transportation (US DOT), "Research and Innovative Technology Administration (RITA)." [online]: <http://www.its.dot.gov/>.
- [57] W. Chen and S. Cai, "Ad Hoc Peer-to-Peer Network Architecture for Vehicle Safety Communications," *IEEE Commn. Mag.*, April 2005.
- [58] K. Tsukamoto, S. Matsuoka, O. Altintas, M. Tsuru, and Y. Oie, "Distributed channel coordination in cognitive wireless vehicle-to-vehicle communications," in *Proceedings of the Wireless Access in Vehicular Environments (WAVE) Conference*, (Dearborn, MI, USA), Dec. 2008.
- [59] K. Tsukamoto, Y. Omori, O. Altintas, M. Tsuru, and Y. Oie, "On spatially-aware channel selection in dynamic spectrum access multi-hop inter-vehicle communications," in *Proceedings of the IEEE Vehicular Technology Conference - Fall*, (Anchorage, AK, USA), Sept. 2009.

-
- [60] C. Lacatus, R. Vuyyuru, O. Altintas, D. Borota, and I. Seskar, "Evaluation of energy-based spectrum sensing algorithm for vehicular networks," in *Proceedings of the SDR Forum Technical Conference*, (Washington DC, USA), Dec. 2009.
- [61] S. Pagadarai and A. Wyglinski, "A Quantitative Assessment of Wireless Spectrum Measurements for Dynamic Spectrum Access," in *4th International Conference on Cognitive Radio Oriented Wireless Networks and Communications (CROWNCOM) 2009.*, pp. 1–5, 2009.
- [62] N. Otsu, "A Threshold Selection Method from Gray-Level Histograms," *IEEE Trans. on Sys., Man and Cyber.*, vol. SMC-9, pp. 62–66, Jan 1979.
- [63] A. J. Petrin, *Maximizing the Utility of Radio Spectrum: Broadband Spectrum Measurements and Occupancy Model for Use by Cognitive Radio*. Ph.d dissertation, Georgia Institute of Technology, Atlanta, Georgia, USA, August 2005.
- [64] D. Datla, "Spectrum Surveying for Dynamic Spectrum Access Networks," Master's thesis, University of Kansas, Lawrence, KS, USA, Feb 2007.
- [65] J. Fox, *Applied Regression, Generalized Linear Models, and Related Methods*. Sage Publications Inc., 2008.
- [66] D. Datla, R. Rajbanshi, A. M. Wyglinski, and G. J. Minden, "An adaptive spectrum sensing architecture for dynamic spectrum access networks," *IEEE Transactions on Wireless Communications*, 2009. To Appear.
- [67] Khaled Ben Letaief and Wei Zhang, *Cognitive Wireless Communication Networks*, ch. 4. Netherlands: Springer, 2007.
- [68] C. Stevenson, C. Cordeiro, E. Sofer, G. Chouinard, "Functional Requirements for the 802.22 WRAN Standard, doc.: IEEE 802.22-05/0007r48." [Online]: <https://mentor.ieee.org/802.22/dcn/05/22-05-0007-48-0000-draft-wran-rqmts-doc.doc>, Nov. 2006.
- [69] D. Gurney, G. Buchwald, L. Ecklund, S. L. Kuffner, J. Grosspietsch, "Geo-Location Database Techniques for Incumbent Protection in the TV White Space," in *IEEE Int. Symp. Dynamic Spectrum Access Netw.*, (Chicago, IL, USA), October, 2008.
- [70] C. M. Cordeiro, M. Ghosh, D. Cavalcanti, and K. Challapali, "Spectrum Sensing for Dynamic Spectrum Access of TV Bands," in *Proc. CROWNCOM*, (Orlando, FL, USA), August 2007.
- [71] "Fixed TV White Space Solutions for Wireless ISP Network Operators." [online]: [http://www.motorola.com/staticfiles/Business/Product Lines/Motowi4/wi4](http://www.motorola.com/staticfiles/Business/Product%20Lines/Motowi4/wi4)

Fixed/Point-to-Point Multipoint/Canopy/_ChannelDetails/_Documents/_Static files/WB_TV White Space Position Paper_V2.11.08.pdf, Nov 2008.

- [72] Federal Communications Commission, “Notice of Proposed Rule Making: FCC-04-113A-1.” [online]: http://hraunfoss.fcc.gov/edocs_public/attachmatch/FCC-04-113A1.doc, May 25 2005.
- [73] FCC Media Bureau, “TVQ TV Database Query.” [online]: <http://www.fcc.gov/mb/video/tvq.html>.
- [74] Federal Communications Commission, “FM and TV Propagation Curves Calculations.” [online]: <http://www.fcc.gov/mb/audio/bickel/curves.html>.
- [75] T. Wang, J. Proakis, and J. Zeidler, “Interference Analysis of Filtered Multitone Modulation Over Time-Varying Frequency-Selective Fading Channels,” *IEEE Transactions on Communications*, vol. 55, pp. 717–727, April 2007.
- [76] J. Mitola III, *Cognitive Radio: An Integrated Agent Architecture for Software Defined Radio*. Ph.d dissertation, KTH (Royal Institute of Technology), Stockholm, Sweden, 2000.
- [77] W. Kozek and A. Molisch, “Nonorthogonal Pulseshapes for Multicarrier Communications in Doubly Dispersive Channels,” *IEEE Journal on Selected Areas in Communications*, vol. 16, pp. 1579–1589, October 1998.
- [78] P. Prinz, “Calculating the Dual Gabor Window for General Sampling Sets,” *IEEE Transactions on Signal Processing*, vol. 44, pp. 2078–2082, August 1996.
- [79] S. Qian and D. Chen, “Discrete Gabor Transform,” *IEEE Transactions on Signal Processing*, vol. 41, pp. 2429–2438, July 1993.
- [80] I. Cosovic and T. Mazzoni, “Suppression of Sidelobes in OFDM Systems by Multiple-Choice Sequences,” *European Transactions on Telecommunications*, vol. 17, no. 6, pp. 623–630, 2006.
- [81] S. Pagadarai, A. Wyglinski, and R. Rajbanshi, “A Novel Sidelobe Suppression Technique for OFDM-Based Cognitive Radio Transmission,” in *3rd IEEE Symposium on New Frontiers in Dynamic Spectrum Access Networks, 2008 (DySPAN '08)*, pp. 1–7, October 2008.
- [82] S. Pagadarai and A. Wyglinski, “A Quantitative Assessment of Wireless Spectrum Measurements for Dynamic Spectrum Access,” in *4th International Conference on Cognitive Radio Oriented Wireless Networks and Communications*, pp. 1–5, 2009.

-
- [83] S. Pagadarai, A. Wyglinski, and C. Anderson, "An Evaluation of the Bayesian CRLB for Time-Varying MIMO Channel Estimation Using Complex-Valued Differentials," in *2011 IEEE Pacific Rim Conference on Communications, Computers and Signal Processing*, pp. 818–823, August 2011.
- [84] G. J. Foschini, "Layered Space-Time Architecture for Wireless Communication in a Fading Environment When Using Multi-Element Antennas," *Bell Labs Technical Journal*, vol. 1, no. 2, pp. 41–59, 1996.
- [85] N. Merhav, G. Kaplan, A. Lapidoth, and S. Shamai Shitz, "On Information Rates for Mismatched Decoders," *IEEE Transactions on Information Theory*, vol. 40, pp. 1953–1967, November 1994.
- [86] A. Lapidoth and P. Narayan, "Reliable Communication Under Channel Uncertainty," *IEEE Transactions on Information Theory*, vol. 44, pp. 2148–2177, October 1998.
- [87] M. Medard, "The Effect Upon Channel Capacity in Wireless Communications of Perfect and Imperfect Knowledge of the Channel," *IEEE Transactions on Information Theory*, vol. 46, pp. 933–946, May 2000.
- [88] A. Lapidoth and S. Shamai, "Fading Channels: How Perfect Need "Perfect Side Information" Be?," *IEEE Transactions on Information Theory*, vol. 48, pp. 1118–1134, May 2002.
- [89] R. Negi and J. Cioffi, "Pilot Tone Selection for Channel Estimation in a Mobile OFDM System," *IEEE Transactions on Consumer Electronics*, vol. 44, pp. 1122–1128, August 1998.
- [90] S. Adireddy, L. Tong, and H. Viswanathan, "Optimal Placement of Training for Frequency-Selective Block-Fading Channels," *IEEE Transactions on Information Theory*, vol. 48, pp. 2338–2353, August 2002.
- [91] M. Dong and L. Tong, "Optimal Design and Placement of Pilot Symbols for Channel Estimation," *IEEE Transactions on Signal Processing*, vol. 50, pp. 3055–3069, December 2002.
- [92] S. Ohno and G. Giannakis, "Optimal Training and Redundant Precoding for Block Transmissions with Application to Wireless OFDM," *IEEE Transactions on Communications*, vol. 50, pp. 2113–2123, December 2002.
- [93] J. Manton, I. Mareels, and Y. Hua, "Affine Precoders for Reliable Communications," in *Proceedings of the 25th IEEE International Conference on Acoustics, Speech, and Signal Processing, 2000 (ICASSP '00)*, vol. 5, pp. 2749–2752, June 2000.

-
- [94] S. Ohno and G. Giannakis, "Capacity Maximizing MMSE-Optimal Pilots for Wireless OFDM over Frequency-Selective Block Rayleigh-Fading Channels," *IEEE Transactions on Information Theory*, vol. 50, pp. 2138–2145, September 2004.
- [95] X. Ma, L. Yang, and G. Giannakis, "Optimal Training for MIMO Frequency-Selective Fading Channels," *IEEE Transactions on Wireless Communications*, vol. 4, pp. 453–466, March 2005.
- [96] J. Baltersee, G. Fock, and H. Meyr, "Achievable Rate of MIMO Channels With Data-Aided Channel Estimation and Perfect Interleaving," *IEEE Journal on Selected Areas in Communications*, vol. 19, pp. 2358–2368, December 2001.
- [97] B. Hassibi and B. Hochwald, "How Much Training is Needed in Multiple-Antenna Wireless Links?," *IEEE Transactions on Information Theory*, vol. 49, pp. 951–963, April 2003.
- [98] D. Samardzija and N. Mandayam, "Pilot-Assisted Estimation of MIMO Fading Channel Response and Achievable Data Rates," *IEEE Transactions on Signal Processing*, vol. 51, pp. 2882–2890, November 2003.
- [99] A. Vosoughi and A. Scaglione, "On the Effect of Receiver Estimation Error Upon Channel Mutual Information," *IEEE Transactions on Signal Processing*, vol. 54, pp. 459–472, February 2006.
- [100] M. Coldrey and P. Bohlin, "Training-Based MIMO Systems-Part I: Performance Comparison," *IEEE Transactions on Signal Processing*, vol. 55, pp. 5464–5476, November 2007.
- [101] M. Ding and S. Blostein, "Maximum Mutual Information Design for MIMO Systems With Imperfect Channel Knowledge," *IEEE Transactions on Information Theory*, vol. 56, pp. 4793–4801, October 2010.
- [102] G. Giannakis, "Filterbanks for Blind Channel Identification and Equalization," *IEEE Signal Processing Letters*, vol. 4, pp. 184–187, June 1997.
- [103] M. Stojanovic, J. Proakis, and J. Catipovic, "Analysis of the Impact of Channel Estimation Errors on the Performance of a Decision-Feedback Equalizer in Fading Multipath Channels," *IEEE Transactions on Communications*, vol. 43, pp. 877–886, February/March/April 1995.
- [104] C. Komninakis, C. Fragouli, A. Sayed, and R. Wesel, "Multi-Input Multi-Output Fading Channel Tracking and Equalization Using Kalman Estimation," *IEEE Transactions on Signal Processing*, vol. 50, pp. 1065–1076, May 2002.

-
- [105] I. E. Telatar, "Capacity of Multi-Antenna Gaussian Channels," *European Transactions on Telecommunications*, vol. 10, pp. 585–595, 1999.
- [106] H. Schulze and C. Lueders, *Theory and Applications of OFDM and CDMA: Wideband Wireless Communications*. Hoboken, NJ: John Wiley & Sons Inc., 2005.
- [107] A. Vosoughi and A. Scaglione, "Everything You Always Wanted to Know About Training: Guidelines Derived Using the Afne Precoding Framework and the CRB," *IEEE Transactions on Signal Processing*, vol. 54, pp. 940–954, March 2006.
- [108] I. Barhumi, G. Leus, and M. Moonen, "Optimal Training Design for MIMO OFDM Systems in Mobile Wireless Channels," *IEEE Transactions on Signal Processing*, vol. 51, pp. 1615–1624, June 2003.
- [109] J. Yang and S. Roy, "On Joint Transmitter and Receiver Optimization for Multiple-Input-Multiple-Output (MIMO) Transmission Systems," *IEEE Transactions on Communications*, vol. 42, pp. 3221–3231, December 1994.
- [110] D. Palomar, M. Lagunas, and J. Cioffi, "Optimum Linear Joint Transmit-Receive Processing for MIMO Channels with QoS Constraints," *IEEE Transactions on Signal Processing*, vol. 52, pp. 1179–1197, May 2004.
- [111] S. M. Kay, *Fundamentals of Statistical Signal Processing, Vol. I - Estimation Theory*. Englewood Cliffs, NJ: Prentice Hall, 1993.
- [112] D. Vaughan, "A Nonrecursive Algebraic Solution for the Discrete Riccati Equation," *IEEE Transactions on Automatic Control*, vol. 15, pp. 597–599, October 1970.
- [113] A. Laub, "A Schur Method for Solving Algebraic Riccati Equations," *IEEE Transactions on Automatic Control*, vol. 24, pp. 913–921, December 1979.
- [114] R. Leland, "An Alternate Calculation of the Discrete-Time Kalman Filter Gain and Riccati Equation Solution," *IEEE Transactions on Automatic Control*, vol. 41, pp. 1817–1819, December 1996.
- [115] H. Minn and N. Al-Dhahir, "Optimal Training Signals for MIMO OFDM Channel Estimation," *IEEE Transactions on Wireless Communications*, vol. 5, pp. 1158–1168, May 2006.
- [116] M. Dong, L. Tong, and B. Sadler, "Optimal Insertion of Pilot Symbols for Transmissions Over Time-Varying Flat Fading Channels," *IEEE Transactions on Signal Processing*, vol. 52, pp. 1403–1418, May 2004.

- [117] Y.-S. Choi, P. Voltz, and F. Cassara, "On Channel Estimation and Detection for Multicarrier Signals in Fast and Selective Rayleigh Fading Channels," *IEEE Transactions on Communications*, vol. 49, pp. 1375–1387, August 2001.
- [118] A. Stamoulis, S. Diggavi, and N. Al-Dhahir, "Intercarrier Interference in MIMO OFDM," *IEEE Transactions on Signal Processing*, vol. 50, pp. 2451–2464, October 2002.
- [119] Mary J. Lindstrom and Douglas M. Bates, "Nonlinear mixed effects models for repeated measures data," *Biometrics*, vol. 46, no. 3, pp. 673–687, 1990.
- [120] A. Hjørungnes and D. Gesbert, "Complex-Valued Matrix Differentiation: Techniques and Key Results," *IEEE Transactions on Signal Processing*, vol. 55, pp. 2740–2746, June 2007.
- [121] Harry L. Van Trees, *Detection, Estimation, and Modulation Theory, Part I*. USA: Wiley-Interscience, 2001.
- [122] A. Hjørungnes, D. Gesbert, and D. Palomar, "Unified Theory of Complex-Valued Matrix Differentiation," in *IEEE International Conference on Acoustics, Speech and Signal Processing*, vol. 3, pp. 345–348, April 2007.